5-2016

Interference Mitigation in Multi-Hop Wireless Networks with Advanced Physical-Layer Techniques

Yantian Hou
Utah State University

INTERFERENCE MITIGATION IN MULTI-HOP WIRELESS NETWORKS WITH ADVANCED PHYSICAL-LAYER TECHNIQUES

by

Yantian Hou

A dissertation submitted in partial fulfillment
of the requirements for the degree

of

DOCTOR OF PHILOSOPHY

in

Computer Science

Approved:

Ming Li, Ph.D. Major Professor	Nicholas Flann, Ph.D. Committee Member
Haitao Wang, Ph.D. Committee Member	Rose Qingyang Hu, Ph.D. Committee Member
Ryan M. Gerdes, Ph.D. Committee Member	Mark R. McLellan, Ph.D. Vice President for Research and Dean of the School of Graduate Studies

UTAH STATE UNIVERSITY
Logan, Utah

2016

ABSTRACT

Interference Mitigation in Multi-hop Wireless Networks with
Advanced Physical-layer Techniques

by

Yantian Hou, Doctor of Philosophy
Utah State University, 2016

Major Professor: Ming Li, Ph.D.
Department: Computer Science

In my dissertation, we focus on the wireless network coexistence problem with advanced physical-layer techniques. For the first part, we study the problem of Wireless Body Area Networks (WBAN)s coexisting with cross-technology interference (CTI). WBANs face the RF cross-technology interference (CTI) from non-protocol-compliant wireless devices. We first experimentally characterize the adverse effect on BAN caused by the CTI sources. Then we formulate a joint routing and power control (JRPC) problem, which aims at minimizing energy consumption while satisfying node reachability and delay constraints. We reformulate our problem into a mixed integer linear programing problem (MILP) and then derive the optimal results. A practical JRPC protocol is then proposed. For the second part, we study the coexistence of heterogeneous multi-hop networks with wireless MIMO. We propose a new paradigm, called cooperative interference mitigation (CIM), which makes it possible for disparate networks to cooperatively mitigate the interference to/from each other to enhance everyone's performance. We establish two tractable models to characterize the CIM behaviors of both networks by using full IC (FIC) and receiver-side IC (RIC) only. We propose two bi-criteria optimization problems aiming at maximizing both networks' throughput, while cooperatively canceling the interference between them based on our two

models. In the third and fourth parts, we study the coexistence problem with MIMO from a different point of view: the incentive of cooperation. We propose a novel two-round game framework, based on which we derive two networks' equilibrium strategies and the corresponding closed-form utilities. We then extend our game-theoretical analysis to a general multi-hop case, specifically the coexistence problem between primary network and multi-hop secondary network in the cognitive radio networks domain. In the final part, we study the benefits brought by reconfigurable antennas (RA). We systematically exploit the pattern diversity and fast reconfigurability of RAs to enhance the throughput of MWNs. We first propose a novel link-layer model that captures the dynamic relations between antenna pattern, link coverage and interference. Based on our model, a throughput optimization framework is proposed by jointly considering pattern selection and link scheduling, which is formulated as a mixed integer non-linear programming problem.

(138 pages)

PUBLIC ABSTRACT

Interference Mitigation in Multi-hop Wireless Networks with
Advanced Physical-layer Techniques
Yantian Hou

With the ever-growing number of wireless systems, the problem of spectrum scarcity is becoming more important than ever. Many devices coexist in the same frequency band, e.g., IEEE 802.11 (WiFi), 802.15.4 (ZigBee), 802.16 (WiMax), and Bluetooth in the ISM bands. Coexisting in the crowded spectrum bands inevitably leads to mutual interferences. For a wireless network, the interference could be from external sources such as microwave oven and cordless phone, or from internal nodes within multi-flow and multi-hop wireless networks. All these interferences can be detrimental to the performance of co-locating networks if they are not properly mitigated. In my dissertation, we try to improve the maximum throughputs of coexisting multi-hop wireless networks by utilizing advanced physical-layer techniques, such as wireless MIMO and reconfigurable antennas (RA). The advance of such new physical-layer techniques provides new optimization freedoms and hasn't been well exploited by previous works.

My first work is about the interference mitigation in wireless body area networks. We propose a joint routing and power control method to select the good-quality links that are not severely affected by the external interference sources. Our scheme could guarantee the quality of service while minimizing the overall energy consumption. My second work is about the cooperative interference mitigation in multi-hop wireless networks, where we utilize the emerging wireless MIMO by cooperatively mitigating internal interferences to enhance the overall network throughputs. In my third and fourth work, I study the coexisting problem using game-theoretical approach. Different from my previous work, we design a game-theoretical framework to capture the competitive and selfish nature of coexisting networks.

My last work is about throughput optimization using reconfigurable antennas, which is another emerging physical-layer technique as wireless MIMO. Our results show that by using reconfigurable antennas, we could improve the overall network throughput as well.

To my family

ACKNOWLEDGMENTS

I would like to express my deep and sincere gratitude to my advisor, Professor Ming Li, for helping me complete this dissertation as well as the research behind it. His strong devotion to work, wide knowledge and strict logic have always been valuable to me. He has always been available for discussion about any academic problems whenever I need to and his very insightful comments and questions make me feel excited about every discussion with him. He always works overnight to review and modify our papers very carefully and this is possible only if he regards my work as his priority. His hard working and great passion for research has set an example that I hope to follow.

I am very thankful to the rest of my dissertation committee: Professor Nicholas Flann, Professor Haitao Wang, Professor Rose Qingyang Hu, and Professor Ryan M. Gerdes, who asked me good questions and gave insightful comments on my work.

I also would like to thank my labmate Boyang Wang, who gave me countless suggestions during my Ph.D. program not only in my research, but also in my life.

I want to thank Dr. Shucheng Yu, Dejun Yang, Kai Zeng for giving me many pieces of advices during my research. I want to thank Hanyu Quan, Shuo Qiu, Min Xian, Jingru Zhang, Shimin Li, Sarbajit Mukherjee, Xu Yuan, Huacheng Zeng, Liang Peng, Qanita Bani Baker, Chong Li, Siyuan Wang, Feifei Li for their all kinds of helps in my life.

Last and most importantly, I am greatly indebted to my parents: Aijun Hou and Yanmei Li, who know nothing about what I do but always unconditionally support anything I am going to do.

I am also greatly indebted to my wife: Min Du, who abandoned her career and move to US as a student, then transferred to Utah to be with me.

I am grateful for the financial support of the National Science Foundation through NSF Grants CNS-1564477, CNS-1218085, and CNS-1619728.

Yantian Hou

CONTENTS

LIST OF TABLES

LIST OF FIGURES

CHAPTER 1

INTRODUCTION

From the local-area networks connecting our laptops and cellphones, to the on-body wireless sensors monitoring our health status [1], wireless networks have been widely used in our daily life. The free transmission of signals on air makes the message sharing among people more convenient. The signals from different networks inevitably cause interference to the coexisting devices. To avoid interference, the most common way is to divide frequencies into multiple bands and each pair of transmitter and receiver within the same spatial space is allocated with a unique band. However, with the ever-growing number of wireless systems, the problem of spectrum scarcity is becoming more important than ever. To utilize the spectrum resources more thoroughly, we need highly efficient spectrum-sharing technologies in wireless networks [2], in which the networks are heterogeneous in hardware capabilities, wireless technologies, or protocol standards, and overlap with each other in the same frequency and space domains. Using wireless body-area networks (WBAN) as example, it is usually deployed in densely populated areas such as hospitals and apartments, where numerous wireless devices coexist, such as cordless phone, baby monitor, microwave, etc. All these devices work in the same industrial, scientific and medical (ISM) band from 2.4GHz to 2.5 GHz. Without carefully dealt with, these devices could severely degrade the WBAN's throughput. In addition, networks with different technologies (e.g., 802.11 and 802.15.4) could interfere with each other [3, 4], causing both networks' throughputs degraded.

Due to the spectrum scarcity problem, we need to utilize the limited frequency resources more wisely. Routing and power control are two commonly used methods, in which we actively select optimal routing path and transmitting power for all links/nodes to mitigate the impact of interference. This method could be effective in such scenarios that channel qualities vary largely, e.g., in the WBAN scenario, some channels are severely affected by

on-body fading, while some others are in good quality due to line-of-sight channels. In addition, some advanced physical-layer techniques such as wireless MIMO and reconfigurable antennas (RA) provide high degree of spatial reusing. By applying these techniques in physical layer, more sophisticated interference mitigation could be achieved to further enhance network throughput. In my dissertation, I will study the joint routing and power control on WBANs to guarantee end-to-end (E2E) reliability. In addition, I will focus on utilizing wireless MIMO and RAs to optimally maximize network throughputs.

1.1 Making Wireless Body Area Networks Robust under Cross-Technology Interference

Wireless Body Area Network is an emerging technology for future healthcare systems. In WBAN, a patient's physiological data are collected by a group of on-body sensors and then transferred through wireless channel to a central controller unit (CU), which could be smartphone or PDA. WBAN is a promising technology that makes remote medical diagnosis more convenient and efficient, which leads to several promising applications such as ubiquitous health monitoring and emergency medical response.

However, the WBAN's transmission reliability is big concern due to the intrinsic open characteristic of wireless channel [5]. Signals transmitted in wireless channel could be easily influenced by noises. WBANs are normally deployed in densely populated areas such as hospitals and apartments, where there could be numerous RF devices generating cross-technology interference (CTI) in the same wireless band. For example, in the widely used ISM band (from 2.4GHz to 2.5GHz), there could be microwave oven, cordless phones, baby monitors, garage doors coexisting in the same spectrum, which makes WBAN in the same band to be easily interfered. Among all the RF sources, the devices such as microwave oven and cordless phone are less friendly due to their *persistent, high-power and broadband* nature. For example, a microwave oven usually occupies at least 25MHz in the 2.4G band. In addition, a cordless phone is usually turned on for conversation for several minutes, which persistently emits electromagnetic signal at a transmission power of 1 Watt (or 30dBm), equivalent to 1,000 times of the power limit of medical devices. All these devices could

damage the data transmissions within WBANs, which has high requirement on E2E link quality. Therefore, a reliable transmission scheme is needed which is robust against powerful external CTI.

To deal with the CTI, one choice is to rely on spectrum licensing. However, the spectrum is becoming increasingly scarcer which makes this harder. The Medical Implant Communications Service (MICS) band spans 402-405 MHz but is dedicated for implanted devices. Although recently, the FCC has allocated additional bandwidth (2360-2400 MHz) for medical BAN services, only those in the 2390-2400 MHz band will be allowed to operate wherever they wish and without coordination of spectrum [6]. As this is adjacent to the ISM band, FCC cautioned that BANs will "need to consider the potential for adverse interaction between their BAN, Wi-Fi and ISM resources" [6]. On the other hand, many existing commercial-off-the-shelf (COTS) medical sensors [5, 7] have adopted one of the wireless technologies under the ISM band. It can be predicted that in the near future many BAN applications will still operate in the ISM band. Also we cannot ignore the interference generated from possible malicious devices, e.g. a wireless jammer, whose goal is to intentionally block the crucial data transmission on a WBAN. Therefore, it is necessary to come up with a solution to make WBAN robust against co-channel CTIs. Our solution is to use joint routing and power control method to select the good-quality links that are not severely affected by CTIs. Meanwhile, we minimize the power level on each node as long as the E2E node reachability requirement is satisfied.

1.2 Cooperative Interference Mitigation for Heterogeneous Multi-hop Wireless MIMO Networks Coexistence

The overlapping of disparate networks in the same spectrum band inevitably leads to CTI. Some examples of existing and future radio devices/networks that create CTI include: IEEE 802.11 (WiFi), 802.15.4 (ZigBee), 802.16 (WiMax), and Bluetooth in the ISM bands, IEEE 802.22 (WRAN) and IEEE 802.11af (WLAN) in the TV white space, etc. The CTI can be detrimental to the performance of co-locating networks if it is not properly mitigated [8, 9]. However, the CTI is harder to handle than *same-technology interference* due to the

differences in physical-layer technology, thus making the communication and coordination among cross-technology devices infeasible. Therefore, it is practically infeasible to use central administration or planning for the coexistence of such networks (unless we use some multi-protocol devices as controller and coordinator, which inevitably exacerbates both hardware and communication overhead). To enable spectrum sharing, current approaches mostly follow the *Interference Avoidance* (IAV) paradigm, where different transmissions are separated in frequency, time, or space domains to avoid collisions, rather than to reduce or eliminate interference.

Recently, interference cancellation (IC) has emerged as a powerful physical-layer approach to mitigate interference [10]. IC is enabled by the use of smart antennas (MIMO), which uses signal processing techniques to minimize or completely cancel the interference from other links. MIMO is gaining popularity in commercial and future systems such as 802.11n, 802.16, and 802.11af. By using IC, we can successfully transmit multiple streams concurrently, as long as the interferences generated are properly canceled at all receivers. Interference alignment (IAL) [11, 12] is a recent advance of IC, which aligns different interferences along the same directions, thus allowing the receiver to cancel all interferences with fewer degree-of-freedom (DoF), By using IAL, the receiver could spend more DoFs on its own transmission, instead of spending on IC. Recent advances in Technology-Independent Multiple-Output (TIMO) [13] even enables the cancellation of the CTI to/from a interferer with a completely different wireless technology. Intuitively, it is possible for two or more multi-hop heterogeneous networks to cooperatively cancel/mitigate the interference to/from each other as long as they (or as long as one of them) are equipped with MIMO, such that everyone's performance can be enhanced simultaneously. We call this the *cooperative cross-technology interference mitigation* (CIM) paradigm.

Previous works have mostly focused on exploiting MIMO IC to enhance throughput within standalone and homogeneous wireless networks [14–17]. However, to date, its potential for interference mitigation across two or more heterogeneous multi-hop networks has not been well understood. There is a lack of study on both the feasibility and theoreti-

cal performance limits of CIM. Recently IC has been adopted to fulfill the "transparent coexistence" or *underlay* paradigm in cognitive radio networks [18], in that the secondary networks should cancel their interferences to/from the primary networks to satisfy FCC policy. However, in this paradigm the responsibility for IC is always assigned to the secondary network, which is only half of the story. This is suitable for a *planned* deployment but not for *unplanned* ones (e.g., networks in the unlicensed bands), where there is no predefined priority among networks, and each network has a competing interest which cannot be solved by single-objective optimization. The work in [19] analyzes the throughput under IAL, and compares it with the one using only traditional IC. However, it also only studied the throughput optimization within a single network without any competing interests. Moreover, interference cancellation among multi-hop networks with *heterogeneous* wireless technologies has not been systematically studied yet.

Our goal is to explore the theoretical performance limit for coexisting heterogeneous multi-hop networks by using CIM paradigm, and compare it with the one by using traditional Interference Avoidance (IAV) paradigm. We consider an unplanned deployment setting, where each network aims at maximizing its own throughput while adopting the CIM paradigm to cooperatively cancel its interference to/from the other. To characterize the performance bounds, the *Pareto-optimal throughput curve* should be found, which is the set of all the points such that both networks cannot simultaneously increase their throughput. The meaning of this Pareto-optimal throughput curve is two-fold: (1) It provides to network designers the quantitative performance-enhancement analysis by using CIM paradigm under arbitrary network settings, such as routing, protocols, and device DoFs. (2) It can guide practical coexisting distributed-algorithm's design, as our Pareto-optimal curve could be used as the theoretical performance bound.

1.3 A Game Theoretical Approach to Coexistence of Heterogeneous MIMO Wireless Networks with Interference Cancellation

With IC and SM, two wireless links can transmit multiple streams concurrently in the same frequency, canceling the interference to and/or from each other. Much work has been

done to increase throughput within standalone or multiple homogeneous/heterogeneous coexisting MIMO networks [14, 15, 17, 20, 21]. A practical MAC protocol (802.11n+) leveraging IC and SM is proposed in [22]. However, these works assume that the coexisting networks are cooperative, i.e., they will unconditionally follow the predefined MAC-layer protocols/rules. On the other hand, several works use game theoretical approaches to study the coexistence in MIMO wireless networks. However, they all assume the coexisting networks to be non-cooperative, so IC is not adopted to cancel the interference to others. Both types of work study the coexistence problem based on a preinstalled assumption of the cooperation incentives.

In this chapter, our goal is to challenge both "Cooperative" and "Non-cooperative" assumptions in previous work, by studying the incentive of each network to comply with/violate the underlying MAC-layer protocol (e.g. 802.11n+) itself. An example is shown in Fig. 4.1. We propose a novel two-round game framework assuming each network is a rational entity. In the second round (lower level), the game refers to the decision making process at the MAC-layer, which includes the DoF allocation for IC and SM. In the first round (upper level), the game refers to a higher-level decision-making function, which takes the second-round game results in as inputs, and determines its best strategy: cooperation or non-cooperation. The first-round strategy imposes restrictions on the second-round strategy by specifying the nature of this round to be cooperative or non-cooperative. Meanwhile, the first-round utilities depend on the second-round utilities. The benefits of modeling it as two-round is that we can clearly analyze the incentives of cooperation for each network.

Based on our framework, we analyze each network's utility and derive the Nash equilibrium via the backward induction approach. For evaluation, we analyze and compare the utilities under equilibrium using different network scenarios and parameters, such as the number of available DoFs and interference ranges. Through numerical results, we found that each network's incentive of cooperation depends on the number of DoFs and the conflict graph. This provides insights and guidance for configuring MIMO wireless networks in a spectrum-resource limited setting.

1.4 Game Theoretical Analysis in MIMO Empowered Multi-hop Cognitive Radio Networks

After introducing our game-theoretical analysis in the single-link wireless network case, we extend it into the general multi-hop case. Specifically, we assume the secondary network possesses multiple flows each with multiple hops. One practical example is the cognitive radio networks, where the single-link primary network needs to coexist with the multi-hop secondary networks.

The biggest challenge of the general multi-hop-case study is the intricacy of link scheduling. In the single-link case, each secondary network only has one link, thus the strategy space is small. In the multi-hop cases, each flow may have multiple links, each having multiple spatial-multiplexing and interference cancellation strategies. These strategies are not independent, i.e., they should be jointly considered to guarantee the solution's feasibility. In order to solve this challenge, we designed an algorithm based on the solution of a mixed-integer-linear-programming problem to derive the optimal link scheduling and DoF allocation. Our algorithm could output the equilibriums of the coexisting game between the primary network and a selfish multi-hop secondary network with MIMO capability. Our simulation results show that we could improve the primary network's utility by extending its interference range, which could consume the secondary network's DoF resources thus turning it into a weaker interference source.

1.5 Throughput Optimization in Multi-hop Wireless Networks with Reconfigurable Antennas

In addition to the wireless MIMO technique, some other techniques such as reconfigurable antennas (RA) [23–26] could also be utilized to enhance multi-hop networks' throughputs. Traditional omni-directional antennas that radiate signals in all directions result in high interference within a multi-hop wireless network (MWN), which prevents spatial reuse and leads to poor capacity scaling laws (especially in dense deployments). Directional antennas (DAs) focus their radiation energy in certain directions, thereby enhancing the antenna gain (and channel quality) while reducing the interference in other directions, which

can potentially improve the performance of a MWN [27–29]. However, legacy DAs have fixed beam directions which cannot be changed on-the-fly, leading to reduced transmission coverage and network connectivity, which may limit the overall throughput gain.

In recent years, RA has emerged as a promising technology to solve the above challenges. By changing its structure electronically, an RA can *swiftly* reconfigure itself in terms of radiation pattern, polarization, and frequency, or combinations of them. There can be a large number of antenna states available; for example, in a type of parasitic-layer based RAs using p-i-n diodes as the switch [30], 10 switches can give $2^{10} = 1024$ different configurations. In addition, the switching between different antenna states can be very fast; for example, within microseconds which is negligible compared with a packet duration [23]. Thus, RAs bring forth two main advantages: antenna state diversity and fast reconfigurability. For pattern-reconfigurable antennas, their radiation patterns are often directional, which means they can cover any direction at a given time by selecting a directional pattern, thus simultaneously maintaining connectivity while reducing the interference. Note that, although smart antennas such as switched/steered beam antennas [31] can also change their radiation patterns, their beam shapes remain the same in each direction and switching is slow (in the order of $100\mu s$ [32]), resulting in very limited pattern diversity. Our goal here is to exploit the antenna reconfigurability and state diversity of RAs to optimize the overall network throughput in multi-hop wireless networks.

1.6 Roadmap

The organization of this dissertation is as follows.

In Chapter 2, we propose the joint routing and power control protocol in WBANs to satisfy E2E-PDR and delay requirement while minimizing energy consumption. In section 2.2, we experimentally study the impact of CTI on WBANs. In section 2.3, we formulate the JRPC problem as a MILP problem. In section 2.4, we propose our joint routing and power control (JRPC) protocol. In section 2.5, we use experiment and simulations to validate the effectiveness of our JRPC protocol. In section 2.6, we conclude this chapter and discuss about the future work.

In Chapter 3, we study the optimal throughput of coexisting-heterogeneous-wireless-MIMO networks. In section 3.2, we give necessary background on MIMO and the motivation. Section 3.3 describes our technology-independent interference cancellation (TIIC) and its feasibility in multi-hop networks. In section 3.4, we present the models of the CIM paradigms and the formulations of our two bi-criteria optimization problems. In section 3.5, we introduce our approach to efficiently derive the optimal-throughput curve by exploiting its stair-shape property. Section 3.6 presents the evaluation results, and section 3.7 concludes this chapter.

In Chapter 4, we propose a game-theoretical framework to study the cooperating incentives of two single-link MIMO wireless networks. Section 4.2 introduces the system model. In section 4.3, we propose the two-round game framework for the coexistence of two single-link MIMO wireless networks. The numerical results are shown in section 4.4. Section 4.5 concludes the chapter.

In Chapter 5, we extend our game-theoretical approach to a more-general multi-hop case. Section 5.2 introduces the system model. In section 5.3, we propose the frameworks for analyzing the coexistence game between the primary network and the multi-hop secondary network. The numerical results are shown in section 5.4. Section 5.5 concludes the chapter.

In Chapter 6, we propose a modeling of RAs in multi-hop wireless networks and study its optimal throughput based on our model. In section 6.2, we illustrate the benefits of reconfigurable antennas in MWNs using three simple examples. In section 6.3, we propose the novel link-layer model for RAs in MWN, based on which we formulate the throughput optimization with reconfigurable antennas (TORA) problem and reformulate it before solving with CPLEX. In section 6.4, we theoretically prove that the reconfigurable antennas can always outperform omni-directional antennas and directional antennas in multi-hop wireless networks under certain conditions. The simulation results are presented in section 6.5, followed by the conclusion in section 6.6.

Chapter 7 presents the conclusion and future research directions of my work.

CHAPTER 2
MAKING WIRELESS BODY AREA NETWORKS ROBUST UNDER CROSS-TECHNOLOGY INTERFERENCE

2.1 Overview

In this chapter, we first study the heterogeneous impact of CTI on WBAN channels. After that we propose and formulate the joint routing and power control problem aiming at minimizing the total energy consumption while guaranteeing the E2E reliability. Then we design a protocol which guarantees the E2E-transmission reliability and delay requirements under the high-power and wide-band CTI. In addition, we reduce total energy consumption as much as possible while satisfying the E2E reliability requirement. The basic idea is to jointly control routing and transmitting power by selecting the good-quality links that are not severely interfered by CTI and lowering the transmitting power level of each node.

2.2 Characterizing the Impact of CTI on a BAN

In this section, we first show through experiments that the high-power and broadband CTIs can severely impact the link quality within a BAN. Then we demonstrate that the interference effect on WBAN is heterogeneous, i.e. the interference power levels detected at nodes are different.

2.2.1 Experimental Setup

In our experiments we use a Sunbeam SGG5702 microwave oven, and a Uniden EXI4560 2.4 Ghz cordless phone as interference sources[1]. Both devices are unfriendly to WBAN as they always generate interference to nearby WBANs when they are working. We use Crossbow Telos RevB sensors with a 802.15.4 compliant transceiver (CC2420) to establish

[1]According to [13], the microwave oven mainly occupies the 2.45 - 2.474 GHz spectrum. The cordless phone in our experiment mainly occupies two 5Mhz channels (2.405-2.415 GHz).

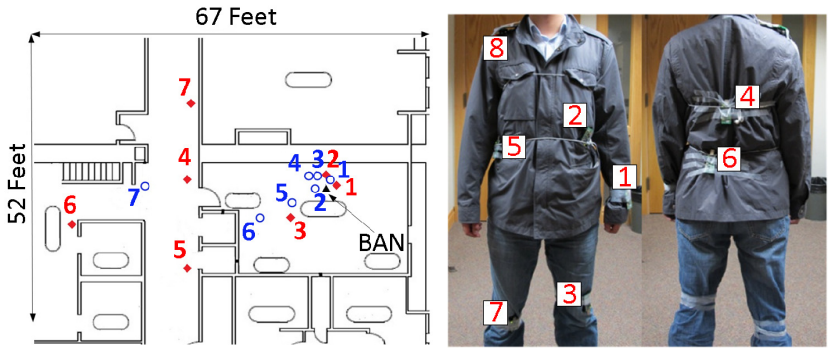

(a) Floor plan and test locations. ♦ - cordless phone, ◯ - microwave oven. (b) Sensor placement on the body.

Fig. 2.1. WBAN experiment setup

the BAN. The power range is from $-24dbm$ to $0dbm$. We fixed the nodes' channel at Channel 11[2], which overlaps with that of the cordless phone. The transmission rate is set to 250kbps. The locations of the WBAN and interference sources are illustrated in Fig. 2.1(a). For the cordless phone, the handset and base are placed very close (5 cm apart from each other).

For sensor placement (Fig. 2.1(b)), we put 8 sensor nodes at different places on a human body. Five of them are placed on the front side of body, and two nodes are placed on the back side. Another node is strapped to the left wrist to emulate the CU. In the first experiment, we measure the received interference signal strengths at all nodes. In the second experiment, we measure the packet delivery ratio (PDR) of each link to show the interference's impact on BAN. When experiments start, each node will broadcast a group of 20 probe packets to all the other nodes in turn, using the lowest power level (-25dBm).

2.2.2 Impact of Cross-Technology Interference on BAN

We first show the RSS of interference at one node. We measured the interference generated from cordless phone and microwave oven respectively. As is shown in Fig. 2.2(a), the RSS from both CTI sources are much stronger compared with background noise (around -93 dBm). For the cordless phone, the signal strength is about -55 dBm and remains

[2]This is because we assume that in reality the spectrum is crowded. All other channels may be simultaneously occupied by multiple CTI sources or other WBAN devices

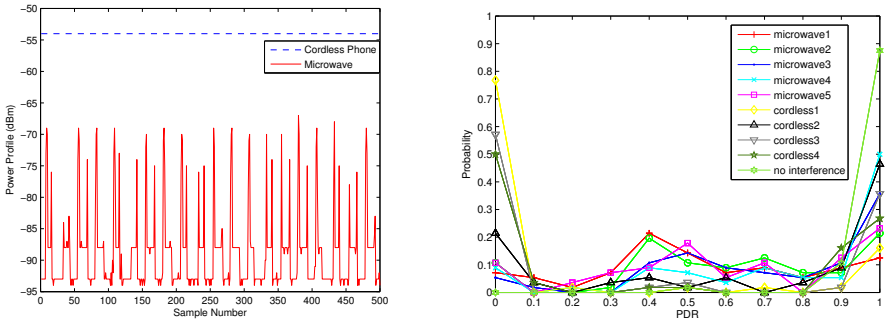

(a) Microwave and cordless phone interference power levels received by one sensor node on body (sample interval is 0.5ms)

(b) PDR distribution of all BAN links under various scenarios

Fig. 2.2. Cross-technology interference (CTI)

constant. For the microwave oven, its power level appears a periodical "ON" and "OFF" pattern over time, which has a roughly 10ms period.

Next we show the impact of CTI on all the 28 links of the BAN. In Fig. 2.2(b), we plot the cumulative distribution function of PDR for each scenario with different interference sources and locations as shown in Fig. 2.1(a). From this figure, we can find that the BAN links are affected by CTIs differently in terms of packet delivering ratio in all scenarios. For example, nearly 90 percent of links' PDRs are nearly 1 when no interference is presented. However, for the 'cordless1' scenario where the distance of interference source is only less than 1 meter, we find that nearly 80 percent of links' PDRs are nearly 0. This phenomenon indicates that the high-power and wide-band cross-technology interference can have severe impacts on BAN's reliability. In addition, there is a correlation between the distance from the BAN to the CTI source and the links' PDR - the nearer the CTI source, the PDRs tend to be smaller.

2.2.3 Making Use of Heterogeneous Link Qualities

We can also see from Fig. 2.2(b) that in each scenario, the links' PDRs have a heterogeneous distribution. This implies that good-quality and bad-quality links simultaneously exist in a BAN under interference. However, a closer look at the 'cordless4' scenario reveals

that many direct links from sensor nodes to CU are severely affected by interference. The interference causes three links' PDRs to drop dramatically to 0 - links $3 \rightarrow 1$, $5 \rightarrow 1$ and $8 \rightarrow 1$. This is due to the larger body shadowing and longer distance of those direct links, which causes a packet's RSS to fall below that of the interference's. On the opposite, some other on-body links have better qualities due to their smaller path losses (nodes can be closer to each other and in line-of-sight). Basically, according to the PDR-SNR relation of sensor devices [33], a packet's RSS needs to overpower that of interference's to make the packet delivered.

In order to enhance WBAN's reliability, one straightforward method is to increase the transmission power of nodes' direct links to CU. However, there are two issues with this approach: (1) Even when those direct links use the maximum possible power (0dBm), there still exists a significant region where BAN communication is disrupted, as we will show in Sec. 2.5. This is mainly due to the very high-power nature of interference. (2) It may not be the most energy-efficient way. Thus, to enlarge the '*reliability zone*' of a BAN under interference and minimize energy consumption, we are motivated to simultaneously exploit the remaining good-quality on-body links (for multi-hop transmission) and power control. In the same scenario (Table 1), the PDR from node 3 to node 1 is 0, the PDR from node 3 to node 6 (= 1) and the PDR from node 6 to node 1 (= 1) are still high. Suppose node 3 needs to use 0dBm (assume node power: 20mW) to achieve a PDR of 1 while -25dBm requires 8mW. Therefore, we can find a path $3 \rightarrow 6 \rightarrow 1$ with high E2E PDR (= 1) with power consumption of $8 + 8 = 16mW$ to transmit a packet for node 3 to 1. In contrast, if we use $3 \rightarrow 1$, this will be $20mW$.

2.3 Problem Formulation

In this section, we first present the models and assumptions, and then formulate the JRPC problem. After that we introduce the main challenges in our problem.

Table 2.1. Example PDR in scenario cordless4

from	node 1	node 2	node 3	node 4	node 5	node 6	node 7	node 8
to node 1	/	1	0	0.9	0	1	1	0
to node 6	0.95	5	1	1	0	/	1	1

2.3.1 Models and Assumptions

Network and Traffic Model

As what we study in this chapter is the data collection in a BAN, thus we use a convergecast model, where each on-body sensor generates a data packet to the CU periodically at constant rate R_s (packets/second). We model the BAN topology as a directed graph $G(V, E)$ and $N =\mid V \mid$, where V is the set of all nodes and E is the set of all links. For each link (i, j) we use $\lambda_{i,j}$ to denote its PDR, which is the probability that a packet sent by i can be directly received by j. Meanwhile, for each node i, we use λ_i to denote the probability that a packet sent by i can be received by the CU (possibly through multi-hop), which is called E2E PDR.

At the link layer, we turned off the CSMA mechanism and adopted a TDMA MAC mechanism which yields bounded delay. For periodical data collection applications, it has been shown that TDMA is better [34]. Time is divided into slots with equal length T - the time needed to transmit one data packet. A "source cycle" $T_S = \frac{1}{R_s \cdot T}$ refers to the number of slots between two consecutive packet generation events. We use "data cycle" $T_D = \sum_i \tau_i$ to represent the number of slots needed to transmit all source packets in one source cycle to the CU, and packet retransmission is not considered. Note that, at each time slot, only one link can transmit to avoid packet collision, because all nodes are considered to be within one conflict graph. Obviously, $T_D \leq T_S$ is necessary to avoid any source congestion.

Interference Model

It is difficult to model the CTI exactly, as in practice the number and types of them are uncertain. Instead, we will model the impact of the CTI on link quality later, by only

Table 2.2. Notations

$\lambda_{i,j}$	link PDR from node i to j
λ_i	node E2E PDR from node i to CU
T_s	length of a source cycle in terms of number of slots, time delay threshold
T_d	length of a data cycle in terms of number of slots
T_{big}	length of a big slot, containing multiple source cycles
T	length of unit slot, used to transmit one data packet
Λ_{th}	node E2E-PDR requirement
τ_i	number of slots T needed to transmit one packet from node i to CU
l_i	transmitting power level at node i
$p_{tx}()$	mapping from power level to transmitting power
$\mathcal{I}_{ij}$	CTI on link (i,j)
$g_{i,j,\mathcal{I}_{ij}}()$	mapping from power level to link PDR, under CTI on link (i,j)
$z_{i,j}$	link (i,j) 's selection status
$P_{tx,k}$	transmitting power at level k
$G_{i,j,k,\mathcal{I}_{ij}}$	link (i,j)'s PDR at level k, under CTI on link (i,j)
α_{ji}, β_{jki}, δ_{ji}	intermediate variables in linear reformulation

assuming that within a time period T_{big} the RSS of the aggregated CTI $\mathcal{I}$ sensed by a node could be denoted as a stationary random process. Though we focus on non-protocol-compliant CTI, this model is applicable to general interference.

Energy Model

We consider each sensor node to have K different transmit power levels $\{P_1, P_2, ..., P_K\}$ (for a TelosB sensor $K = 8$). We denote the transmit power level on each node as l_i. Assuming the circuit power P_{cir} is a constant, then we can obtain the power consumed by the transmitter/receiver on each node:

$$p_{tx}(l_i) = P_{cir} + p_A(l_i) \tag{2.1}$$

$$P_{rx} = P_{cir} \tag{2.2}$$

where $p_A(l_i)$ is the additional circuit power for l_i. Note that this model has also been adopted by previous work [35].

2.3.2 Design Objectives

To deal with cross-technology interference in BAN, we aim at ensuring a certain reliability requirement for each sensor node communicating with the CU, while using a minimum overall energy consumption.

(1) *Energy consumption minimization*: The overall energy consumption accounts for the transmission and reception of all the packets by all nodes. It is proportional to that in one source cycle length, as a feasible source rate requires that $T_D = \sum_i \tau_i \leq T_S$.

(2) *Reliability requirement*: For each node i in a BAN, we require its E2E PDR to the CU λ_i should be above a predefined threshold $\Lambda_{th} \in [0, 1]$. The PDR constraint can ensure that all packets are received successfully with a high-enough probability to perform error correction coding if necessary.

(3) *Time delay constraint*: We aim at confining E2E delay which is an important concern in many BAN applications. In our convergecast model, decreasing the time delay could further enhance E2E data throughput. Note that to satisfy the delay constraint, the retransmission is disabled. However, we can rely on the error-correction coding to guarantee all packets are successfully received.

Given the objectives mentioned above, we formulate our problem aiming at minimizing energy consumption while satisfying the reliability and time-delay constraints.

2.3.3 Formulation of Joint Routing and Power Control

The formulation of our JRPC problem is shown in Fig. 2.3, Eqs. (2.3) - (2.10). The variables are l_i, τ_i, λ_i, $\lambda_{i,j}$, $z_{i,j}$, in which l_i and $z_{i,j}$ are binary variables, λ_i, $\lambda_{i,j}$ are continuous within range $[0, 1]$, and τ_i is integer within $[0, N]$. Here N is the total number of nodes. Our goal is to find a convergecast routing tree $G' = (V, E')$, and link power level l_i assignments satisfying the constraints. Eq.(2.3) is the overall energy consumption in one source cycle. Eq.(2.4) is the E2E PDR constraint, where λ_i is node i's E2E reachability to the gateway node. In Eq.(2.5), $g_{i,j,\mathcal{I}_{ij}}()$ is the mapping function from the transmit power level to link PDR for each link, under the external CTI. This will be derived at the beginning of each big slot by our link PDR estimation algorithm. How to derive this function $g_{i,j,\mathcal{I}_{ij}}()$ in practice

$$\text{minimize} \quad \sum_i ((p_{tx}(l_i) \cdot \tau_i + P_{rx} \cdot (\tau_i - 1)) \tag{2.3}$$

$$\text{subject to} \quad \lambda_i \geqslant \Lambda_{th} \tag{2.4}$$

$$\lambda_{i,j} = g_{i,j,\mathcal{I}_{ij}}(l_i), \forall (i,j) \in E \tag{2.5}$$

$$\lambda_i = \sum_j \lambda_{i,j} \cdot z_{i,j} \cdot \lambda_j, \forall i \neq 0 \tag{2.6}$$

$$\sum_j z_{i,j} = 1, \forall i \neq 0 \tag{2.7}$$

$$\tau_i = (\sum_j \tau_j \cdot z_{j,i}) + 1, \forall i \tag{2.8}$$

$$\sum_i \tau_i \leqslant T_s \tag{2.9}$$

$$\lambda_1 = 1 \tag{2.10}$$

Fig. 2.3. The MINLP formulation of JRPC

is a challenge and will be introduced in detail in the next section. Eq.(2.6) is the definition of λ_i in induction form. Eq.(2.7) is each node's output degree constraint which means that each node only has one parent node; Constraint (2.7) and (2.8) together guarantee that our routing is a convergecast tree. Eq.(2.9) is the node delay constraint, which is equivalent to the flow-balance constraint. τ_i denotes the time delay brought by node i.

The objective function (2.3) and constraints (2.5), (2.6), (2.8) are all non-linear ($g_{i,j,\mathcal{I}_{ij}}()$, $p_{tx}()$ are non-linear functions of l_i [36]). Therefore, our problem is a *mixed integer non-linear programming* (MINLP) problem, which is known as NP-hard in general.

2.3.4 Problem Reformulation

To efficiently solve our JRPC problem, we reformulate it into a linear one. First we remove the non-linear function $g_{i,j,\mathcal{I}_{ij}}()$ and $p_{tx}()$ by discretizing them at each power level. Then we use Reformulation-Linearization Technique (RLT) [37–39] to transform the non-linear product into linear term.

Specifically, for the non-linear function $p_{tx}(l_i)$ in Eq.(2.3), as the valid values for l_i are discrete within the range $[1, K]$, we transform the function into an equivalent linear form:

$$p_{tx}(l_i) = \sum_k P_{tx,k} \cdot l_{i,k} \tag{2.11}$$

$$\sum_{k} l_{i,k} = 1, \forall i/1 \tag{2.12}$$

In Eq.(2.11), $l_{i,k}$ is a binary variable which denotes whether the power level k is selected at node i. Eq.(2.12) means only one power level could be used for each node i. $P_{tx,k}$ is a parameter which denotes the transmitting power at level k. The discrete variable l_i is transformed into binary variable $l_{i,k}$. By removing the non-linear function $p_{tx}(l_i)$, the objective function is transformed into:

$$\sum_{i}((\sum_{k} P_{tx,k} \cdot l_{i,k}) \cdot \tau_i + P_{rx} \cdot (\tau_i - 1)) \tag{2.13}$$

A similar process could be applied on constraint (2.5) to remove non-linear function $g_{i,j,\mathcal{I}_{ij}}(l_i)$. Thus constraint (2.5) is transformed into:

$$\lambda_{i,j} = \sum_{k} G_{i,j,k,\mathcal{I}_{ij}} \cdot l_{i,k}, \forall (i,j) \in E \tag{2.14}$$

Next we use RLT to remove the non-linear terms by introducing new variables. In objective function, we define new variable $\theta_{ik} = \tau_i \cdot l_{ik}$. Thus our objective function becomes:

$$\sum_{i}((\sum_{k} P_{tx,k} \cdot \theta_{ik}) + P_{rx} \cdot (\tau_i - 1)) \tag{2.15}$$

The objective function in (2.15) is now linear. By introducing new variable θ_{ik}, a cluster of several new constraints is needed:

$$\theta_{ik} \geqslant 0; \quad N \cdot l_{ik} - \theta_{ik} \geqslant 0; \quad \tau_i - \theta_{ik} \geqslant 0; \quad N - \tau_i - N \cdot l_{ik} + \theta_{ik} \geqslant 0 \tag{2.16}$$

For the constraints, we remove constraint (2.5) by taking it into constraint (2.6) and then we use similar technique by introducing new variables. We first set $\alpha_{ji} = \lambda_i \cdot z_{ji}$ and then set $\beta_{jki} = \alpha_{ji} \cdot l_{jk}$. For constraint (2.8), we set $\delta_{ji} = \tau_j \cdot z_{ji}$. Therefore, constraints

(2.6) and (2.8) become:

$$\lambda_i = \sum_j \sum_k G_{i,j,k,\mathcal{I}_{ij}} \cdot \beta_{i,k,j} \tag{2.17}$$

$$\tau_i = (\sum_j \delta_{ji}) + 1 \tag{2.18}$$

Again, several new constraints are introduced along with the new variables:

$$\alpha_{ji} \geqslant 0; \quad z_{ji} - \alpha_{ji} \geqslant 0; \quad \lambda_i - \alpha_{ji} \geqslant 0; \quad 1 - \lambda_i - z_{ji} + \alpha_{ji} \geqslant 0 \tag{2.19}$$

$$\beta_{jki} \geqslant 0; \quad l_{jk} - \beta_{jki} \geqslant 0; \quad \alpha_{ji} - \beta_{jki} \geqslant 0; \quad 1 - \alpha_{ji} - l_{jk} + \beta_{jki} \geqslant 0 \tag{2.20}$$

$$\delta_{ji} \geqslant 0; \quad \tau_j - \delta_{ji} \geqslant 0; \quad N \cdot z_{ji} - \delta_{ji} \geqslant 0; \quad N - N \cdot z_{ji} - \tau_j + \delta_{ji} \geqslant 0 \tag{2.21}$$

minimize	Overall energy consumption per round(2.15)	(2.22)
subject to	Node reacheability threshold constraint(2.4)	(2.23)
	Node reachability definition(2.17)	(2.24)
	Node output degree(2.7)	(2.25)
	Power level selection(2.12)	(2.26)
	Node delay definition(2.18)	(2.27)
	Overall delay(2.9)	(2.28)
	New variable constraints(2.16), (2.19), (2.20), (2.21)	(2.29)
	Gateway node reachability(2.10)	(2.30)

Fig. 2.4. The MILP formulation of JRPC

2.3.5 Optimization Problem Complexity Analysis

By applying these reformulation techniques, our JRPC problem is reformulated into a mixed integer linear programing (MILP) problem. MILP problem is NP-hard in general. We will show that by choosing the parameters, a special case of our problem is a non-linear Knapsack problem, which is the general form of the famous NP-complete Knapsack problem.

Assuming for all of the N nodes, only these links have non-zero PDR: $(N-1, N-2)$, $(N-2, N-3)$, ... $(1, 0)$. Therefore, the routing is fixed, which is a (N-1)-hop path from node $N-1$ to node 0. In addition, assume the delay constraint is loose thus it is always satisfied. Now our original problem is simplified as: selecting power level for each node, such that the overall power is minimum, while satisfying $\lambda_{(N-1,N-2)} \cdot \lambda_{(N-2,N-3)} \cdot .... \cdot \lambda_{(2,1)} \geqslant \lambda_{th}$. In addition, assuming for each power level l_i, we have $p_i = l_i$ and $\lambda_{i,i-1} = A_i \cdot l_i$ where A_i is the a fixed coefficient. This problem is formulated in Fig. 2.5.

$$\text{minimize} \quad \sum_{i=1}^{N-1} p_i \cdot (N-i) \tag{2.31}$$

$$\text{subject to} \quad \prod_{i=1}^{N-1} \lambda_{i,i-1} \geqslant \lambda_{th} \tag{2.32}$$

Fig. 2.5. The special-case problem formulation.

By assuming $p_i = l_i$, $\lambda_{i,i-1} = A_i \cdot l_i$ and taking the logarithm on Eq. 2.32, we can rewrite the formulation of the problem in Fig. 2.5 in another form, which is shown in Fig. 2.6:

$$\text{minimize} \quad \sum_{i=1}^{N-1} l_i \cdot (N-i) \tag{2.33}$$

$$\text{subject to} \quad \sum_{i=1}^{N-1} log(l_i) \geqslant log(\lambda_{th}) - \sum_{i=1}^{N-1} log(A_i) \tag{2.34}$$

Fig. 2.6. The transformed-special-case problem formulation.

The problem shown in Fig.2.6 is a non-linear Knapsack problem, a general form of the famous Knapsack problem that has been proven as a NP-complete problem. Through the complexity analysis of this special-case problem, we can conclude that it is hard to find a solution of our general-form JRPC problem in polynomial time.

However, there exists tools such as IBM's CPLEX, which could efficiently solve our problem using Branch and Bound approach. In our case where the network's size is small ($N = 8$), the running time of our problem is only about $1 - 2$ seconds in average. The optimal solutions could be used as comparison to accurately evaluate the effectiveness of our low-complexity heuristic algorithm, which will be introduced in the next section.

2.3.6 Practical Challenges

There are two main practical challenges remaining. First, how to obtain the power-PDR mapping function $g_{i,j,\mathcal{I}_{ij}}()$ (or its equivalent linear form $G_{i,j,k,\mathcal{I}_{ij}}$)? To do this we need to know each link's signal-to-interference-plus-noise ratio (SINR) under all transmitting powers. However, it is inaccurate to apply channel propagation models to estimate the received packet RSS due to the channel dynamics and CTI. Link PDRs are traditionally estimated by actively sending probe packets [40–42]. However, it is impossible to send probe packets using every power level as it brings large time overhead.

Second, though we could obtain optimal solutions by using tools such as CPLEX, it is too computationally demanding. Due to the restricting nature of power and processing ability on sensors, we need a low-complexity algorithm to solve our JRPC problem, as the commercial tools such as CPLEX are not scalable due to their intrinsic complexity.

2.4 Our Solution: the JRPC Protocol

In this section, we introduce our practical JRPC protocol. Our protocol addresses the two practical challenges successfully. We first present our link-PDR estimation and prediction approach which could obtain the power-PDR mapping function $g_{i,j,\mathcal{I}_{ij}}()$. Second we introduce our low-complexity heuristic algorithm to solve the JRPC problem, along with its complexity analysis.

2.4.1 Protocol Overview

To tackle the first challenge, we exploit SINR estimation to derive the links' PDRs under all power levels, which is taken as input to our optimization problem. To solve the second one, we propose an effective and efficient heuristic algorithm (JRPC).

Our protocol consists of two phases. Time is divided into big slots of duration T_{big} consisting of multiple source cycles T_S. First, at the end of each big slot, every BAN node passively calculates its incoming links' PDRs ($\lambda_{i,j}$) in the current big slot based on the received data packets and sensed interference signals, which are measured during gaps of data-packets transmissions. Specifically, each node estimates the mappings $g_{i,j,\mathcal{I}_{ij}}()$ from l_i to $\lambda_{i,j}$ at all transmit power levels $k \in [1, ..., K]$. After estimation, the mapping information is sent to the CU, who predicts the links' PDRs $\lambda_{i,j}$ for the next big slot under all power levels.

In the second phase, using the predicted $g_{i,j,\mathcal{I}_{ij}}$ for the next big slot as input, the JRPC algorithm is ran at the CU to establish the routing tree and assign each node its new power level and route to minimize the power consumption while guaranteeing the node reachability and delay constraint. Our heuristic JRPC algorithm has performance guarantee in terms of E2E reachability. The rationale of our JRPC algorithm is to first guarantee the E2E PDR by establishing a max E2E-PDR tree. We use a variant of Dijkstra's algorithm to build a maximum E2E-PDR tree to maximize the reachability of the BAN in the presence of external CTI. In this way, our algorithm can always guarantee the E2E PDR requirement whenever the optimal solution does. Second, we decrease the transmitting power levels of all the nodes as much as possible while satisfying the E2E PDR constraints. In addition, the lower-level nodes are lifted to upper levels while satisfying the E2E-PDR constraint to decrease time delay in case the delay constraint is not satisfied. The derived route and power level for each node is then distributed to all nodes by sending a notification packet.

To evaluate the effectiveness of JRPC algorithm, we will compare it with the optimal solution derived by CPLEX in Sec. 2.5, which is also assumed to be running at the CU. The protocol framework is illustrated in Fig.2.7.

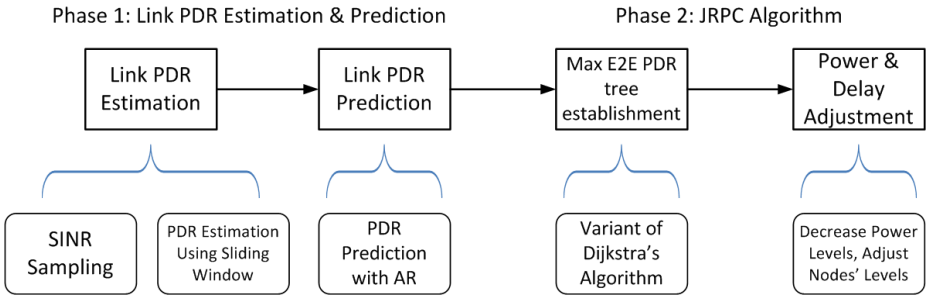

Fig. 2.7. The framework of JRPC protocol

2.4.2 Link PDR Estimation and Prediction under CTI

To assure the reliability under external CTI in our optimization framework, a key issue is to accurately estimate the links' qualities with minimum overhead. The essential question is: for every link (i, j), which transmission power level yields the desired PDR? Previous link power control approaches [43] did not consider CTI, which makes it easier to determine the desired transmit power as the interference is mainly generated from background, which is stable. However, external CTIs' types are usually unknown to BANs and their influence on links' PDR are very different. New modeling techniques must be developed to deal with different CTIs. Thus our solution estimates the dynamic relation between link PDR and transmitting power *on the fly*. First, at the end of each big slot, each node will estimate the PDR of all incoming links under all power levels based on passive measurements of data packets and CTI. Second, we will exploit prediction to estimate the mapping from transmitting power to link PDR for the next big slot, based on previous records.

Estimating Link PDR-Transmit Power Relation

As we know, the probability of successful packet reception is a function of that packet's SINR (signal-to-interference-and-noise-ratio). However, under CTI, the SINR is dynamic (due to the uncertainty of CTI sources and the channel fading). Thus, link PDR estimation boils down to computing the packet's SINR distribution, and mapping that to a PDR.

First, we determine the relationship of packet receiving probability (PRP) w.r.t. SINR: $PRP(\gamma_{i,j})$ where $\gamma_{i,j}$ is the SINR. For sensors, the transition interval from 0 PRP to 1 is

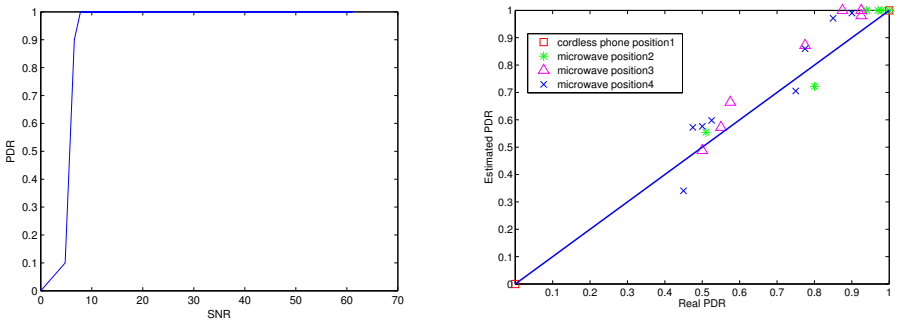

(a) The measured PDR-SINR relation for sensors.

(b) Accuracy of link PDR estimation under various power levels.

Fig. 2.8. Link PDR estimation under CTI.

usually small, which is close to a step function [33]. Our experiments also verify this result (Fig. 2.8(a)). Theoretically, under interference signal $\mathcal{I}$ and a fixed transmit power, the link PDR is a mean value:

$$\lambda_{i,j} = \int_{-\infty}^{\infty} PRP(\gamma_{i,j}) h(\gamma_{i,j}) \mathrm{d}\gamma_{i,j}, \tag{2.35}$$

where $h(\gamma_{i,j})$ is the probability density of $\gamma_{i,j}$. The difficulty here is how to accurately compute $\lambda_{i,j}$ efficiently in reality because it is non-trivial to derive $h(\gamma_{i,j})$. Thus we approximate $\lambda_{i,j}$ by exploiting the property of stationary random process - the ensemble mean equals the temporal mean. The basic idea is using a sliding window and deriving PRP using the minimum SINR within the window, which is illustrated in Fig. 2.9. Assuming the beginning of a packet distributes randomly over time and the packet RSS $RSS_{pkt,k}$ remains constant, based on a sequence of M consecutive interference RSS samples, we obtain an estimation of PDR when transmit power is P_k:

$$\lambda_{i,j,k} = \frac{1}{M} \sum_{m=1}^{M} PRP(\gamma_{i,j,k}(m)), \tag{2.36}$$

where $\gamma_{i,j,k}(m) = \min\{RSS_{pkt,k} - RSS_{\mathcal{I}(m)}, \cdots, RSS_{pkt,k} - RSS_{\mathcal{I}(m+\Delta)}\}$. This is because that one packet transmission duration spans several (Δ) interference RSS samples, while

whenever one part of the packet is corrupted the whole packet cannot be received correctly (error correction code is not implemented in 802.15.4). As the channel fading is usually not significant in a big slot, we set $RSS_{pkt,k}$ as the average packet RSS to average out the effect of fading. In addition, since the wireless channel can be regarded as a linear system, for any transmit power level P_k (dBm) we have:

$$RSS_{pkt,k} = RSS_{pkt,measure} + P_k - P_{measure}, \tag{2.37}$$

where $P_{measure}$ is the transmitting power chosen for link measurement at any specific big slot. Combining the above, we can derive the mapping $g_{i,j,\mathcal{I}_{ij}} : l_i \rightarrow \lambda_{i,j}$ for all power levels k using passive measurements under only one power level.

We design an experiment to validate the effectiveness of our link PDR estimation approach. We place two nodes on different locations of the body, and let one of them transmit 40 probe packets to the other for 8 rounds, each round using a different power (from -25dBm to 0dBm). We record the actual PDRs in each round, and the average packet's and interference samples' RSSes only in the first round (using minimum power -25dBm). Then we run the estimation approach to compare the estimated PDRs with real ones for the other 7 rounds. We use $\Delta = 8$ for a 1.6ms long packet, since the interference sample interval is $0.2ms$; We choose $M = 100$ which is large enough to characterize CTI. Results are shown in Fig. 2.8(b). It can be seen that the estimated and real PDR match very well.

Link Parameter Collection and Synchronization

After estimating link PDRs at all power levels through link measurement, each node then sends the estimated link-PDR list to the CU, which runs our JRPC algorithm to make centralized decision. In the protocol bootstrapping, the link-PDR lists are sent by each node using maximum transmitting power and broadcasting. Each broadcasting packet is relayed by all other nodes before an ACK packet from CU is received. After bootstrapping, each node sends the link-PDR list using normal data packets within one TDMA cycle at

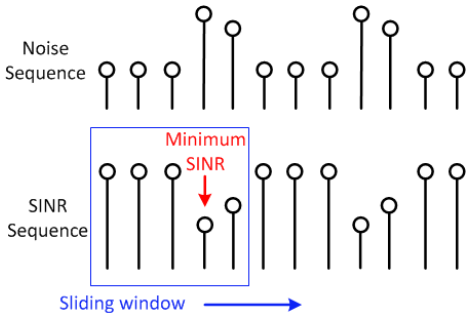

Fig. 2.9. Estimate link PDR by using a sliding window

the end of each big slot. As our JRPC protocol runs in a TDMA manner, at the beginning of each big slot, all nodes are synchronized by the notifying packet from CU and then send data packets to the CU in order. Though our network is multi-hop, the synchronization is precise: given the 40-ppm clock requirement of Zigbee, the accumulated error is less than $48\mu s$ for a $1.2s$ big slot (as shown in Sec. 2.5), which is negligible compared to each of the 2ms-long packet.

Predicting links' PDRs under Various Power Levels

For each of the past T_{big} period, each node j obtains a list of PDR estimations under all power levels: $\{\lambda_{i,j,k}\}_{i\neq j,1\leq k\leq K}$ and sends to the CU. Based on these historical data, the CU can predict the link quality under every power level for the next big slot using **autoregression** (AR). The AR model is a tool for predicting a time series of data [44]. Formally $AR(p)$ is defined as: $z_l = c + \sum_{i=1}^{p} \phi_i z_{l-i} + \epsilon_l$, where c is a constant, p is order, ϕ_i is AR coefficient, and ϵ_l the zero-mean Gaussian white noise error. This model can be updated continuously to adaptively enhance predicting accuracy. A concrete model can be found in [45, 46]. Intuitively, the AR exploits the correlation inside the time series.

2.4.3 Algorithm Design

In our JRPC problem, our goal is to minimize the power consumption. To solve this problem, we first show that when the links' PDRs are binary variables, we can find a simple polynomial-time algorithm. Then we explore the general case in which the links' PDRs are

Algorithm 1 Building maximum E2E PDR tree

input: graph $G(V, E)$, links' PDRs $\{\lambda_{i,j,K}\}_{(i,j)\in E}$
output: maximum E2E-PDR tree T_{tree}

1: Insert CU node 1 into tree T_{tree}; $\lambda_1 \leftarrow 1$.
2: Put all other nodes into set S
3: **while** $S \neq \emptyset$ **do**
Select the node d with maximum λ_d from T_{tree}.
4: **if** there are ties among any set of nodes **then**
5: Select the node that brings the minimum ΔE.
6: **end if**
Insert d into T_{tree}, delete d from S. Update $\lambda_j \leftarrow max_{\forall i \in T_{tree}}\{\lambda_i \cdot \lambda_{j,i,K}\}$ for all $j \notin T_{tree}$.
7: **end while**

continuous and then propose an effective heuristic algorithm.

Binary Link-PDR Model

When dealing with some stable CTI, i.e., the interference signal's RSSI does not change frequently, the detected PDRs under such CTI are normally either 1 or 0. This is because of the step-shape PRP-SINR function as shown in Fig. 2.8(a).

In this case, due to the monotonicity of the function between link PDR and power level, we can find the minimum power $p_{i,j,k_{min}} = p_{tx}(l_{i,j,k_{min}}) + P_{rx}$ of each link that guarantees $\lambda_{i,j} = 1$, where $l_{i,j,k_{min}}$ denotes the minimum power level on link (i, j) that guarantees $\lambda_{i,j} = 1$. If we set $p_{i,j,k_{min}}$ as the weight of each link, the Dijkstra's algorithm can be adopted directly to find the "shortest" path from each source node to the sink. The path's 'distance' denotes the energy consumed per time unit for each source node. The minimum-overall energy consumption (Eq. (2.3)) could be easily derived by adding the 'distances' for all source nodes and then multiplying the length of each time slot.

Continuous Link-PDR Model

In the general case where the links' PDRs are continuous, our proposed JRPC algorithm consists of two steps.

Step 1 Our primary goal is to ensure BAN's reliability under the presence of interference. Therefore, we first build a maximum reliability tree to guarantee that we can always find a feasible solution of our JRPC problem whenever it exists. The idea is to first set the

power level for each node to be maximum, because the E2E PDR for each node is a non-decreasing function of any link's transmitting power. Then we use a variant of Dijkstra's algorithm, in which we use each link's PDR as its weight. And we search the 'max-E2E PDR', which has similar deriving logic as that of 'shortest path'. Specifically, in each step of the algorithm, we always insert the node i which yields the maximum E2E PDR λ_i into the tree. To resolve ties, we insert the node which brings the minimum additional energy consumption (ΔE, which equals the tx/rx power sum of all the links from it to the root) to the existing tree. By doing so, in the resulting tree every node's E2E PDR achieves its maximum. The algorithm is described in Alg. 1.

Step 2 In this step we decrease the transmitting power level of each node and the overall time delay based on the derived max-E2E PDR tree. Our objective is to minimize the overall energy consumption and decrease delay while satisfying the E2E PDR requirement $\lambda_i \geq \Lambda_{th}$ for all nodes. The essential question is: which order should we follow to decrease nodes' transmit powers?

We propose a greedy strategy, in which the transmitting powers of the nodes at higher levels of the tree are decreased first. The intuition is, the higher a node's level is, the more transmitting opportunity (traffic load) it has, thus decreasing its power level first is more effective for the overall energy reduction. E.g., assuming node a has M child nodes, it thus needs to transmit $M + 1$ (including its own) sets of data to its parent node in each round while the parent node needs to send $M + 2$ sets of data at least in the same round. This is the intrinsic property of the convergecast tree: the higher level nodes always have higher workloads thus these nodes run out of energy faster in practice. Care should be taken as changing one node i's transmitting power may affect all the nodes lower than i in the tree. Thus, for each node i from top to the bottom level (except the CU), we continue to decrease its transmitting power level until for any node j in i's subtree, we have $\lambda_j < \Lambda_{th}$ (including i itself). This algorithm is depicted in Alg. 2. In addition, we also decrease the overall time delay by moving low-level nodes to upper levels if the time-delay constraint is not satisfied. This is because the higher a node's level is, the fewer intermediate relaying nodes

are needed, thus less slots are consumed.

2.4.4 Protocol Summary

In each big slot, every on-body node j first measures and records the RSSes of the received *data packets* from each node $i \neq j$ sent using a power level $k_{measure}$ derived from previous big slot. After all nodes finish transmitting, each node will record M consecutive samples of the CTI's RSS. Then each j will estimate $\lambda_{i,j,k}, \forall i \neq j$ under all power levels $l_i \neq k_{measure}$ using Eqs. (2.36) and (2.37): $\{\lambda_{i,j,k}\}_{k\in[1,\ldots,K]}, \forall i \neq j$. Next, each node sends the list of $\lambda_{i,j,k}$ to the CU at the end of the current big slot using the current power and routing scheme. Based on the historical data, the CU first predicts the links' PDRs for the next big slot $\{\widehat{\lambda}_{i,j,k}\}_{k\in[1,\ldots,K]}, \forall i \neq j$, runs our JRPC algorithm using these as input, and then broadcasts the new power and routing scheme to all nodes: $\{i, l_i, n_i\}_{i\in V}$, where l_i and n_i are the power level and the next-hop node of i, respectively.

2.4.5 Complexity Analysis

The complexity of step 1 in our heuristic algorithm is the same as Dijkstra's algorithm's, which runs in $O((N+M)\log N)$ time in average and $O(N^2 \log N)$ in the worst case ($N =\mid V \mid, M =\mid E \mid$). In step 2, we decrease every node's power level from the top to bottom. For the d-th node in the ordered set, the lower-level nodes in its subtree should not be more than $N-1-d$ (except the root), thus we need to check $N-1-d$ nodes' E2E PDRs at most. For the whole tree, in the worst case we need to compute node E2E PDRs $O(N^2)$ times, as there are $N-1$ nodes. For each node, we have to check for all L power levels at most. As L is a constant, the complexity for this step is still $O(N^2)$.

2.5 Performance Evaluation

We use both experiment and simulation to validate the performance of our JRPC protocol. First, we implement our link-quality measurement, estimation and prediction modules on real Crossbow Telos RevB sensor motes. The data rate is $250kb/s$ as in previous experiments. 8 power levels are used in total, ranging from $-25dbm$ to $0dbm$. We show the

Algorithm 2 Decreasing Nodes' Transmitting Powers and Delay

input: tree T_{tree}, links' PDRs $\{\lambda_{i,j,k}\}_{(i,j)\in E, 1\leq k\leq K}$
output: transmitting power levels $l_i, \forall i \in T_{tree}\backslash 1$; adjusted tree T_{tree}

1: Sort all nodes in $T_{tree}\backslash 1$ in the order of their tree level (top to bottom).
2: **for** all nodes i in the sorted order **do**
$l_i \leftarrow$ the minimum power level s.t. $\lambda_j \geq \Lambda_{th}, \forall j \in T_{tree}$ with level lower than node i, including i itself.
3: **end for**
4: **while** delay constraint violated **do**
5: lift the bottom nodes j if $\lambda_j \geq \Lambda_{th}$ after adjusting.
6: **end while**

PDR prediction results in both static and dynamic scenarios. The result of PDR estimation at different transmitting power levels are also presented, based on which the transmitting power levels will be adaptively adjusted. This serves as a primitive operation in each big slot in our protocol. Second, we attach 8 sensors to a human body to emulate the BAN (Fig. 2.1(b)), from which the link parameters: {power level, link PDR} of every link in each big slot are obtained. We put these link parameters into our JRPC algorithm and optimization solver, which is solved with Matlab and CPLEX respectively.

For other parameter settings, we choose each big slot to contain 40 TDMA cycles, and each TDMA cycle includes T_D TDMA slots. For delay constraint, we set $T_D \leqslant 15$. Transmitting one 29-byte packet with 250kbps rate needs about 2ms in ZigBee, thus a big slot is usually smaller than 1.2s. In each big slot, we choose the number of interference samples as $M = 100$.

2.5.1 Accuracy of Link Quality Prediction under CTI

We designed two experiments to validate the effectiveness of our link quality prediction method. Our single-link experiments successfully validate the effectiveness of our prediction approach, as both channel fading and the CTI's dynamic characteristics are taken into account.

First, we test the prediction accuracy under a single transmitting power (the minimum level). We implement the autoregressive algorithm in [45] using orders $p = 1, 2$. The transmitter and receiver are placed on the right knee and left wrist, respectively. To emulate a real BAN, the former periodically sends 40 data packets (29 byte payload) with 30ms

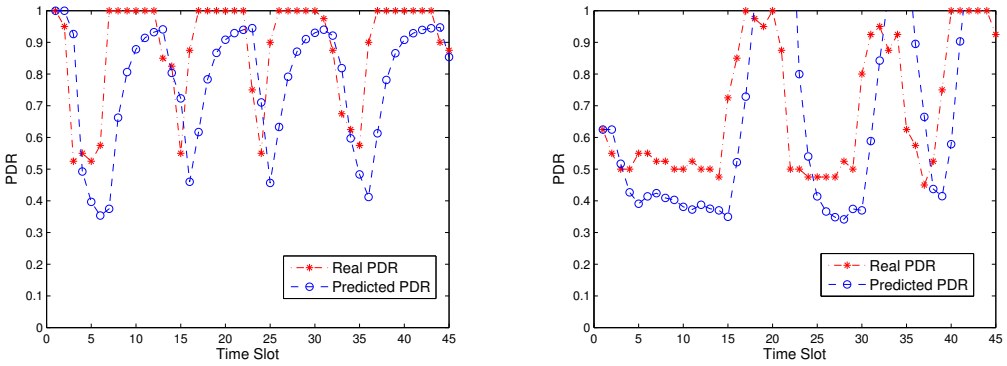

(a) Scenario 1 (b) Scenario 2

Fig. 2.10. Comparison between predicted PDR and real PDR with AR prediction order as 1. (a) the result in scenario 1 with static body while periodically turning on and off the microwave. (b) the result in scenario 2 with dynamic body movement while microwave is turned on all the time.

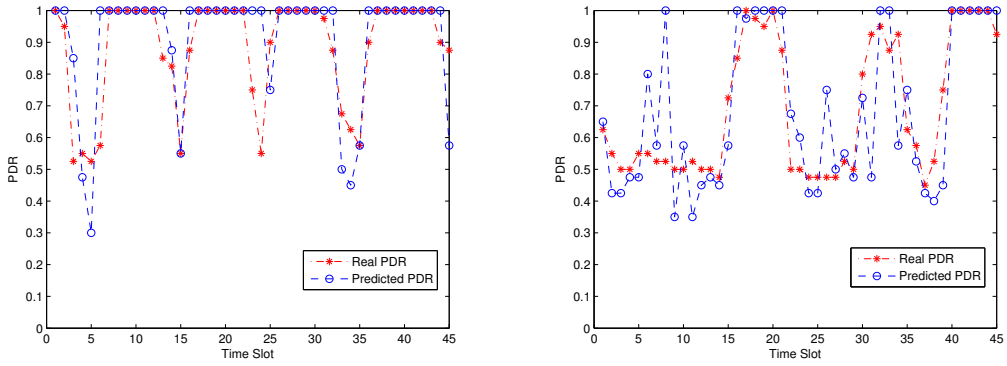

(a) Scenario 1 (b) Scenario 2

Fig. 2.11. Comparison between predicted PDR and real PDR with AR prediction order as 2. (a) the result in scenario 1 with static body while periodically turning on and off the microwave. (b) the result in scenario 2 with dynamic body movement while microwave is turned on all the time.

interval. We use a microwave oven as the CTI source, which locates $0.5m - 1.5m$ away from the body. In scenario 1, the person sits in a chair. The microwave oven is periodically turned on and off every 10 seconds. In scenario 2, the person periodically walks towards and away from the microwave oven every 10 seconds while the latter is turned on all the time. The predicted results of using different orders are shown in Fig. 2.10 and 2.11. The

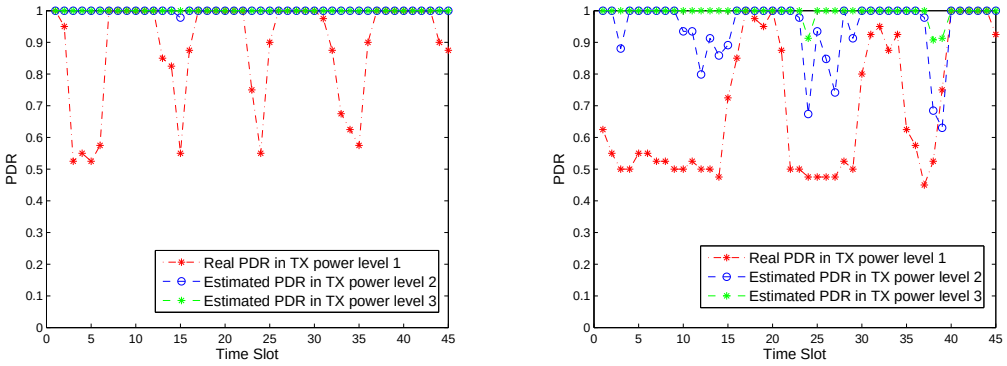

(a) Scenario 1 (b) Scenario 2

Fig. 2.12. PDR estimation at different power levels. (a) the result in scenario 1 with static body while periodically turning on and off the microwave. (b) the result in scenario 2 with dynamic body movement while microwave is turned on all the time.

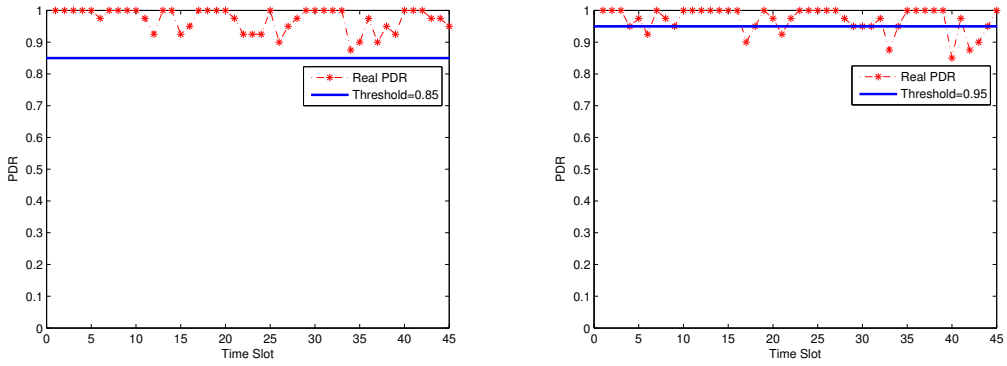

(a) $\Lambda_{th} = 0.85$ (b) $\Lambda_{th} = 0.95$

Fig. 2.13. Link PDR with transmitting-power-level control, in the environment with dynamic body movement while microwave is turned on all the time.

results show that by using AR we could predict the link PDR with considerable accuracy. Especially when using order 2, the predicted PDRs are mostly close to the real ones.

The second experiment evaluates the effectiveness of link PDR - transmit power estimation and prediction via power control. The experiment setting is unchanged and the AR order is 2. In each big slot, the receiver first estimates the PDR under each power level, and then predicts the link PDR under each power level for the next big slot based on the estimated PDR sequences under all power levels in the past. After the estimation and pre-

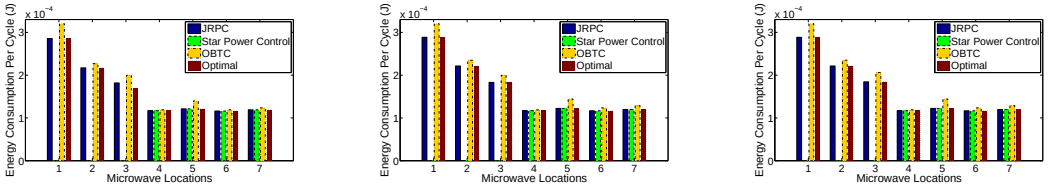

(a) $\Lambda_{th} = 0.85$ (b) $\Lambda_{th} = 0.95$ (c) $\Lambda_{th} = 0.98$

Fig. 2.14. Power consumption in one cycle in the presence of cordless phone interference

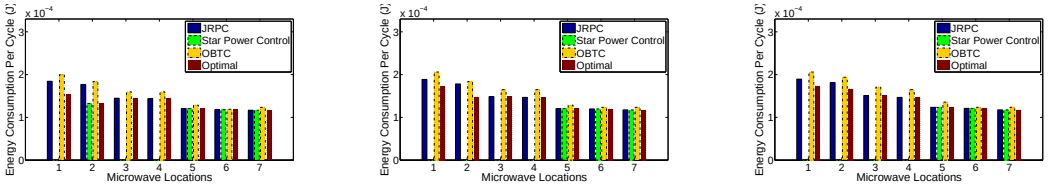

(a) $\Lambda_{th} = 0.85$ (b) $\Lambda_{th} = 0.95$ (c) $\Lambda_{th} = 0.98$

Fig. 2.15. Power consumption in one cycle in the presence of microwave oven interference

diction, it chooses the minimum power level satisfying the PDR threshold and notifies the transmitter to use this level in the next big slot. The estimated PDR sequence are shown in Fig. 2.12, in which the sequences under power level $1, 2, 3$ are shown. After obtaining the feedback from receiver, the transmitter will adjust its power. In Fig. 2.13, we collect the real PDR sequence under the adjusted power level to test whether this power level can guarantee the PDR threshold on a single link. We set two link PDR thresholds: 0.85 and 0.95. From Fig. 2.13, one can see that the predicted power level can guarantee link PDR for most of the time. The above results imply that, as long as our JRPC algorithm outputs a feasible link power assignment and routing scheme, our protocol can ensure the PDR requirement for each node in practice.

2.5.2 Robustness and Effectiveness of JRPC

We now evaluate the robustness and effectiveness of our JRPC algorithm, which ran on the CU in practice. Our experimental scenarios include two CTI sources (cordless phone and microwave oven) placed at different locations. Using the collected link qualities as input, we compare the overall energy consumption output by our JRPC algorithm with the

optimal results derived by CPLEX, and two other strategies including a star topology with only-power-control method, and a previous opportunity based topology control (OBTC) approach [47]. We choose different E2E reliability requirements and evaluate their influences on the energy consumption.

Figs. 2.14 and 2.15 show the energy consumption in one TDMA cycle under the presence of CTI from the cordless phone and microwave oven, respectively. The meaning of energy consumption in one cycle is to show the overall energy consumed by all nodes to transmit one unit of data each. The locations are sorted by increasing distance to the body (see Fig. 2.1(a) for floor plan). We compare our optimal result and heuristic-approach result with two other approaches, the straight-forward star topology with power control, and the OBTC [47] approach. The reason we choose OBTC for comparison is that we both use similar PDR-based link model. As the problem in [47] is not exactly the same as ours, we make some modifications on OBTC to make our works comparable: First, in their work they didn't consider time delay, thus we add our time-delay step after the tree establishment to guarantee the delay requirement. Second, we add a simple power control by choosing the minimal and same power level for all nodes. In Fig. 2.14, the star-topology based power control fails to guarantee the E2E PDR requirement when the cordless phone is at locations 1, 2, and 3, even with the highest transmit power level. The reason is that the links from nodes $1-7$ to node 0 (the gateway) are in poor link qualities due to high-level interferences, thus they cannot satisfy the E2E-PDR constraints of 0.85, 0.95, 0.98. *In contrast, remarkably, our JRPC algorithm can always guarantee the E2E PDR (up to 0.98) in the presence of the strong CTI, even when the cordless phone is closest to the body (held beside the head and making a phone call).* Similar cases with microwave CTI can be seen in Fig. 2.15. Our protocol outperforms the traditional star-topology based method as it adaptively utilizes the high-PDR links instead of the ones severely affected by the CTI. Note that, in our protocol the control packets are treated the same way as data packets, thus their reliability is ensured as well. Meanwhile, the OBTC approach could also guarantee the reliability constraint in all scenarios just as our JRPC approach. The reason is that both

approaches are based on Dijkstra's algorithm in maximizing E2E reliability of all nodes. However, our JRPC approach always outperforms the OBTC approach in terms of energy efficiency due to our delicate power control on each node. We could also note that with the distance between WBAN and interference source becoming smaller, the performance gap of energy efficiency between JRPC and OBTC is larger. The reason is that smaller distance brings larger and more complex interferences, which leads to heterogenous link PDRs. Thus we need more delicate power control to separately adjust each node's power level as in JRPC. Moreover, by comparing the energy consumptions under different E2E-PDR constraints, we find that the energy consumption increases with the increasing of E2E-PDR constraint, but only slightly in average. The reason could be explained by Fig. 2.8(a): the link PDR experiences a step change with the increasing of SINR. The consequence is that a slight increase in transmitting power could enhance link PDR remarkably. Therefore, with our delicate power control, we could continuously satisfy the increasing link-reliability requirements in an energy-efficient way.

Meanwhile, the results also show that our algorithm is very energy-efficient by comparing with the optimal solutions. In most scenarios for cordless phone, our algorithm achieves the same energy consumptions as the optimal solutions. Only in a few scenarios, such as positions 1 and 2 for microwave oven, the energy-consumption difference is noticeable between JRPC algorithm and the optimal solution. These results indicate the effectiveness of our heuristic algorithm.

In addition, our algorithm yields low end-to-end delay for each source packet. As we can see from Tables. 2.3 and 2.4, assuming each TDMA slot is $T = 2ms$, the end-to-end delay values are very small even with the strictest E2E PDR requirement ($\Lambda_{th} = 0.98$). As comparison, the star topology could always result in the lowest time delay, which is $14ms$ in our 8-sensor scenarios. However, this delay is meaningful only when the E2E PDR constraint is satisfied first. In locations $1, 2, 3, 4$ in Table. 2.3 and locations $1, 2, 3$ in Table. 2.4, the E2E PDR constraint is violated by using star topology. For the other two thresholds (0.85 and 0.95), the delay is almost the same, thus is not shown here.

Table 2.3. End-to-end delay by using JRPC algorithm in the presence of microwave oven CTI at different locations

Locations	1	2	3	4	5	6	7
$\Lambda_{th} = 0.98$, JRPC	20 ms	20 ms	16 ms	16 ms	14 ms	14 ms	14 ms
$\Lambda_{th} = 0.98$, Star	-	-	-	-	14 ms	14 ms	14 ms

Table 2.4. End-to-end delay by using JRPC algorithm in the presence of cordless phone CTI at different locations

Location	1	2	3	4	5	6	7
$\Lambda_{th} = 0.98$, JRPC	30 ms	22 ms	20 ms	14 ms	14 ms	14 ms	14 ms
$\Lambda_{th} = 0.98$, Star	-	-	-	14 ms	14 ms	14 ms	14 ms

We also simulate and test the impact of inaccurate link-PDR estimation. We assume the measurement of link SINR has an uniformly distributed and zero-mean error, which leads to inaccurate link PDRs. Given these link PDRs, we run our JRPC protocol to get the overall energy consumption and calculate the differences. The SNR error variance is set as 10 and the results are shown in Tab. 2.5. The SNR-variance error is large enough according to our calculation: given Fig 2.8(a), the SNR-PDR curve is approximately a linear function between $4dB$ to $7dB$ segment. From our experiment shown in Fig. 2.8(b), we can derive the PDR-error variance as 0.07. Given the linear model, we derive the SNR-error variance as less than 1. By adding such a noise, the final energy consumption is hardly noticeable. We further relax the SNR-error variance ten-times larger, and the enlarged energy-consumption error is shown in Tab. 2.5. Given this result, we find that the average energy difference is about 3.7%, meaning that overall energy consumption is not obviously affected by a relatively large link-PDR-estimation error.

2.5.3 Protocol Overhead

Our protocol has minimal traffic overhead, as in the link-PDR measurement and prediction phase the data packets are used instead of specialized-probing packets, which are only needed for one big slot duration initially to bootstrap the protocol. For the same reason, the time overhead is also minimal as we do not need to allocate additional slots to measure the links' quality. In each big slot, only two extra TDMA cycles are needed

Table 2.5. WBAN overall energy consumption differences given inaccurate link-PDR estimation with JRPC algorithm.

Cordless phone locations	1	2	3	4	5	6	7
Energy consumption difference	4.6 %	1.7 %	12.4 %	0.6 %	7.4 %	0.7 %	0.9 %
Microwave oven locations	1	2	3	4	5	6	7
Energy consumption difference	8.7 %	2.1 %	1.9 %	0.5 %	0.3 %	0.3 %	1.7 %

separately for the nodes to report their incoming link's PDR estimations to the CU, and for the CU to broadcast the derived power assignments and routing decisions. These control packets are transmitted using the same power and routing scheme as that of normal data packets. In our implementation a big slot contains 40 TDMA cycles, thus the overhead in terms of communication, delay, and energy is merely 5%. Note that, although our current algorithm is centralized, as a BAN has a small physical span, it is not an overkill. A distributed algorithm may lead to lower overhead, but will also be less optimal.

2.6 Summary

In this chapter, for the first time we study the problem of reliability assurance under external CTI in a BAN, especially those from non-protocol-compliant sources that are much harder to mitigate than the CTI from 802.x devices. We formulate a joint routing and power control problem aiming at overcoming the impact of such strong CTI in a BAN, while using minimal overall energy consumption. The optimal results are derived by using CPLEX after reformulated into linear form. We then propose a practical JRPC protocol which exploits passive measurement and prediction to model the uncertain impact of CTI on link qualities and a heuristic algorithm to efficiently solve our JRPC problem. Remarkably, evaluation results show that our JRPC protocol can effectively enlarge the "reliability zone" of the BAN, even when the CTI source is closest to the body. Our protocol also achieves high efficiency, low-energy consumption and overhead.

CHAPTER 3
COOPERATIVE INTERFERENCE CANCELLATION IN COEXISTING HETEROGENEOUS MULTI-HOP WIRELESS MIMO NETWORKS

3.1 Overview

In the previous chapter, we studied the detrimental impact of non-protocol-compliant CTI on body area networks. In our daily life, the protocol-compliant interference is also hard to deal with. E.g., the networks applying 802.11 and 802.15.4 could not coordinate, thus they could only apply the interference avoidance strategy to mitigate the interference. The recent advance of IC could achieve interference mitigation between transmitter and receiver nodes through measuring the channel. However, for networks running different protocols, this is hard as the coexisting nodes could not communicate with each other. In this chapter, we first explore the feasibility of cooperative interference mitigation (CIM) among heterogeneous multi-hop networks by exploiting only partial CSI (or channel ratio information, CRI). Specifically, we show that compared with full CSI, such CRI does not affect the satisfiability of DoF constraints (or computability of transmit/receive vectors) in each network. We discuss practical methods to measure CRI and achieve cooperative technology-independent interference cancellation (TIIC). Then we propose two tractable models for CIM that accurately capture both networks bilateral cooperative IC decisions, link scheduling, and various forms of system heterogeneity, based on recent advances in MIMO link-layer modeling. One of our models captures full IC (CIM- FIC) which considers both transmitter-side and receiver-side IC, while the other model only captures traditional receiver-side cancellation (CIM-RIC). Furthermore, for our CIM-FIC model, we theoretically analyze its ability to support interference alignment and use an example to prove it. Based on our CIM models, we formulate two bi-criteria optimization problems, in which both coexisting networks maximize their own respective throughput. As both

of our problems are mixed integer linear programming (MILP) problems, we rely on the Reformulation-Linearization Technique (RLT) to reformulate them. In order to find the Pareto-optimal curve efficiently, we exploit the inherent stair-shape property determined by our model, thus reducing the number of MILP problems needed to be solved, which is extremely time-consuming in practice. The derived curve under our model could be regarded as a lower bound to the outer bound of the capacity region of two multi-hop heterogeneous networks in the DoF sense.

3.2 Background and Motivation

MIMO Background. There are two key techniques enabled by MIMO communication: spatial multiplexing (SM) and interference cancellation (IC). The DoF [10] at a node represent the available number of interference-free signaling dimensions. SM refers to transmitting multiple streams simultaneously on a single MIMO link using multiple DoFs, which is upper limited by $min(A_t, A_r)$ where A_t and A_r are the antenna numbers at the transmitter and receiver sides, respectively. IC refers to a node's capability to cancel unintended interference using some of its DoFs, which can be done either by a transmitter or receiver. Assume transmitter t's link carries s_t streams and another receiver r's link carries s_r streams. For transmitter-side IC, the number of DoF required at t is equal to s_r (i.e., t can cancel its interference at r iff. $A_t - s_t \geq s_r$). For receiver-side IC, the number of DoFs required at a receiver is equal to s_t (i.e., r can cancel t's signal iff. $A_r - s_r \geq s_t$). As an advance of IC, the IAL is built upon receiver-side IC, which aligns the interferences from different transmitters along the same directions in the receiver's nulling space. As a result, the receiver could deal with multiple aligned interfering streams as if dealing with fewer streams. To achieve SM and IC, antenna weights are assigned to transmitters and receivers such that the signals received will be combined in the desired way.

IC depends on full channel state information (CSI) at each node which is usually estimated via training symbols in an orthogonal frequency-division multiplexing (OFDM) packet. However, with the CTI from a different wireless technology, the full CSI may not be obtained (or very costly to obtain) due to the generally unknown signal structure. If the

other wireless network also uses OFDM at the physical layer and its preamble is known, then we can assume full CSI is available. But in reality this requires prior knowledge of the protocol standard of various coexisting networks, which incurs significant overhead and cannot handle new systems. Fortunately, Gollakota et al. [13] proposed Technology-Independent Multiple-Output (TIMO), which enables an 802.11 MIMO link to completely cancel the high power and wide-bandwidth interference to/from a non-802.11 device (e.g., a ZigBee sensor and microwave oven), by only measuring the *channel ratio* information. TIMO is *agnostic* to the interferer's technology, making it possible to enhance coexistence among *heterogeneous* networks.

Motivation. The advancement of both MIMO and TIMO makes it possible for two or more coexisting networks to cooperatively enhance everyone's throughput. Fig. 3.1 illustrates this idea using a simple two-interfering-link setting. Link 1 is equipped with two antennas at both transmitter and receiver sides, while link 2 only has one antenna. Assume we divide time into multiple slots, and define each link's throughput to be the average number of streams transmitted (or DoF for SM) over all time slots. Fig. 3.1 (b) shows their optimal throughput curve, which is derived from the convex hull of all the possible base-rate combinations: $(2,0),(1,1),(1,0),(0,1),(0,0)$. Suppose we want to achieve proportional fairness, and let the throughput ratio of two links to be the same as that of their maximum throughput without interference (i.e., 2:1, equaling to the ratio of their antenna numbers). Under the interference avoidance paradigm, the Pareto-optimal fair throughput pair is $(1, 0.5)$. In contrast, under CIM (link 1 uses both transmitter- and receiver-side IC), the new pair is $(\frac{4}{3}, \frac{2}{3})$, which is achieved by sending $(1,1),(1,1),(2,0)$ streams during three consecutive slots for each link. Note that this also requires link 2 to cooperate by not transmitting during the third slot. This example clearly shows the potential by using CIM.

To enable such cooperation among heterogeneous multi-hop networks, information including active sessions and the interference graph in each network needs to be shared with others. This can be difficult in unplanned deployments, as there lacks a common commu-

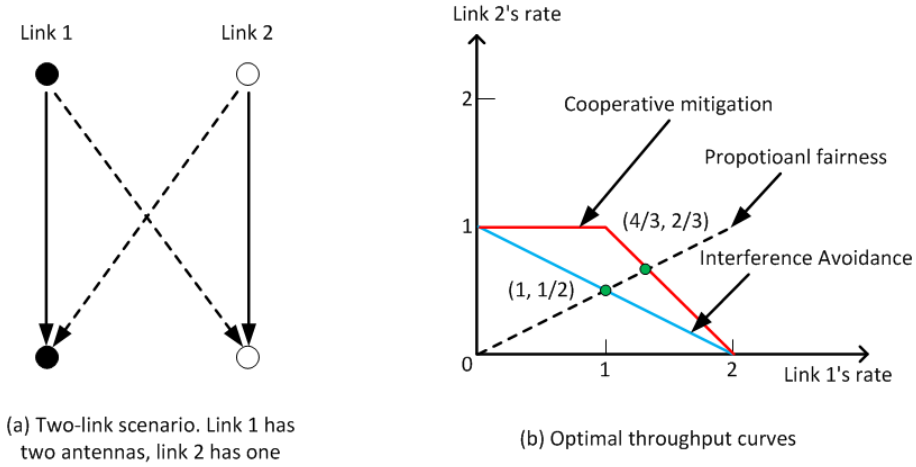

Fig. 3.1. Overall throughput with Cooperative MIMO interference mitigation

nication channel (CCC) between networks with different protocol standards. However, it is possible to obtain such information without a CCC. For example, Zhang and Shin [48] proposed GapSense, a lightweight protocol to coordinate among heterogeneous wireless devices based on energy sensing. It can be regarded as a side channel using implicit communication. In reality, we can assume each network has a central controller or base station, and these controllers can exchange necessary information for CIM using implicit communications. The performance bounds for each network form a Pareto-optimal curve. In reality, to choose from one feasible point on the curve, two networks can make agreements based on certain criteria like fairness (max-min or proportional) or max total rate. This can be achieved because we assume that the networks are cooperative. In the case that both networks are selfish and may deviate from cooperation, a game-theoretic approach is needed, which will be left for our future work.

Key Challenges. There involves a unique set of challenges to realize CIM in a multi-hop network setting. (1) How to cancel the interference from/to nodes in another multi-hop network running different wireless technology without having the full CSI? So far TIMO has only been applied to the single-link and non-cooperative setting, but its feasibility in multi-hop networks is unexplored. In a multi-hop network, there can be multiple simultaneous active links in each network generating interference to a link of the other network. Then, how to design the transmit/receive vectors to satisfy all nodes' DoF constraints?

(2) To theoretically model and quantify the performance limit of CIM among heterogeneous MIMO networks, the intrinsic complexity involves both networks' cooperative link scheduling, MIMO DoF allocation for spatial multiplexing (SM), IC for both intra- and inter-network. The model must capture network heterogeneity: different PHY technologies, number of antennas, transmit power, data rates, etc. (3) Networks have competing interests such that each wants to maximize its own throughput. One may think of extending the capacity-region concept to derive the Pareto-optimal throughput curve of the "combined network". Previously, Toumpis and Goldsmith studied the capacity region of SISO multi-hop wireless networks [49], which showed the region can be derived from the convex hull of a set of base-rate points via arbitrary time-sharing. However, it remains open for MIMO ad hoc networks due to the intractability of SNR model. Even if we adopt a DoF model, the deriving of base-rate pairs is still non-trivial as we need to enumerate not only the link scheduling but also DoF allocation on each link. To the best of our knowledge, this problem also remains open to date.

3.3 Feasibility of Cooperative TIIC among Multi-hop Networks

In this section, we study the feasibility of realizing cooperative TIIC across heterogeneous multi-hop networks, which is the essence in our CIM paradigms. Specifically, considering the basic scenario of two coexisting networks, is it possible to schedule the links' transmissions in both networks such that all the interference from/to each other can be canceled (subject to the DoF constraints at each node)? In the case of a single MIMO network, [14–18, 50] show it is feasible that links can cancel all the interference in the same network by allocating their transmission DoFs for SM and IC. However, the previous results are derived under the assumption of full CSI. To deal with cross-technology interference, only partial CSI can be obtained (such as channel ratio in TIMO [13]). Thus the natural question is, is it possible to make MIMO and TIMO work together in heterogeneous multi-hop networks (use the former for intra-network IC and the latter for inter-network IC)?

TIIC Based on Channel Ratio Information (CRI). We first give a theoretical

treatment of TIIC based on CRI. We adopt the matrix representation of MIMO IC based on the Zero-Forcing beamforming (ZFBF) [51], which is used by previous works [50]. W.l.o.g., consider the cross-technology interference from the transmitter $Tx(l)$ of a link l to receiver $Rx(k)$, where node i has A_i antennas. For each active link l, denote z_l as the number of data streams and s_{li} the signal of stream i ($1 \leq i \leq z_l$). Denote $\mathbf{H}_{(l,k)}$ the $A_{Tx(l)} \times A_{Rx(k)}$ channel gain matrix between nodes $Tx(l)$ and $Rx(k)$ which is full-rank (assuming a rich scattering environment). Let transmitter $Tx(l)$'s transmitting-weight vectors be $\mathbf{u}_{li}, 1 \leq i \leq z_l$, and receiver $Rx(k)$'s receiving-weight vectors be $\mathbf{v}_{kj}, 1 \leq j \leq z_k$. The interference to data stream j on link k is:

$$\Big(\sum_{i=1}^{z_l} \mathbf{u}_{li} s_{li}\Big)^T \mathbf{H}_{(l,k)} \mathbf{v}_{kj} = \sum_{i=1}^{z_l} ((\mathbf{u}_{li})^T \mathbf{H}_{(l,k)} \mathbf{v}_{kj}) \cdot s_{li}.$$

To cancel this interference, the following constraints should be satisfied:

$$(\mathbf{u}_{li})^T \mathbf{H}_{(l,k)} \mathbf{v}_{kj} = 0, \quad (1 \leq i \leq z_l, 1 \leq j \leq z_k). \tag{3.1}$$

However, the complete matrix $\mathbf{H}_{(l,k)}$ is unknown due to different technology. In the special case where link l has only one antenna, we have $z_l = 1$ and $\mathbf{u}_{li}$ equals to a constant while $\mathbf{H}_{(l,k)}$ is an $A_{\mathrm{Rx}(k)}$ dimensional vector $\mathbf{h}_{(l,k)}$. Then we get $\sum_{d=1}^{A_{\mathrm{Rx}(k)}} h_{(l,k)}(d) \cdot v_{kj}(d) = 0$. Since $h_{(l,k)}(1) \neq 0$ w.h.p., if we divide $h_{(l,k)}(1)$ on both left and right sides, we obtain

$$\mathbf{h}_{(l,k)} \cdot \mathbf{v}_{kj} = v_{kj}(1) + \sum_{d=2}^{A_{\mathrm{Rx}(k)}} \beta_{l,k}(d) v_{kj}(d) = 0, \quad (1 \leq j \leq z_k), \tag{3.2}$$

where the "*channel ratio*" between link l's transmitter and link k's receiver is defined as: $\beta_{l,k}(d) = \frac{h_{(l,k)}(d)}{h_{(l,k)}(1)}$, $2 \leq d \leq A_{\mathrm{Rx}(k)}$. Note that, Eq. (3.2) is equivalent to Eq. (3.1) thus it does not change the rank of the coefficient matrix of $\mathbf{v}_{kj}$. This means the DoF consumed by all constraints in Eq. (3.2) is unchanged. It has been shown in TIMO that we are able to solve Eq. (3.2), i.e. to find $\mathbf{v}_{kj}$ such that the interference from node l is canceled, as long as we can get $\beta_{l,k}(d)$, which can be easily realized by broadcasting the vector $\mathbf{u}_{li}$ in

probing packet before data transmission. The deriving of channel ratio information $\beta_{l,k}(d)$ in multi-hop networks will be introduced later. Note that, under channel-reciprocity model, similar results can be derived for transmitter-side IC.

When the CTI links have multiple antennas, we need to define "*extended channel ratio*" β'. Observe that in Eq. (3.1), $(\mathbf{u}_{li})^T\mathbf{H}_{(l,k)} = \mathbf{h}'_{(l,k)}$ which is an $A_{\mathrm{Rx}(k)}$ dimensional vector, where $h'_{(l,k)}(d) = \sum_{j'=1}^{A_{\mathrm{Tx}(l)}} u_{li}(j') \cdot h_{(l,k)}(j', d)$, where $h'_{(l,k)}(1) \neq 0$ with high probability. Then,

$$\beta'_{l,k}(d) = \frac{h'_{(l,k)}(d)}{h'_{(l,k)}(1)}, \quad (2 \leq d \leq A_{\mathrm{Rx}(k)}). \tag{3.3}$$

By replacing $\mathbf{h}_{(l,k)}$ with $\mathbf{h}'_{(l,k)}$ and $\beta_{l,k}(d)$ with $\beta'_{l,k}(d)$ in Eq.(3.2), we can use the same methodology as that in TIMO to derive $\mathbf{v}_{kj}$ in the multi-antenna CTI case.

Hereafter, we use *channel ratio information* (CRI) to refer to the union of channel ratio and extended channel ratio.

DoF Criterion. Next we analyze the DoF consumption in our multi-hop networks. First, we consider the coexisting of two single-link networks. Assume link 1 and link 2 are transmitting s_1 and s_2 streams respectively. W.l.o.g., we assume link $Rx(1)$ tries to cancel the interference from link $Tx(2)$. Because in a CRI-based TIIC scheme, every IC-constraint equation is equivalent to the original one by a constant factor (e.g. (3.1) and (3.2)), the number of consumed DoF of a node due to a set of linear constraints is unchanged compared with the one with full CSI. Therefore, the consumed DoF will be s_2 at $Rx(1)$, as each interfering stream generates one equation, thus consume one DoF. Then, we assume link 2 tries to cancel its interference towards $Rx(1)$. In this case, the DoF consumed will be s_1 at $Tx(2)$.

Now we explore the feasibility of TIIC in general for two multi-hop networks. Assume there is a global "node ordering" π among the nodes in the "combined network"; denote $\pi_{Tx(l)}$ and $\pi_{Rx(k)}$ as the positions of nodes $Tx(l)$ and $Rx(k)$ in the node-ordering list, respectively. Based on Lemma 5 in [50], we have the following lemma:

Lemma 1. *Consider the cross-technology interference from $Tx(l)$'s z_l streams to $Rx(k)$'s z_k streams. Based on only CRI, from the IC constraints in Eq. (3.1), we have (i) if*

$\pi_{Tx(l)} > \pi_{Rx(k)}$, then the number of DoFs consumed by IC are z_k and 0 at Tx(l) and Rx(k), respectively. If $A_{Tx(l)} = 1$ and $z_k \geq 1$, then $z_l = 0$ at Tx(l). (ii) If $\pi_{Tx(l)} < \pi_{Rx(k)}$, then the number of DoFs consumed by IC are 0 and z_l at Tx(l) and Rx(k), respectively.

The proof is straightforward. Such a node ordering is both sufficient and necessary to ensure the feasibility of transmit/receive vector allocation on each link, thus showing that the CRI-based TIIC can be used in multi-hop networks along with standard IC with full CSI.

Measuring the Channel Ratio Information in Multi-hop Networks. In order to obtain the CRI, TIMO can be used to measure the channel ratio for single-antenna interference sources. Its current implementation is limited to single concurrent and co-channel interferer. Extending to multiple interferers is possible but the IC algorithm will be more complex. Therefore, we propose an alternative, cooperative approach to suit the CIM paradigm.

Our idea is to ensure only one of the interferers' signals is present at a time such that the channel ratios can be measured directly. We assume time is slotted (e.g., TDMA is used), which is necessary for optimized transmission scheduling. Each interferer sends a short probing packet (PP) at different times sequentially. Suppose there are M active nodes in total within one slot according to link scheduling, each of them can broadcast a PP within a non-overlapping mini-slot (M in total). Upon each probing, the channel ratios on each interfered node are obtained by taking the ratio of the received symbols on each antenna. After all the probings, the signal-of-interest and interference signals may transmit concurrently.

The extended channel ratio can be obtained in a similar way as the channel ratio. An active node on link l sends a weighted probing signal $\mathbf{u}_{li}^T \cdot s_p$ during each mini-slot $i (1 \leq i \leq z_l)$ where s_p is the probe packet, and z_l is the intended number of streams to transmit on l. The received signal vector on all the antennas of Rx(k) is $(\mathbf{u}_{li})^T \mathbf{H}_{(l,k)} s_p = \mathbf{h}'_{(l,k)} s_p$. Then, dividing the signal on the dth antenna by that of the 1st antenna yields $\beta'_{l,k}(d)$.

The above describes the use of receiver-side IC, which means the CTI transmitter Tx(l)

determines its transmit vectors $\mathbf{u}_{li}$ first, and the receiver Rx(k) decides its receive vectors $\mathbf{v}_{kj}$ afterwards. The same approach can be easily extended to transmitter-side IC (Tx(k) cancels its CTI to Rx(l)), for which the receiver Rx(l) transmits a probing signal, and then Tx(k) can estimate the CRI based on channel reciprocity [13].

The probing order is determined by the node order π. This is because that the order π must be followed when determining vector $\mathbf{u}$, $\mathbf{v}$ [50], and the probing behavior logically plays a '*vector-notifying*' role in practice.

Feasibility of IAL. After elaborating the importance of node-ordering in our CIM paradigm. Next, we show that node-ordering is an effective mechanism to achieve IAL in practice.

In Fig. 3.2, assume each node's order is the same as its index number, i.e. node i's order is also i. Assume each node has 2 antennas. The dash lines denotes the interference relations. At an arbitrary time point, assuming node 1 transmits one stream to node 2. By using our CIM, it will broadcast a probing packet using its transmitting vector $\mathbf{u}_1$ to all other nodes. Note that as node 1 has highest priority in the global order π, its vector $\mathbf{u}_1$ could be arbitrarily chosen. Based on the channel ratio information β measured on all its antennas, node 4 will compute its receiving vector $\mathbf{v}_4$ satisfying $\mathbf{u}_1^T\mathbf{H}_{1,4}\mathbf{v}_4 = \mathbf{0}$, then broadcast a probing packet using the receiving vector $\mathbf{v}_4$. Next the nodes $5, 7$ will use the same methodology to derive $\mathbf{u}_{5/7}$, such that $\mathbf{u}_{5/7}^T\mathbf{H}_{5/7,4}\mathbf{v}_4 = \mathbf{0}$. In this way, we can see that node 5 and 7 align their interfering streams $\mathbf{u}_5$, $\mathbf{u}_7$ along the direction of $\mathbf{u}_1$.

The example in Fig. 3.2 is a special case where IAL is achieved by using our ordering mechanism. However, we do not claim that our ordering mechanism could achieve IAL in all cases. E.g., in Fig. 3.3, assuming all settings are the same as in Fig. 3.2, except that node 4 has three antennas. In this case, all interfering streams from node $1, 5, 7$ are casted into node 4's nulling space, which is a two-dimensional plane. In general, we have the following theorem:

Theorem 1. *Under any feasible ordering π, the interference alignment is supported by our CIM-FIC model, i.e., given a node ordering π, any feasible DoF allocation using IAL could*

be equivalently derived using CIM-FIC.

The basic idea of this theorem is that the IAL is feasible under our CIM model as long as it is feasible given any ordering π. Note that our CIM paradigm supports IAL only under full-IC (FIC) model, as IAL is feasible only if transmitter-side IC is feasible.

Discussion. Here we discuss the overhead of our CRI-based cooperative TIIC scheme. First, the exchange of network flow information and interference graph (input to the optimization problem) is done at the beginning, which is a one-time overhead and can be amortized. Second, regarding probing signals, the number of mini-slots needed in the worst case is $(A_1 \cdot N_1 + A_2 \cdot N_2)$, where A_i is the number of DoFs for each node in the ith network. In reality it can be much smaller because not all active nodes are involved in cross-technology interference. Besides, the probing frequency depends on the channel coherence time, which is typically hundreds of milliseconds in static indoor environments [52]. In that case, the overhead can be amortized over multiple data slots. Third, time synchronization among networks is only required in our analytical optimization framework, which can be relaxed in practice. For example, if a CSMA-like MAC protocol is used in both networks, neither probing nor synchronization is needed. CRI measurement can be done by opportunistically exploiting the overheard non-interfered signals from RTS/CTS/Data/ACK packets.

3.4 Modeling and Formulation

In this and the next section, we systematically study the performance bounds of two (or more) heterogeneous multi-hop MIMO wireless networks under the CIM paradigm. Due to the absence of central administration, we consider each network aiming at maximizing its own throughput, assuming they cooperatively cancel/mitigate the interference to/from each other. However, the networks' objectives conflict with each other because of their mutual interference. Thus, we will develop a *bi-criteria optimization* framework, and characterize the *Pareto-optimal throughput curve* rather than a single optimal point. In order to be tractable, we adopt a recent DoF model from [50], and assume that time is slotted and finite instead of continuous assumed in capacity region research. Since arbitrary time sharing is

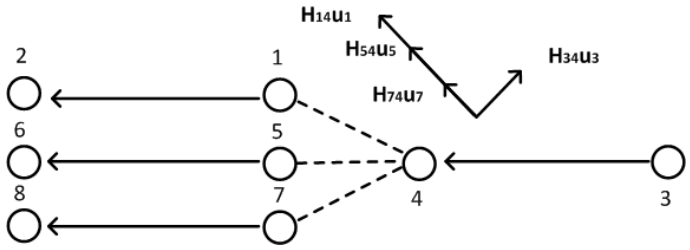

Fig. 3.2. Example 1 of interference alignment by using our CIM paradigm. 1 stream on node 1,3,5,7. The streams transmitted by node 1,5,7 are aligned along the same direction.

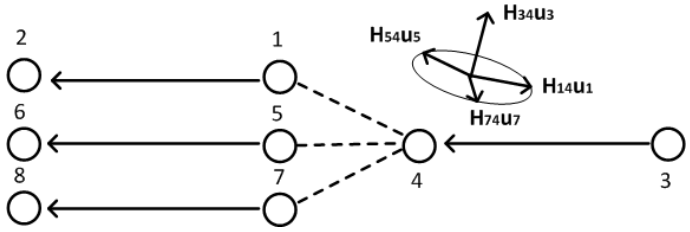

Fig. 3.3. Example 2 of interference alignment by using our CIM paradigm. 1 stream on node 1,3,5,7. The streams transmitted by node 1,5,7 are casted into the nulling space of node 4.

not supported by a finite number of slots T, our result can be regarded as a lower bound to the case when $T \to \infty$.

3.4.1 Mathematical Modeling

System Model. Consider two unplanned multi-hop wireless networks $\mathcal{N}_1 = (\mathcal{V}_1, \mathcal{E}_1)$ and $\mathcal{N}_2 = (\mathcal{V}_2, \mathcal{E}_2)$ with heterogeneous technologies that interfere with each other, and $N_1 = \|\mathcal{V}_1\|$ and $N_2 = \|\mathcal{V}_2\|$. Assume the nodes in at least one network possesses MIMO capability (e.g., an 802.11n ad hoc network v.s. WiMax, or ZigBee with SISO links). The MIMO nodes also use our cooperative TIIC scheme to cancel the CTI from/to another disparate network using different technology[1]. The networks operate in the same band, and we consider T time slots are available to both networks[2]. Let $\mathcal{F}_i$ represent the set of multi-hop sessions in network i, and $r(f)$ denotes the rate of session $f \in \mathcal{F}_i$. Assume routing is

[1]We assume that the networks' technologies are unknown to each other, thus complete CSI across networks is not obtainable.

[2]This reflects that spectrum is crowded. We can also extend this to model an additional set of channel resources.

given and denote $\mathcal{L}_i$ the set of active links in network i. Let $z_l(t)$ be the number of data streams transmitted over link $l \in \mathcal{L}_i$ during slot t. If a network is SISO, then $z_l(t) = 1$ when link l is active during slot t, otherwise $z_l(t) = 0$. Each network's goal is to maximize its own utility (function of session rates: $\sum_{f \in \mathcal{F}_i} h[r(f)]$) while using CIM.

Modeling the CIM Paradigm with Full IC. In the full-IC model, we assume both transmitter and receiver have the ability to perform interference cancellation. We describe the general case where both networks are MIMO. To model channel access, we consider half-duplex transceivers for both networks. Denote binary variables $x_i(t)$ and $y_i(t)$ $(i \in \mathcal{V}_1 \cup \mathcal{V}_2, 1 \leq t \leq T)$ as if node i transmits or receives at slot t. We have:

$$x_i(t) + y_i(t) \leq 1 \qquad (i \in \mathcal{V}_1 \cup \mathcal{V}_2, 1 \leq t \leq T) \tag{3.4}$$

To realize CIM, both networks should use some of their resources to mitigate the interference with each other. For a MIMO network, each node can use MIMO IC to cancel the interference either to/from other nodes within the same network, or to/from nodes in the other network. While for a SISO network, it is not able to carry out any IC. Thus its cooperative behavior can be regarded as refraining from transmitting on a subset of its links that will interfere with the MIMO network during each slot, through link scheduling. The main complexity of the problem is due to the lack of predefined order/priority between any two networks so the responsibility of cooperation is in both networks in general. There are numerous combinations as to how the nodes should cancel the interference to/from links in its own network, and to/from the other network, and scheduling its transmission to not interfere with another network in case of SISO.

To this end, we adopt a recent MIMO link-layer model [50], which introduces an ordering among the nodes for DoF allocation to ensure the feasibility of IC and avoid unnecessary duplication of IC. By inserting a formulation of the ordering relationship into a specific optimization problem, an optimal ordering can be found. In our case, a global order of nodes in both networks needs to be established in each time slot. Denote $1 \leq \pi_i(t) \leq N = N_1 + N_2$ as the global ordering of node i in slot t, and $\theta_{ji}(t)$ as the relative order between nodes j

and i ($\theta_{ji}(t) = 1$ if j is before i and 0 otherwise). Then we have the following relationship:

$$\pi_i(t) - N \cdot \theta_{ji}(t) + 1 \leq \pi_j(t) \leq \pi_i(t) - N \cdot \theta_{ji}(t) + N - 1, \quad (i, j \in \mathcal{V}_1 \cup \mathcal{V}_2, 1 \leq t \leq T) \tag{3.5}$$

Next we describe the constraints for DoF consumption at each node, which include DoFs spent on spatial multiplexing (SM), intra- and inter-network IC. With the above MIMO link model, a transmitter i needs only to cancel the interference to the set of neighboring nodes $\mathcal{I}_i \subset \mathcal{V}_1 \cup \mathcal{V}_2$ (within its interference range) that are before itself in the ordered list, and the DoF spent is equal to the number of streams received by those interfered nodes. A similar rule is used for a receiver. If node i is transmitting/receiving, its DoF consumptions cannot exceed the total number of DoFs of itself. Denote $\mathcal{L}_{i,out}$ and $\mathcal{L}_{i,in}$ as the set of outgoing and incoming links from node i, respectively. The transmitter-side DoF constraints are:

$$x_i(t) \leq \sum_{l \in \mathcal{L}_{i,out}} z_l(t) + [\sum_{j \in \mathcal{I}_i} (\theta_{j,i}(t) \sum_{k \in \mathcal{L}_{j,in}}^{Tx(k) \neq i} z_k(t))] x_i(t) \leq A_i x_i(t), \quad (i \in \mathcal{V}_1 \cup \mathcal{V}_2, 1 \leq t \leq T) \tag{3.6}$$

The receiver-side's DoF constraints are similar:

$$y_i(t) \leq \sum_{l \in \mathcal{L}_{i,in}} z_l(t) + [\sum_{j \in \mathcal{I}_i} (\theta_{j,i}(t) \sum_{k \in \mathcal{L}_{j,out}}^{Rx(k) \neq i} z_k(t))] y_i(t) \leq A_i y_i(t), \quad (i \in \mathcal{V}_1 \cup \mathcal{V}_2, 1 \leq t \leq T) \tag{3.7}$$

By analyzing the constraint (3.7), we can clearly see that the IAL is supported intrinsically by our model. In the component $[\sum_{j \in \mathcal{I}_i} (\theta_{j,i}(t) \sum_{k \in \mathcal{L}_{j,out}}^{Rx(k) \neq i} z_k(t))]$, it can be seen that only the interferences from transmitting nodes j that are prior to node i in the ordering list π are canceled by i using receiver-side IC. The streams from nodes j that are behind i in ordering list π are not canceled and thus will not consume any DoF at node i. As a result, these non-interfering streams must be casted into the nulling space of node i, in which *aligning*

along one direction is a special case.

Note that the constraints (3.6) and (3.7) are also satisfied under SISO ($A_i = 1$). This is because a SISO node either transmits/receives or keeps silent (for latter case, either $x_i = \sum_{l \in \mathcal{L}_{i,out}} z_l(t) = 0$, or $y_i = \sum_{l \in \mathcal{L}_{i,in}} z_l(t) = 0$).

For the link-capacity model, to reflect heterogeneous data rates, we multiply with a different constant weight w_n for each network:

$$c_l = w_n \cdot \frac{1}{T} \sum_{t=1}^{T} z_l(t), \quad (\forall l \in \mathcal{L}_n, n \in \{1, 2\}, 1 \leq t \leq T) \tag{3.8}$$

Then we have the flow-rate constraints for each session of our two coexisting networks:

$$r(f) \leqslant c_l \quad (\forall l \in f, f \in \mathcal{F}_1), \quad r(g) \leqslant c_l \quad (\forall l \in g, g \in \mathcal{F}_2) \tag{3.9}$$

Modeling the CIM Paradigm with Receiver-side IC. The model of CIM with only receiver-side IC is different than the one using full IC in terms of receiver-side's DoF constraint. In the previous model, multiple streams from different transmitters could be casted into the receiver's nulling space. However, in the receiver-side-IC model, all interfering streams are handled by receiver, thus each interfering stream will consume one DoF at the receiver. To eliminate transmitter-side IC, we just need to modify the receiver-side IC constraint by assuming all incoming-interfering streams should be canceled by every receiver i. Based on the analysis in [19], we modify the receiver's DoF constraint:

$$y_i(t) \leq [\sum_{l \in \mathcal{L}_{i,in}} z_l(t) + \sum_{j \in \mathcal{I}_{i,in}} \alpha_{ji}(t)] \cdot y_i(t) \leq A_i y_i(t), \quad (i \in V_1 \cup V_2, 1 \leq t \leq T) \tag{3.10}$$

in which the variant $\alpha_{ij}(t)$ denotes the number of interfering streams from transmitter i to receiver j. The definition of $\alpha_{ij}(t)$ is given as follows:

$$\alpha_{ij}(t) = y_j(t) \cdot \sum_{l \in \mathcal{L}_{i,out}}^{Rx(l) \neq j} z_l(t), \quad (j \in \mathcal{I}_i, 1 \leqslant i \leqslant N, 1 \leqslant t \leqslant T) \tag{3.11}$$

Reformulation. In order to convert the non-linear constraints into linear ones, we reformulate Eqs. (3.6) and (3.7) into the following. First, by imposing an upper bound (large constant) $B = \sum_{j\in\mathcal{I}_i} \sum_{k\in\mathcal{L}_{j,in}}^{Tx(k)\neq i} A_k$, and $B' = \sum_{j\in\mathcal{I}_i} \sum_{k\in\mathcal{L}_{j,out}}^{Tx(k)\neq i} A_k$, where $\mathcal{I}_i$ is the interference node set of link i, Eq. (3.6) can be converted into Eq. (3.12), and Eq. (3.7) can be converted into Eq. (3.13).

$$\sum_{l\in\mathcal{L}_{i,out}} z_l(t) + [\sum_{j\in\mathcal{I}_i} (\theta_{j,i}(t) \sum_{k\in\mathcal{L}_{j,in}}^{Tx(k)\neq i} z_k(t))] \leq x_i(t)\cdot A_i + (1-x_i(t))B, \quad (i\in\mathcal{V}_1\cup\mathcal{V}_2, 1\leq t\leq T) \tag{3.12}$$

$$\sum_{l\in\mathcal{L}_{i,in}} z_l(t) + [\sum_{j\in\mathcal{I}_i} (\theta_{j,i}(t) \sum_{k\in\mathcal{L}_{j,out}}^{Rx(k)\neq i} z_k(t))] \leq y_i(t)\cdot A_i + (1-y_i(t))B', \quad (i\in\mathcal{V}_1\cup\mathcal{V}_2, 1\leq t\leq T) \tag{3.13}$$

Then, we apply the Reformulation-Linearization Technique (RLT) [37] to transform the above to linear constraints. Specifically, define $\lambda_{j,i}(t) = \theta_{j,i}(t) \sum_{k\in\mathcal{L}_{j,in}}^{Tx(k)\neq i} z_k(t)$, Eq. (3.12) to be rewritten as:

$$\sum_{l\in\mathcal{L}_{i,out}} z_l(t) + \sum_{j\in\mathcal{I}_i} \lambda_{j,i}(t) \leq x_i(t)\cdot A_i + (1-x_i(t))B, \quad (i\in\mathcal{V}_1\cup\mathcal{V}_2, 1\leq t\leq T) \tag{3.14}$$

Because we also have $\theta_{j,i}(t)\geq 0$, $1-\theta_{j,i}(t)\geq 0$, $\sum_{k\in\mathcal{L}_{j,in}}^{Tx(k)\neq i} z_k(t)\geq 0$ and $A_j - \sum_{k\in\mathcal{L}_{j,in}}^{Tx(k)\neq i} z_k(t)\geq 0$, we can obtain the following linear constraints by multiplying them together:

$$\lambda_{j,i}(t) \geq 0, \tag{3.15}$$

$$\lambda_{j,i}(t) \leq A_j \cdot \theta_{j,i}(t), \tag{3.16}$$

$$\lambda_{j,i}(t) \leq \sum_{k \in \mathcal{L}_{j,in}}^{Tx(k) \neq i} z_k(t), \tag{3.17}$$

$$\lambda_{j,i}(t) \geq A_j \cdot \theta_{j,i}(t) - A_j + \sum_{k \in \mathcal{L}_{j,in}}^{Tx(k) \neq i} z_k(t), \tag{3.18}$$

for all $i \in \mathcal{V}_1 \cup \mathcal{V}_2, j \in \mathcal{I}_i, 1 \leq t \leq T$. Eqs. (3.14)-(3.18) are equivalent with Eq. (3.12). Similarly, define $\mu_{j,i}(t) = \theta_{j,i}(t) \sum_{k \in \mathcal{L}_{j,out}}^{Rx(k) \neq i} z_k(t)$, Eq. (3.13) can be replaced by:

$$\sum_{l \in \mathcal{L}_{i,in}} z_l(t) + \sum_{j \in \mathcal{I}_i} \mu_{j,i}(t) \leq y_i(t) \cdot A_i + (1 - y_i(t))B', \quad (i \in \mathcal{V}_1 \cup \mathcal{V}_2, 1 \leq t \leq T) \tag{3.19}$$

$$\mu_{j,i}(t) \geq 0, \tag{3.20}$$

$$\mu_{j,i}(t) \leq A_j \cdot \theta_{j,i}(t), \tag{3.21}$$

$$\mu_{j,i}(t) \leq \sum_{k \in \mathcal{L}_{j,out}}^{Rx(k) \neq i} z_k(t), \tag{3.22}$$

$$\mu_{j,i}(t) \geq A_j \cdot \theta_{j,i}(t) - A_j + \sum_{k \in \mathcal{L}_{j,out}}^{Rx(k) \neq i} z_k(t), \tag{3.23}$$

where $i \in \mathcal{V}_1 \cup \mathcal{V}_2, j \in \mathcal{I}_i, 1 \leq t \leq T$.

The constraint in (3.11) is also nonlinear. Again, by choosing a large constant $B \geqslant A_i$, we use RLT to transform it into two equivalent linear constraints:

$$0 \leqslant \sum_{\mathcal{L}_{i,out}}^{Rx(l) \neq j} z_l(t) - \alpha_{ij}(t) \leqslant (1 - y_j(t)) \cdot B, \quad (j \in \mathcal{I}_i, 1 \leqslant i \leqslant N, 1 \leqslant t \leqslant T) \tag{3.24}$$

$$0 \leqslant \alpha_{ij}(t) \leqslant y_j(t) \cdot B, \quad (j \in \mathcal{I}_i, 1 \leqslant i \leqslant N, 1 \leqslant t \leqslant T) \tag{3.25}$$

3.4.2 Formulation

The mathematical formulations of the throughput maximization problems with FIC and RIC are shown in Fig. 3.4 and Fig. 3.5 respectively, which are bi-criteria mixed-integer linear programing (MILP) problems. In the objective function, $h(\cdot)$ denotes network utility function.

As shown in the formulation, the objective is to maximize both networks' utilities simultaneously while satisfying all constraints. The optimization variables include: network 1 and 2's session rates $r(f)$ and $r(g)$, $\pi_i(t)$, $\theta_{ji}(t)$, $z_l(t)$, $x_i(t), y_i(t)$, and additional variables $\lambda_{ji}(t)$, $\mu_{j,i}(t)$ in the reformulated problem. The challenge is that even the single-objective version of the general MILP problem is NP-hard. We will show that this can be converted into multiple (a small number of) single-objective MILP problems, where there exists highly efficient optimal and approximation algorithms such as branch-and-bound with cutting planes [53], or heuristic algorithms such as sequential fixing algorithms [18] to solve it. We use the off-the-shelf solver CPLEX to solve the MILP problems in our case.

3.5 Pareto-Optimal Throughput Curve

In this section, we explore a novel approach to find the optimal throughput curve of two heterogeneous multi-hop MIMO networks. We consider the linear case[3] where $h[r(f)] = d_1 \cdot r(f)$ and $h[r(g)] = d_2 \cdot r(g)$, such that $\sum_{f \in \mathcal{F}_1} h[r(f)]$ and $\sum_{g \in \mathcal{F}_2} h[r(g)]$ represent the weighted throughput of each network, respectively. Here d_1, d_2 are two constants.

We want to find all the *Pareto-optimal* throughput pairs (u_1, u_2) where there does *not* exists another solution (u_1', u_2') such that $u_1' \geq u_1$ and $u_2' \geq u_2$. By fixing one objective $(u_1 = u_1^*)$ and finding the optimal value of the other (u_2), we will solve a single optimization

[3] Non-linear throughput functions will be our future work.

$$\max U_1 = \sum_{f \in \mathcal{F}_1} h[r(f)]$$
$$\max U_2 = \sum_{g \in \mathcal{F}_2} h[r(g)]$$
s.t. (for both networks)
Half duplex constraints:(3.4);
Node ordering constraints:(3.5);
Tx/Rx DoF constraints:$(3.14) - (3.18), (3.19) - (3.23)$;
Flow rate $\leq$ link capacity:(3.9);
Link capacity model:(3.8)

Fig. 3.4. Original bi-criteria optimization formulation with FIC (BOPT-FIC).

$$\max U_1 = \sum_{f \in \mathcal{F}_1} h[r(f)]$$
$$\max U_2 = \sum_{g \in \mathcal{F}_2} h[r(g)]$$
s.t. (for both networks)
Half duplex constraints:(3.4);
Node ordering constraints:(3.5);
Tx DoF constraints:$(3.14) - (3.18)$;
Rx DoF constraints:(3.10);
Interference degree:$(3.24, 3.25)$;
Flow rate $\leq$ link capacity:(3.9);
Link capacity model:(3.8)

Fig. 3.5. Original bi-criteria optimization formulation with RIC (BOPT-RIC).

problem:

$$OPT(u_1) : \max u_2, \tag{3.26}$$
$$\text{s.t. } u_1 = u_1^*, \text{and all constraints in BOPT-FIC/BOPT-RIC}$$

One can obtain a one-to-one mapping $u_2 = f(u_1)$ which defines an optimal throughput curve containing all the *weakly Pareto-optimal* points. A weakly Pareto-optimal point is a throughput pair (u_1, u_2) where there does *not* exist another solution (u_1', u_2') such that $u_1' > u_1$ and $u_2' > u_2$. A Pareto-optimal point is also weakly Pareto-optimal, but not vice

versa.

Since u_1 and u_2 are continuous, a naive approach to approximate the curve is to discretize $[0, u_{1,max}]$ into a large number of equal intervals, solve $OPT(u_1)$ for each discrete u_1, and connect the corresponding optimal values u_2 via line segments. However, each instance is an MILP problem (NP-hard in general), thus this method incurs high complexity and does not give any performance guarantee.

Instead of brute-force or trying approximation approaches, through exploiting the property of the curve itself we find that the exact curve can be obtained (under our formulation). Firstly, it is easy to see the curve is *non-increasing* with u_1, because when u_1 increases the interference to network 2 also increases. Interestingly, we have the following Theorem which gives the basis of our method:

Theorem 2. *When T is finite, the optimal throughput curve $u_2 = f(u_1)$ is a stair-shape non-continuous function, and the minimum unit stair width is $d_1 \cdot w_1/T$.*

This theorem means that we only need to compute the points on the curve where $u_1 = d_1 w_1 k/T, 0 \leq k \leq k_{max}$, and connect them using stair-shape line segments. Each computation corresponds to solving one $OPT(u_1)$ instance. But the following theorem shows it is not necessary to cover all $0 \leq k \leq k_{max}$:

Theorem 3. *There exists two special Pareto-optimal points $(u_{1s}, u_{2s}), (u'_{1s}, u'_{2s})$ on the optimal throughput curve that $u_{2s} = u_{2,max}$ and $u'_{1s} = u'_{1,max}$.*

Given theorem 3, we can further reduce computation complexity by first identifying two Pareto-optimal points on the curve (which can be obtained by only two instances of $OPT(\max\{u_1\})$ and $OPT(\max\{u_2\})$), then focusing on finding the curve points between them. Our method can also be extended to more than two networks, where the curve becomes multi-dimensional.

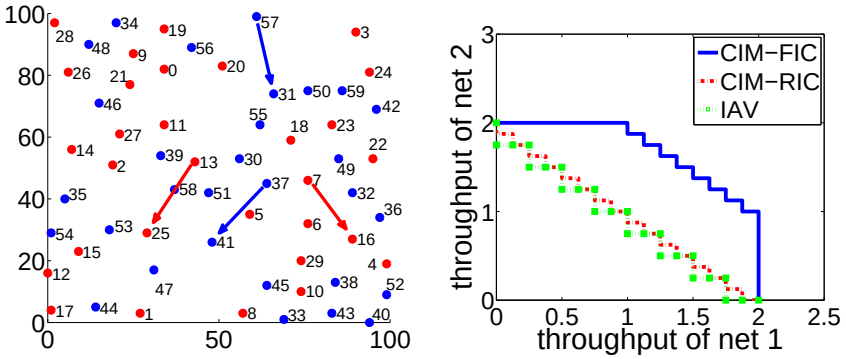

(a) (b)

Fig. 3.6. Flow setting and throughput curve. (a) Active flow sessions in two heterogeneous networks (blue: Net 1, red: Net 2). (b) The optimal throughput curve for the two networks under CIM and IAV.

3.6 Evaluation

In this section, we use numerical results to show the throughput gain by using our CIM with full IC and receiver-side IC. We compare our CIM paradigm with the interference-avoidance paradigm, where each network only cancels/mitigates the interference within itself but not to/from another network. We also examine the impacts of various types of interference scenarios and network heterogeneity.

3.6.1 A Case Study

We use a case study to show the gain brought by CIM paradigm. Consider two multi-hop networks (topology and sessions shown in Fig. 3.6 (a)) with 30 nodes each, deployed in a 100×100 area. Networks 1 and 2 both have two active sessions (8 active nodes in total) and min-hop routing is used. We assume both networks have two antennas for each node. For simplicity, assume $w_1 = w_2 = 1$ and $d_1 = d_2 = 1$. All nodes' transmission and interference ranges are 30 and 50, respectively. All networks coexist in one frequency band. Time is divided into 8 slots. We use CPLEX to solve for the exact solution of each $OPT(u_1)$ instance. The results are generated by an Intel 4 core i5-2400 with a 3.1GHz CPU and 8GB RAM.

The derived stair-shape curve is shown in Fig. 3.6 (b). The blue line denotes the

curve when using CIM with FIC, and the red line denotes the one using CIM with RIC. The throughput curve derived by IAV is drawn in green line. It can be seen that the minimum unit step is 1/8. Obviously, one can find that every point on the IAV's curve is Pareto-dominated by two points on CIM-FIC's and CIM-RIC's curves respectively, which verifies the large throughput gain from IAV. Besides, the throughput curve of CIM-FIC also dominates the one of CIM-RIC, which shows the performance enhancement brought by transmitter-side IC. All computations for the curve finished within a reasonable amount of time.

To verify the networks' cooperative behavior under CIM, we randomly pick a set of points from the curve with network 1's throughput equaling to 1.25.

In Table 3.1, we list the stream allocation during all the slots for all the links. In this table, 'x' denotes that no stream is allocated in the corresponding time slot. First, we can verify that all interferences are canceled. For example, in slot 2, links $37 \rightarrow 41, 13 \rightarrow 25$ are active in CIM-RIC. Both nodes use 1 out of their 2 total DoFs for SM. By analyzing the node ordering $\theta_{41,13}$ and $\theta_{37,25}$, we found that node 41 cancels the interference from node 13 while node 37 canceling its interference to node 25. We can see that no alignment is applied here. For CIM-FIC, using slot 2 as well, links $57 \rightarrow 31$, $37 \rightarrow 41$, $13 \rightarrow 25$ are active, with one stream transmitting on each link. We can see that the IAL is applied in this slot as node 31 receives one stream while dealing with the interferences from node 13 and 37 simultaneously. This is only possible when the two interfering streams are aligned in one direction, otherwise node 31 cannot handle three streams concurrently (1 receiving stream and 2 interfering streams) with only two antennas.

Various special points can be identified on this curve. For max-min fairness (MMF), the optimal throughput-pair obtained is $(1.5, 1.5)$ when using CIM-FIC, compared with $(1, 1)$ by using IAV. For proportional fairness, the optimal throughput-pair is also $(1.5, 1.5)$ due to the symmetric antenna numbers in our example (both networks have 2 antennas for each node).

3.6.2 Impact of Different Interference Degrees

We further compare CIM's performance with that of IAV's, by changing the extent to which both networks interfere with each other. For example, we change the distance between the two networks to study the interference's impact on throughputs.

In Fig. 3.7, we choose two scenarios containing one session in each network, while Fig. 3.8 illustrates two scenarios containing 2 sessions in each network. In Fig. 3.7 (a), the two sessions are far apart so as to not interfere with each other, while in Fig. 3.7 (b) they are near enough to severely interfere with each other. In Fig. 3.8 (a), the interference degree is approximately equal to that of Fig. 3.8 (b). We can observe in Fig. 3.7 (a), the curves derived by CIM and IAV are exactly the same. In contrast, the throughput ranges derived by CIM-FIC and CIM-RIC are larger than the one by IAV shown in Fig. 3.7 (b). The gaps between CIM and IAV are nearly the same in Fig. 3.8 (a) and Fig. 3.8 (b), though the CIM-RIC brings more benefits in (b) due to its slightly more-crowded network setting. These two sets of results successfully verified that FIC and RIC could enhance both networks' throughputs which coexist in the same space and frequency domain.

We randomly generate 50 scenarios to show the better performances brought by our CIM paradigms compared with the one using IAV in an average sense. We calculate the maximum overall throughput of both networks. Network 1 and Network 2 are equipped with 1 and 4 antennas respectively to reflect heterogeneity. All sessions are randomly generated within the range shown in Fig. 3.6 (a). The results are presented in Table. 3.2. It can be seen that the maximum overall throughputs under CIM paradigms are significantly larger than the ones under IAV in some cases. By using FIC and RIC, the overall throughput are never lower than the ones using IAV. Similar results can be obtained under other throughput-allocation criteria such as max-min or proportional fairness, which are not elaborated in this chapter.

3.6.3 Impact of Network Heterogeneity

We test our CIM paradigms in several other heterogeneous aspects, such as different transmit power/range and data rates. This heterogeneity exists in practical coexisting

Table 3.1. Link stream allocation in each slot

Sessions	Path Link	FIC Time Slot	FIC DoF of SM	Rate	RIC Time Slot	RIC DoF of SM	Rate
Session1-1	57 → 31	0	1	0.75	0	2	0.25
		2	1		x	x	
		4	1		x	x	
		5	1		x	x	
		6	1		x	x	
		7	1		x	x	
Session1-2	37 → 41	1	1	1	1	1	0.5
		2	1		2	1	
		3	1		4	1	
		4	1		5	1	
		5	1		x	x	
		6	1		x	x	
		7	1		x	x	
		8	1		x	x	
Session2-1	7 → 16	0	1	0.625	3	2	0.375
		1	1		6	1	
		3	1		x	x	
		4	1		x	x	
		5	1		x	x	
Session2-2	13 → 25	1	1	0.625	1	1	0.875
		2	1		2	1	
		3	1		4	1	
		6	1		5	1	
		7	1		6	1	
		x	x		7	2	

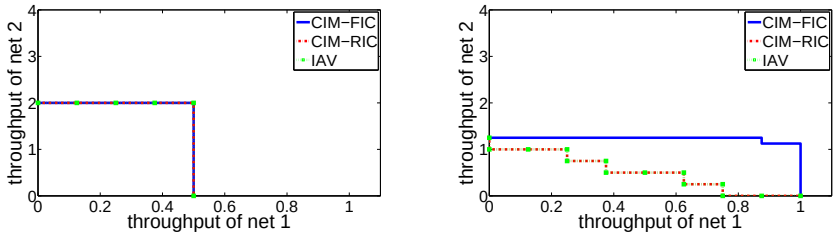

(a) (b)

Fig. 3.7. Throughput curves. (a) Network 1 has 1 session: 45 → 38 →52. Network 2 has 1 session: 26 → 0 → 20. (b) Network 1 has 1 session: 50 → 30. Network 2 has 1 session: 21 → 2 → 13 → 5.

environment, such as the coexisting of 802.11 with 802.15.4 networks.

In Fig. 3.9 (a), we set the transmission ranges for networks 1 and 2 as 20 and 40, and the interference ranges as 30 and 60, respectively. In Fig. 3.9 (b), we increase network 1's transmission range to 33, interference range to 50. One can see that both the throughput region and the gap between CIM and IAV enlarge in Fig. 3.9 (b). There are two insights: (1) Larger transmission range decreases hop count, thus increases one's own throughput;

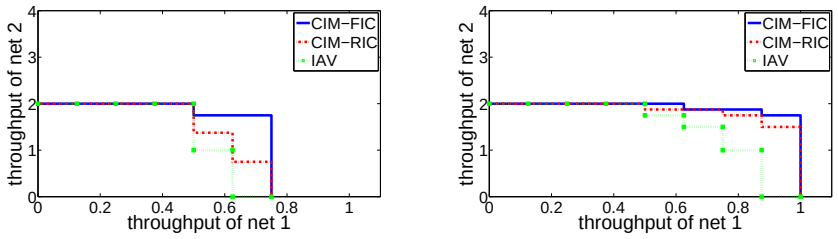

(a) (b)

Fig. 3.8. Throughput curves. (a) Network 1 has 2 sessions:35 → 53 → 47, 37 → 32 → 36. Network 2 has 2 sessions: 10 → 5 → 18, 12 → 1 → 25. (b) Network 1 has 2 sessions: 41 → 30 → 55, 48 → 34 → 56. Network 2 has 2 sessions: 8 → 10 → 4, 5 → 7 → 23.

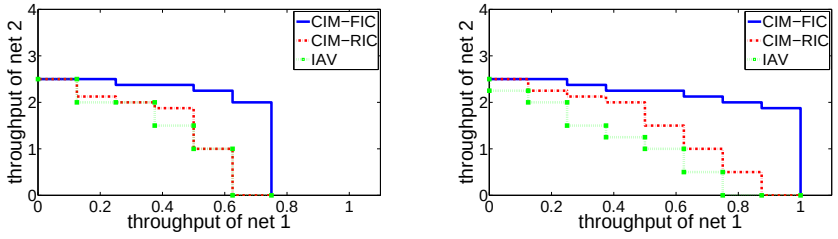

(a) (b)

Fig. 3.9. Throughput curves. (a) Network 1 has 2 sessions:39 → 51 → 41, 55 → 50 → 59 → 42. Network 2 has 2 sessions: 28 → 0 → 27, 10 → 5 → 18. In (b) Network 1 has 2 sessions:39 → 41, 55 → 31 → 42. Network 2 has 2 sessions: 28 → 0 → 27, 10 → 5 → 18. (a) the transmission ranges: (20,40), the interference ranges: (30,60). (b) the transmission ranges: (33,40), the interference ranges: (50,60).

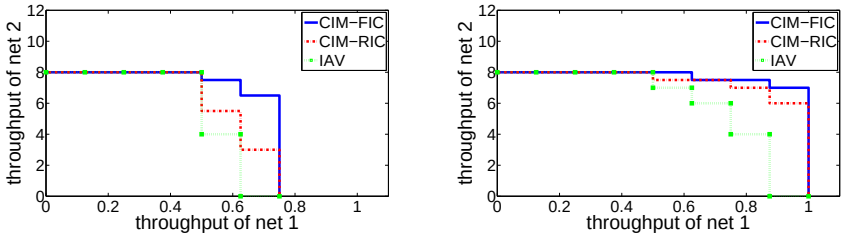

(a) (b)

Fig. 3.10. Throughput curves. (a) Network 1 has 2 sessions:35 → 53 → 47, 37 → 32 → 36. Network 2 has 2 sessions: 10 → 5 → 18, 12 → 1 → 25. (b) Network 1 has 2 sessions: 41 → 30 → 55, 48 → 34 → 56. Network 2 has 2 sessions: 8 → 10 → 4, 5 → 7 → 23.

(2) When the mutual interference degree is higher, more gains could be obtained by using CIM paradigms, thus making the coexisting networks more willing to cooperatively mitigate

Table 3.2. Max. total throughput comparison between CIM and IAV

Scenarios	CIM-FIC	CIM-RIC	IAV	Scenarios	CIM-FIC	CIM-RIC	IAV
0	3.25	2.5	2.5	25	4.25	4.25	4.25
1	4	4	4	26	4.25	4.25	4
2	6	6	6	27	4	4	4
3	5	5	5	28	4.5	4.5	4.5
4	4	4	4	29	2.5	2.5	2.5
5	2.75	2.5	2.5	30	4	4	4
6	9	9	9	31	6.5	6	6
7	4	4	4	32	2	2	2
8	4.25	4.25	4.25	33	5.25	5.25	5.25
9	8	8	8	34	3.5	3	3
10	2	2	2	35	4	4	4
11	4	4	4	36	5	5	5
12	6	6	6	37	2.5	2	2
13	3	2.625	2.5	38	4	4	4
14	4	4	4	39	2	2	2
15	5	5	5	40	3	3	3
16	4.25	4.25	4.25	41	4	4	4
17	2.25	2	2	42	4	4	4
18	5	5	5	43	4	4	4
19	6	6	6	44	4	4	4
20	4	4	4	45	5	5	5
21	2.125	2	1.875	46	4.5	4.5	4.5
22	4.25	4.25	4.25	47	5	5	5
23	2.125	2.125	2	48	8	8	8
24	5.25	5.25	5.25	49	2.5	2.5	2.5

the interference. For different data rates, suppose $w_2 = 4w_1$ (such as 1Mbps in WiFi and 250kbps in ZigBee) instead of $w_2 = w_1$. The results are shown in Fig. 3.10. Compared with Fig. 3.8, the throughput curve scales by a factor of 4 in the y-axis.

3.7 Summary

This chapter offered a thorough study of the cooperative cross-technology interference mitigation (CIM) paradigm for heterogeneous multi-hop networks in unplanned settings. The main technical challenges are due to the lack of a predefined network priority in unplanned deployments, and various forms of network heterogeneity. We first show that general technology-independent interference cancellation (TIIC) is feasible for heterogeneous

multi-hop networks with different protocol standards, and then introduce our two CIM models with different interference cancellation (IC) techniques. We characterize the performance bounds of CIM via deriving the Pareto-optimal throughput curve. Through extensive simulation results we show that the CIM paradigms with full IC and receiver-side IC can both offer significant performance gains in throughput to the coexisting networks compared with the traditional interference-avoidance (IAV) paradigm. The models and results in this chapter will guide practical CIM protocol design, and pave the way to ultimately change the coexistence paradigm for unplanned heterogeneous networks in unlicensed bands and TV white spaces. In the following chapters, we will investigate the incentives of cooperation for multiple independent networks, and study the coexisting problem with a game-theoretical approach.

CHAPTER 4
A GAME THEORETICAL APPROACH TO COEXISTENCE OF HETEROGENEOUS MIMO WIRELESS NETWORKS WITH INTERFERENCE CANCELLATION

4.1 Overview

In the previous chapter, we perform centralized optimization on the multi-hop networks coexistence problem. Our work assumes all coexisting entities are cooperative, i.e., they will follow the decisions made by our central controller. In fact, all previous algorithms and protocol design (e.g., 802.11 n+) have similar assumptions by considering all entities will follow the predefined algorithms or protocols unconditionally. However, the incentive of complying with such algorithm/protocols has never been studied, which is what we will conduct in this chapter. Our goal in this chapter is to adopt a new perspective to study the coexistence of heterogeneous wireless MIMO networks, by investigating each network's incentive to comply with/violate the underlying MAC protocols. To this end, we establish a new two-round game framework, which incorporates both the high-level cooperation strategy and the MAC-layer transmission strategies. We analytically derive the utility functions and the Nash equilibrium for both networks, based on a common DoF model. From numerical results, we gain several insights which are helpful in future wireless network design.

4.2 System Model

In this chapter, we consider a simple model with two single-link networks $\mathcal{N}_1(\mathcal{V}, \mathcal{E})$ and $\mathcal{N}_2(\mathcal{V}, \mathcal{E})$. Each network is considered as a player, and its nodes are coordinated by a central controller which can determine the strategy to adopt. Time is divided into slots and the interference graph is assumed to be known by both networks.

In our single-link coexistence problem, we assume each network first chooses whether

to be cooperative or non-cooperative. After that, both networks compete for the channel at each time slot and the winner could access the channel first with probability p_i. This network will act as leader to determine its low-level strategy first (in terms of DoF allocation). The other network j that accesses channel secondly must determine its low-level strategy as response based on network i's strategy which has already been made. Both networks are assumed to be non-malicious, i.e. each network will not intentionally generate interference to the other one.

4.3 Game Formulation

In this section, we propose the game formulation for our single-link coexistence problem. We assume each network has knowledge of both networks' DoF and interference-range information. We will derive both networks' optimal strategies and the Nash equilibrium.

4.3.1 Game Framework

As the 'cooperative/non-cooperative strategy' and 'DoF allocation' are logically in two different levels, we need to split them in our game framework. We model our problem as a 2-level game played in 2 rounds separately. In the first round, the strategy space is {'Cooperative','Non-cooperative'}. The strategy in this round corresponds to the decision made on top of MAC-layer protocols. In the second round, the strategy space is DoF allocation for SM and IC. The second round strategy corresponds to the decisions made at the MAC layer. The second-round's strategy space is split into four sub-spaces by using the first-round strategies as constraints. Our two-round game is illustrated in Figs. 4.2.

4.3.2 First-round Game

Strategy Space

The first-round game is modeled as a static game. The strategy space of the first-round game is {'Cooperative','Non-cooperative'}. In this round, each network determines whether to comply with the underlying MAC protocol. By choosing 'Cooperative' strategy, it will

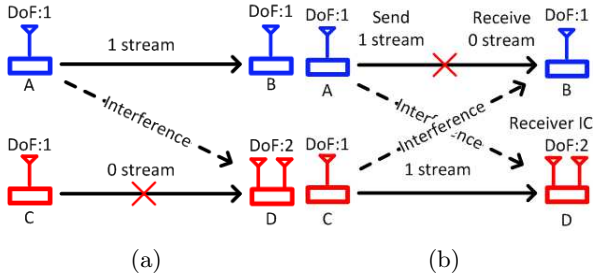

Fig. 4.1. Throughput comparison with cooperative and non-cooperative coexisting networks. (a) network 1 (nodes A, B) accesses channel first, and network 2 complies with the 802.11n+ protocol. (b) network 1 accesses channel first, and network 2 selfishly violates the 802.11 n+ protocol.

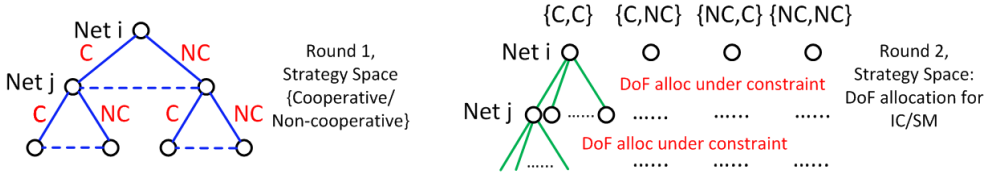

Fig. 4.2. Detail formulation of the first and second round games

transmit its own streams without generating interference to the other network which accesses the channel before it. By choosing 'Non-cooperative', it maximizes its own throughput without considering its interference to the other network.

Utility

In this round, the utility $U_i(X, Y)$ is the expected throughput of network i under a certain first-round strategy pair (X, Y), in which X and Y are network 1 and 2's first-round strategies respectively. As in the first round, the strategy space has two elements: cooperative, non-cooperative. So in the second-round game, it has $2 * 2 = 4$ possible constraints. Each element is explained in Eq. (4.1).

$$\begin{aligned} U_i(C,C) &= p_i \cdot U_{iL}(C,C) + p_j \cdot U_{iF}(C,C) \\ U_i(NC,C) &= p_i \cdot U_{iL}(NC,C) + p_j \cdot U_{iF}(NC,C) \\ U_i(C,NC) &= p_i \cdot U_{iL}(C,NC) + p_j \cdot U_{iF}(C,NC) \\ U_i(NC,NC) &= p_i \cdot U_{iL}(NC,NC) + p_j \cdot U_{iF}(NC,NC) \end{aligned} \tag{4.1}$$

In Eq. (4.1), p_i denotes the probability that network i accesses channel first. $U_{iL}(X,Y)$, $U_{iF}(X,Y)$ denote network i's throughputs when it acts as leader or follower under the constraints of first-round strategy (X,Y).

4.3.3 Second-round Game

The second-round game is modeled as a Stackelberg Game. At any time slot, both networks compete and then one of them wins the priority to access the channel. Therefore, it will act as the leader to determine its strategy first. Meanwhile, the other network will choose its strategy as a follower. Each network tries to maximize its own utility.

Strategy Space

The strategy space includes the selection of DoFs used for SM with the remaining used for IC. The selection of the second-round strategy should be under the constraint of the first-round strategy. Specifically, the DoFs used in SM and IC should be subjected to the 'cooperative/non-cooperative' strategy chosen in the first-round game.

Utility

The utility of the second-round game is the successfully received number of streams. E.g. assume network i firstly sends M streams. It could receive M streams iff $M \leqslant B$ (B denotes the DoF number of network i's receiver) while coexisting with a cooperative follower, or $M+N \leqslant B$ with a non-cooperative follower, where N is the number of streams transmitted by the other network j. In the above cases, we have $U_{iL} = M$. Otherwise, $U_{iL} = 0$.

4.3.4 Equilibrium

Next we analyze the equilibrium of our two-round game. We will show that in each round there is an equilibrium. The derivation of final equilibrium is by using backward-induction, as the equilibrium of the first-round game depends on the equilibrium of the

second-round game. Therefore, first we will analyze the equilibrium of the second-round game.

Second-round Game's Equilibrium

Assume that network 1 has A and B antennas at transmitter and receiver, and network 2 has C and D at transmitter and receiver. Without losing generality, we assume network 1 is leader and network 2 is follower. First we define the interference function $r(t_i, r_j)$.

$$r(t_i, r_j) = \begin{cases} 1 & \text{if } r_j \text{ is in } t_i\text{'s interference range} \\ 0 & \text{if } r_j \text{ is out of } t_i\text{'s interference range} \end{cases} \tag{4.2}$$

As defined in Eq. (4.2), we use $r(t_i, r_j)$ to denote the interference impact from transmitter t_i to receiver r_j.

Follower Cooperative Case: First assume the follower network 2 is cooperative. We use $S_{iL}(X, Y)$ and $S_{iF}(X, Y)$ to denote network i's number of transmitted streams being as leader/follower respectively. Then it is easy to see that the leader network 1 will choose $S_{1L}(C/NC, C) = min(A, B)$ to maximize its utility. Here C/NC denotes that network 1's first-round strategy could be either cooperative or non-cooperative. Meanwhile, network 2 will try to cancel its interference to network 1's receiver by using IC. Assuming network 1 chooses its optimal strategy $S^*_{1L}(C/NC, C) = min(A, B)$, then the network 2's optimal strategy could be derived as $S^*_{2F}(S^*_{1L}(C/NC, C), C/NC, C) = max[0, min(D - min(A, B) \cdot r(t_1, r_2), C - min(A, B) \cdot r(t_2, r_1))]$. These optimal strategies for networks 1 and 2 are equilibriums in the cooperative follower case.

Follower Non-cooperative Case: Second we consider the non-cooperative follower case. This case is more complex than the cooperative case because the non-cooperative follower will ignore its interference to the leader's receiver, thus the leader's utility is affected by the follower's response. For simplicity, in this subsection we use S_{1L} to denote $S_{1L}(C/NC, NC)$, and S_{2F} to denote $S_{2F}(S_{1L}(C/NC, NC), C/NC, NC)$. First we could derive the follower network's best response function.

Lemma 2. *The best response of the non-cooperative follower network* 2 *is* $S^*_{2F}(S_{1L}) = max(0, min(D - S_{1L} \cdot r(t_1, r_2), C))$.

The proof is omitted. As the follower is considered to be non-malicious, so its utility equals its strategy in terms of quantity, i.e. $U_{2F} = S^*_{2F}(S_{1L})$.

We also derive the leader's utility function given the follower's arbitrary response:

Lemma 3. *The leader network* 1*'s utility function in the presence of the non-cooperative follower network* 2 *is* $U_{1L}(C/NC, NC) = S_{1L} \cdot f(B - S_{1L} - S_{2F}(S_{1L}) \cdot r(t_2, r_1))$,

$$f(x) = \begin{cases} 1 & \text{if } x \geqslant 0 \\ 0 & \text{if } x < 0 \end{cases}$$

If we substitute the follower's optimal response shown in Lemma 2 into 3, we could derive the leader's utility under the follower's optimal response:

$$\begin{aligned} U_{1L}(C/NC, NC) = & S_{1L} \cdot f(B - S_{1L} - max(0, \\ & min(D - S_{1L} \cdot r(t_1, r_2), C)) \cdot r(t_2, r_1)) \end{aligned} \tag{4.3}$$

From this utility function in Eq. (4.3), we could derive the optimal leader's strategies in different interference-range cases:

Lemma 4. *Assuming both networks are in a single collision domain, i.e.* $r(t_1, r_2) = 1, r(t_2, r_1) = 1$. *The optimal leader strategy* S^*_{1L} *of network* 1 *is:*

$$S^*_{1L} = \begin{cases} min(A, B) & \text{if } B \geqslant D \\ max(0, B - C) & \text{if } B < D \end{cases} \tag{4.4}$$

By now we have derived the equilibriums in both cooperative-follower and non-cooperative-follower cases. The utilities of both networks under second-round equilibrium in the single-collision-domain scenario are shown in Eq. (4.5).

$$
\begin{aligned}
&U_{1L}(C/NC, C) = min(A, B) \\
&U_{2F}(C/NC, C) = max[0, min(D - min(A, B), C - min(A, B))] \\
&U_{2L}(C, C/NC) = min(C, D) \\
&U_{1F}(C, C/NC) = max[0, min(A - min(C, D), B - min(C, D))] \\
&U_{1L}(C/NC, NC) = f(B, D) \cdot min(A, B) + (1 - f(B, D)) \\
&\cdot max(0, B - C) \\
&U_{2F}(C/NC, NC) = max[0, min(D - [f(B, D) \cdot min(A, B) \\
&+ (1 - f(B, D)) \cdot max(0, B - C)], C)] \\
&U_{2L}(NC, C/NC) = f(D, B) \cdot min(C, D) + (1 - f(D, B)) \\
&\cdot max(0, D - A) \\
&U_{1F}(NC, C/NC) = max[0, min(B - [f(D, B) \cdot min(C, D) \\
&+ (1 - f(D, B)) \cdot max(0, D - A)], A)]
\end{aligned}
\tag{4.5}
$$

Using similar analysis approaches, we could derive the second-round equilibrium under other conflict-graph scenarios, in which $r(t_i, r_j) = 1$ or 0, for $\forall i, j$. Due to space limitations, these analyses are omitted in this section.

Theorem 4. *$(S^*_{1L}, S^*_{2F}(S^*_{1L}))$ is the equilibrium of the second-round game in non-cooperative follower case, where S^*_{1L} and $S^*_{2F}(S_{1L})$ are defined in Lemma. 4 and 2 respectively.*

First-round Game Equilibrium

Theorem 5. *For the outer level game, (NC, NC) is always an equilibrium.*

Subgame Perfect Nash Equilibrium

A subgame of a game is a sub-tree which begins at an information set containing only one decision node. All decision nodes following the initial node belong to the subgame.

The Subgame Perfect Nash Equilibrium denotes a set of strategies which forms a Nash Equilibrium in every subgame. For our two-round game, we can prove that there exists a Subgame Perfect Nash Equilibrium (SPNE). The SPNE is shown in Theorem 6.

Theorem 6. *The SPNE of our game is* $(NC \quad \overline{\boldsymbol{S}^*_{1L}}(X,Y)), \quad NC \quad \overline{\boldsymbol{S}^*_{2F}}(\overline{\boldsymbol{S}_{1L}}(X,Y),X,Y))$*, in which* (X,Y) *denotes network* 1 *and* 2*'s first-round strategy.*

Based on our utility and equilibrium analysis, we could infer each network's incentive of cooperation.

Corollary 1. *1) Assuming network* 1 *has* A *and* B *antennas on transmitter and receiver, and network* 2 *has* C *and* D *antennas. If* $B \geqslant min(C,D) + min(A,B)$*, then network* 1 *always has the incentive to behave non-cooperatively.*

4.4 Numerical Results

4.4.1 Overview

In this section, we first use two examples to study the leader's utilities under follower's optimal response in the second round. Then we study the first-round equilibriums under different network settings.

4.4.2 Second-round Equilibrium Numerical Results

In Fig. 4.3, we show both networks' utilities under leader's different strategies, while assuming the follower network uses its optimal response. Based on our analysis (e.g. Lemma 4), the optimal leader's strategy is $S^*_{1L}(C/NC, C) = 3$ for cooperative follower and $S^*_{1L}(C/NC, NC) = 1$ for non-cooperative follower in the subfigure (a)'s setting, and $S^*_{1L}(C/NC, C) = 3$ for cooperative follower and $S^*_{1L}(C/NC, NC) = 0$ for non-cooperative follower in the subfigure (b)'s setting. From the results, we can see that the leader achieves its maximum utility by choosing the optimal strategy derived from our theoretical analysis.

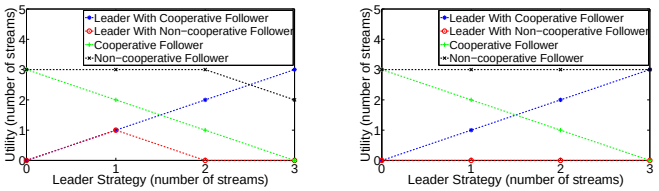

(a) (b)

Fig. 4.3. The leader network 1's second-round utilities by choosing different strategies. (a) $A = 3, B = 4, C = 3, D = 5$, $r(t_1, r_2) = r(t_2, r_1) = 1$. (b) $A = B = C = D = 3$, $r(t_1, r_2) = 0, r(t_2, r_1) = 1$.

4.4.3 Cooperation Incentives

We choose different numbers of antennas, and different conflict graphs to evaluate each network's cooperation incentives under different settings.

Unbalanced DoF Scenario

We analyzed the unbalanced DoF scenario. In this scenario, the antenna numbers of the two networks are unbalanced. From the results in Table 4.1, 4.2, 4.3, we can see that the network with more receiving antennas (network 2 in Table 4.2 and network 1 in Table 4.3) has incentive to be non-cooperative, while the network with less receiving antennas has no incentive to be non-cooperative.

Table 4.1. The utilities in equilibrium of second-round game in unbalanced DoF scenario

	A=2;B=2;C=3;D=3; $r(t_1, r_2) = 1$; $r(t_2, r_1) = 1$;	A=2;B=5;C=3;D=3; $r(t_1, r_2) = 1$; $r(t_2, r_1) = 1$
$U_{1L}(C/NC, C)$	2	2
$U_{2F}(C/NC, C)$	1	1
$U_{2L}(C, C/NC)$	3	3
$U_{1F}(C, C/NC)$	0	0
$U_{1L}(C/NC, NC)$	0	2
$U_{2F}(C/NC, NC)$	3	1
$U_{2L}(NC, C/NC)$	3	1
$U_{1F}(NC, C/NC)$	0	2

Table 4.2. The utilities in equilibrium of first-round game in unbalanced DoF scenario with $A = B = 2, C = D = 3$, $r(t_1, r_2) = 1$, $r(t_2, r_1) = 1$

	Net 2, Cooperate	Net 2, Non-cooperate
Net 1, Cooperate	$(1, 2)$	$(0, 3)$
Net 1, Non-cooperate	$(1, 2)$	$(0, 3)$

Table 4.3. The utilities in equilibrium of first-round game in unbalanced DoF scenario with $A = 2, B = 5, C = D = 3$, $r(t_1, r_2) = 1$, $r(t_2, r_1) = 1$

	Net 2, Cooperate	Net 2, Non-cooperate
Net 1, Cooperate	$(1, 2)$	$(1, 2)$
Net 1, Non-cooperate	$(2, 1)$	$(2, 1)$

Unbalanced Interference Scenario

The second scenario is the unbalanced-interference scenario. The results are shown in Tables. 4.4 ,4.5, 4.6. In this case, we place network 1's receiver far away from network 2's transmitter. Therefore, network 1 is not interfered by network 2's transmission. From the results, we can see that network 1 always has incentive to be non-cooperative. Especially, for the $A = B = C = D = 1$ case, it corresponds to the traditional single-antenna case.

Table 4.4. The utilities in equilibrium of second-round game in unbalanced interference scenario

	A=2;B=2;C=2;D=2; $r(t_1, r_2) = 1$; $r(t_2, r_1) = 0$	A=1;B=1;C=1;D=1; $r(t_1, r_2) = 1$; $r(t_2, r_1) = 0$
$U_{1L}(C/NC, C)$	2	1
$U_{2F}(C/NC, C)$	0	0
$U_{2L}(C, C/NC)$	2	1
$U_{1F}(C, C/NC)$	0	0
$U_{1L}(C/NC, NC)$	2	1
$U_{2F}(C/NC, NC)$	0	0
$U_{2L}(NC, C/NC)$	0	0
$U_{1F}(NC, C/NC)$	2	1

Several insights can be found from the results. We can see that more receiving antennas gives a network the incentive to be non-cooperative as it can make the network less likely to be affected by the other network. Also, the network whose receiver is beyond the other

Table 4.5. The utilities in equilibrium of first-round game in unbalanced interference scenario with $A = B = C = D = 2$, $r(t_1, r_2) = 1$, $r(t_2, r_1) = 0$

	Net 2, Cooperate	Net 2, Non-cooperate
Net 1, Cooperate	$(1, 1)$	$(1, 1)$
Net 1, Non-cooperate	$(2, 0)$	$(2, 0)$

Table 4.6. The utilities in equilibrium of first-round game in unbalanced interference scenario with $A = B = C = D = 1$, $r(t_1, r_2) = 1$, $r(t_2, r_1) = 0$

	Net 2, Cooperate	Net 2, Non-cooperate
Net 1, Cooperate	$(0.5, 0.5)$	$(0.5, 0.5)$
Net 1, Non-cooperate	$(1, 0)$	$(1, 0)$

transmitter's interference range has the incentive to be non-cooperative as it will not be affected by the other network. More results can be found in our technical report [54].

4.5 Summary

In this chapter, we study the coexistence problem of MIMO wireless networks. Different from previous works, we focus on this problem from a new point of view at a higher level: the incentive of complying with/violating the underlying MAC protocols. We establish a new multi-level game framework which incorporates both the high-level cooperative/non-cooperative strategies, and the low-level DoF allocation strategies. The game is played in two rounds, in which the first round is modeled as a static game and the second round is modeled as a Stackelberg game. Both the utilities and strategies in equilibrium are analyzed and derived in this chapter. By studying the equilibriums in different scenarios, we have insights of the cooperation incentives in the coexistence of single-link MIMO wireless networks. In the following chapter, we will study the coexistence game in the multi-hop network case.

CHAPTER 5

GAME THEORETICAL ANALYSIS OF COEXISTENCE IN MIMO-EMPOWERED COGNITIVE RADIO NETWORKS

5.1 Overview

In this chapter, we will study the coexistence problem in MIMO empowered multi-hop cognitive radio networks (CRNs) using game theoretical approach. We will analyze both the primary and secondary networks' optimal strategies in the coexistence game. We study two types of secondary networks categorized by their cooperative behaviors: 1) type-1 secondary network, which is selfish-compliant in following the spectrum-accessing rules without generating interferences to the primary network; 2) type-2 secondary network, which is selfish-non-compliant meaning that it non-compliantly maximizes its own throughput without controlling its interference to the primary network. We derive the equilibriums of both primary and each of the two types of secondary networks respectively. Our numerical results imply that the multi-hop secondary networks always have incentive to play type-2. Through analyzing its strategy by decomposing our algorithms, we unveil some insights in dealing with such type of multi-hop secondary networks.

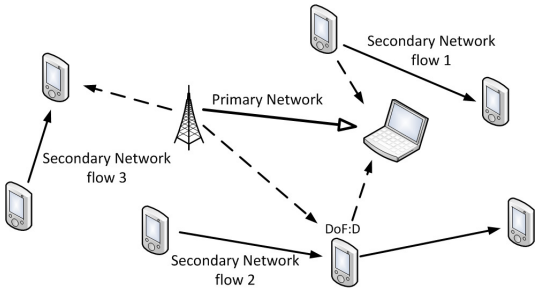

Fig. 5.1. Coexistence example: a single-link primary network coexists with a multi-hop and multi-flow secondary network

5.2 System Model

We assume a single-link primary network $\mathcal{N}_p(\mathcal{V}_p, \mathcal{E}_p)$ coexists with a general multi-hop secondary network $\mathcal{N}_s(\mathcal{V}_s, \mathcal{E}_s)$ with multiple flows. Each network has MIMO capability [22], using which each device could perform IC to mitigate interference from/to any other device and SM to transmit multiple streams concurrently. Each network is considered as a player, and its nodes are coordinated by a central controller which determines what strategy to adopt. Both controllers have the complete information about their own network topologies respectively. In addition, the primary network's controller also has the complete selfish-type, topology and flow information of the secondary network. The interference graph is assumed known by both networks. Both networks coexist within a single frequency band. We assume the primary and secondary networks could arbitrarily select their strategies in terms of the number of spatial-multiplexing DoFs and interference-cancellation DoFs. As multi-hop network is considered, we divide time into a number of discrete time slots $t \in \{1, 2..T\}$. However, the primary network is not as agile as the secondary network, i.e., it is not capable of swiftly changing its strategy in each time slot.

We assume that the primary network always accesses the spectrum first by freely selecting its accessing strategy, and the secondary network determines its spectrum access responsive strategy afterwards. Two types of secondary networks are studied, which are 1) type-1: selfish-compliant network meaning that the secondary network aims at maximizing its throughput without generating interference to the primary network, and 2) type-2: selfish-non-compliant network meaning that the secondary network maximizes its own throughput regardless of its interference to the primary network. We assume each network's device could have arbitrary number of antennas.

5.3 Game Theoretical Analysis

In CRNs, the primary network always has the priority in spectrum access. Therefore, our game is formulated as a Stackelberg game, in which the primary network makes spectrum access decision first, and the secondary network makes its decision afterwards. Each network tries to maximize its throughput. We will study a general multi-hop case,

Table 5.1. Major Notations

$s_p, \boldsymbol{s}_s$	strategy of primary and secondary network
$\theta_{i,j}(t), \pi_i(t)$	relative and global cancellation ordering on nodes i, j
$z_l(t)$	number of streams sent on link l in time slot t
u_p, u_s	primary and secondary network's utility

in which the primary network coexists with the secondary network, in the type of either selfish-compliant or selfish-non-compliant.

The multi-hop secondary-network case is more complicated than the single-link case. This is mainly due to the intricacy of link scheduling in multi-hop networks. We will show that though we cannot express the optimal response strategy in closed-form, we can still derive the optimal response strategy of the secondary network through solving a mixed integer linear programming (MILP) problem. Based on the optimal response, we can further derive the optimal leading strategy of the primary network through an algorithm, in which we calculate the interference degree generated by the secondary network and then check each primary network strategy's feasibility.

5.3.1 Strategy Space

For the single-link primary network, the strategy $s_p = z_{l_p}$ denotes the number of DoFs spent on transmitting streams concurrently on link l_p, which should be bounded by its antenna number $min(A_{p_t}, A_{p_r})$. We assume the primary network's receiver uses the remaining DoFs for receiver-side IC to mitigate the possible interferences back from secondary network.

For the secondary network, the strategy $\boldsymbol{s}_s = [\boldsymbol{z}_{l_0} ... \boldsymbol{z}_{l_L}]$, where $\boldsymbol{z}_{l_k} = [z_{l_k}(0), ... z_{l_k}(T)]$, $k \in \{0, ...L\}$ denotes the number of streams transmitted in each time slot $t \in \{0, ...T\}$ on each link l_k. The remaining DoFs are used for performing interference cancellation at both the transmitter and receiver sides. Similarly, the secondary network's strategy should also be bounded by the antenna number on each of its devices. In addition, it should also satisfy several intra-network constraints [50] including half-duplex, node ordering, transmitter-side

and receiver-side IC constraints to guarantee the strategy's feasibility:

$$x_i(t) + y_i(t) \leq 1 \qquad (i \in \mathcal{V}_s, 1 \leq t \leq T) \tag{5.1}$$

$$\pi_i(t) - N \cdot \theta_{j,i}(t) + 1 \leq \pi_j(t) \leq \pi_i(t) - N \cdot \theta_{j,i}(t) + N - 1, \quad (i, j \in \mathcal{V}_s, 1 \leq t \leq T) \tag{5.2}$$

$$x_i(t) \leq \sum_{l \in \mathcal{L}_{i,out}} z_l(t) + [\sum_{j \in \mathcal{I}_i,} (\theta_{j,i}(t) \sum_{k \in \mathcal{L}_{j,in}}^{Tx(k) \neq i} z_k(t))] x_i(t) \leq A_i x_i(t), \quad (i \in \mathcal{V}_s, 1 \leq t \leq T) \tag{5.3}$$

$$y_i(t) \leq \sum_{l \in \mathcal{L}_{i,in}} z_l(t) + [\sum_{j \in \mathcal{I}_i} (\theta_{j,i}(t) \sum_{k \in \mathcal{L}_{j,out}}^{Rx(k) \neq i} z_k(t))] y_i(t) \leq A_i y_i(t), \quad (i \in \mathcal{V}_s, 1 \leq t \leq T) \tag{5.4}$$

The variables $x_i(t), y_i(t)$ denote whether node i sends or receives at time slot t. $z_l(t)$ denotes the number of streams sent on link l. $\theta_{i,j}$ denotes the cancellation order between node i and j. $\pi_i(t)$ denotes the global cancellation order of node i. A_i is the antenna number parameter at node i. $\mathcal{I}_i$ denotes the interference set of node i. $\mathcal{L}_{i,in}$ and $\mathcal{L}_{i,out}$ denote node i's inward and outward link sets. The constraint (5.1) requires each node to be half-duplex thus can not send and receive simultaneously. The node ordering constraint in (5.2) is used to establish a cancellation order for each pair of nodes, which ensures the feasibility of the stream transmitting strategy $\boldsymbol{s}_s$. Constraints (5.3)(5.4) guarantee that the overall number of DoFs used for spatial multiplexing and interference cancellation at each node

should be bounded by its antenna number. Through these constraints, we can guarantee the secondary network stream-transmitting strategy's feasibility inside its network.

5.3.2 Utility

The utility u_p and u_s is the total number of streams successfully transmitted on all flows in all time slots for the primary and secondary networks respectively. When calculating the utilities, we should take the other network's strategies into account, as these strategies could generate external interferences. For the secondary network, as it could have multiple flows $f \in \mathcal{F}_s$ each with multi-hops where $\mathcal{F}_s$ denotes the set of flows in secondary network, its utility is defined as the summation of all flows' rates $r(f)$ which is the time-average throughput of this flow. We denote its utility as $u_s = \sum_{f \in \mathcal{F}_s} r(f)$. We will show how to derive its utility under the interferences from primary network in next subsection. For the leading primary network, its utility is defined as:

$$u_p(\boldsymbol{s}_s, s_p) = \begin{cases} s_p & \text{if } s_p + \mu_{r_p}(\boldsymbol{s}_s) < A_{r_p} \\ 0 & \text{if } s_p + \mu_{r_p}(\boldsymbol{s}_s) > A_{r_p} \end{cases} \tag{5.5}$$

where $\mu_{r_p}(\boldsymbol{s}_s)$ denotes the maximum total number of interference received back from the secondary network. (5.5) denotes that the primary network's utility is 0 if it is interfered with by the secondary network. This is because we assume primary network's QoS should be always guaranteed.

5.3.3 Equilibrium

We will first analyze the optimal response strategy of the secondary network. After that we will derive the optimal leading strategy of the primary network and finally the equilibrium.

Type-1 Multi-hop Secondary Network

When dealing with the type-1 secondary network, the primary network's optimal strategy is shown in lemma 5.

Lemma 5. $s_p^* = min(A_{t_p}, A_{r_p})$

Proof. The proof is very straightforward, as the primary network knows the complete information of the secondary network's compliant behaviors, it should choose to transmit as many streams as it could. □

For the optimal response, given any primary network's strategy, the secondary network will choose its strategy without generating interference to the primary network. Different from the single-link case, it is more difficult to derive the closed-form expression of the optimal response. However, we show that the optimal response could be derived through solving a MILP problem (ORT1), which is very similar to that in [55]. To use their optimization model, we need to set $z_{l_p}(t) = s_p^*, \forall t$. The optimization solution and result are the secondary network's optimal response and utility respectively against primary network's optimal strategy.

Lemma 6. *The solution of problem ORT1 is the optimal response of type-1 secondary network* $\boldsymbol{s}_s^*(s_p^*)$ *against primary network's optimal strategy* s_p^*.

Proof. According to the model in [55], the secondary network takes the primary network's transmitted streams into its transmitter-side constraint, thus the primary network is not interfered with. □

Theorem 7. $(s_p^*, \boldsymbol{s}_s^*(s_p^*))$ *is the equilibrium of the type-1 secondary-network follower case, where* s_p^* *and* $\boldsymbol{s}_s^*(s_p^*)$ *are defined in Lemma. 5 and Lemma. 6 respectively.*

Type-2 Multi-hop Secondary Network

The type-2 secondary network follows no predefined rule, thus it does not manage its interference towards the primary network. We first need to establish the model of our coexistence problem. The first one is primary network's strategy. Similar as defined in the type-1 case, we use z_{l_p} to denote the number of streams sent on primary link l_p:

$$z_{l_p}(t) = s_p, \quad \forall t \tag{5.6}$$

The second one is the canceling order constraint, in which we let all nodes in secondary network $\mathcal{N}_s$ to cancel the interferences from primary network's transmitter p_t.

$$\theta_{p_t,i} = 1, \quad \forall i \in \mathcal{N}_s \tag{5.7}$$

The secondary network also needs to satisfy all the constraints in (5.1) (5.2) (5.3) to guarantee the solution feasibility. In addition, the secondary network needs to cancel the interference generated by primary network's strategy s_p by adding it into its receiver-side constraint:

$$y_i(t) \leq \sum_{l \in \mathcal{L}_{i,in}} z_l(t) + [\sum_{j \in \mathcal{I}_i} (\theta_{j,i}(t) \sum_{k \in \mathcal{L}_{j,out}}^{Rx(k) \neq i} z_k(t)) + \theta_{p_t,i}(t) z_{l_p}(t)] y_i(t) \leq A_i y_i(t), \quad (i \in \mathcal{V}_s, 1 \leq t \leq T) \tag{5.8}$$

Note that we do not change the transmitter-side constraint in (5.3) as the secondary network is selfish-non-compliant thus it does not control its interference to the primary network. We have link capacity constraint (5.9) and flow-rate constraint (5.10) to calculate the secondary network's throughput utility. c_l denotes link l's capacity. $r(f)$ denotes rate on flow f.

$$c_l = \frac{1}{T} \sum_{t=1}^{T} z_l(t), \quad (\forall l \in \mathcal{L}_s, 1 \leq t \leq T) \tag{5.9}$$

$$r(f) \leqslant c_l \quad (\forall l \in f, f \in \mathcal{F}_s) \tag{5.10}$$

To derive the equilibrium, we start from secondary network's optimal-response strategy. The definition of the ORS2 problem is shown in Fig. 5.2.

Lemma 7. *Solution of problem ORS2(s_p) is the type-2 secondary network's optimal response strategy $\boldsymbol{s}_s^*(s_p)$ under arbitrary primary network's strategy s_p. The objective value is*

$$\max\ u_s = \sum_{f \in \mathcal{F}_s} r(f)$$

s.t.

Primary network strategy constraint(5.6)
Cancelling ordring constraint(5.7)
Half duplex constraint(5.1)
Node ordering constraints(5.2)
Tx DoF constraints: no IC to primary netwok(5.3)
Rx DoF constraints (5.8)
Link capacity model(5.9)
Flow rate $\leq$ link capacity(5.10)

Fig. 5.2. Optimal response of the secondary network (ORS2(s_p)) given primary network's strategy

the secondary network's maximum utility u_s^* *under* $\boldsymbol{s}_s^*(s_p)$.

Proof. The canceling-order constraint (5.7) and transmitter-side constraint (5.3) guarantees the secondary network does not take the primary network's receiver into account when performing transmitter-side IC. Therefore, the response is selfish-non-compliant. □

We have shown that the optimal response of the secondary network could be derived through solving a mixed-integer-nonlinear-programming (MINLP) problem shown in Fig. 5.2. Through comparing the formulations of ORS2 and ORS1, we could find that in ORS2, the strategy space is loosened as no transmitter-side IC is considered towards the primary network. We reformulate our problem into a mixed-integer-linear-programming (MILP) problem, which is NP-hard in general. To solve this problem, we choose IBM's CPLEX solver, which is based on branch and bound technique. We will leave the more-efficient approximation approach in future work. The remaining problem is how to derive the optimal primary network's strategy. To derive primary network's optimal strategy, we first need to know the primary network's utility under secondary network's interference in return, which could be derived by Alg. 3. Using Alg. 3 as a building block, we derive the optimal leader's strategy through Alg. 4.

Algorithm 3 Calculating primary network's utility under secondary network's strategy

input: Network topology G, secondary network's strategy $\boldsymbol{s}_s$; primary network's strategy s_p
output: Primary network's utility u_p

for $t = 1 : T$ **do**
  $\mu_{r_p,t} = 0$, μ denotes the interferences received by a node
  for all $i \in \mathcal{I}_{r_p}$ **do** $\mu_{r_p,t} += z_{l_{k:tx=i}}(t)$, $\mathcal{I}$ denotes the link sets that cause interference
  end for
end for
$\mu_{r_p}(\boldsymbol{s}_s) = \max_t\{\mu_{r_p,t}\}$
if $s_p + \mu_{r_p}(\boldsymbol{s}_s) \leqslant A_{r_p}$ **then** $u_p(\boldsymbol{s}_s, s_p) = s_p$
else $u_p(\boldsymbol{s}_s, s_p) = 0$
end if

Algorithm 4 Finding primary network's optimal strategy

input: Network topology G
output: Primary network's optimal strategy s_p^*, and corresponding optimal utility u_p^*

for $s_p = 1 : min(A_{t_p}, A_{r_p})$ **do**
  Solve problem ORS2(s_p), record solution $\boldsymbol{s}_s^*(s_p)$
  Run Alg.3 with input $\boldsymbol{s}_s^*(s_p)$, s_p
  Collect $u_p(\boldsymbol{s}_s^*(s_p), s_p)$
end for
$s_p^* : s.t. u_p^* = \max_{s_p}\{u_p(\boldsymbol{s_s}^*(s_p), s_p)\}$

Lemma 8. *The output of Alg. 4 is the primary network's optimal strategy s_p^* when coexisting with a type-2 multi-hop secondary network.*

Proof. In Alg. 4, each primary-network strategy's corresponding utility is traversed and calculated according to our utility definition by calling Alg. 3, thus the output is the maximum. □

Theorem 8. *$(s_p^*, \boldsymbol{s}_s^*(s_p^*))$ is the equilibrium of the type-2 secondary-network follower case, where s_p^* and $\boldsymbol{s_s}^*(s_p^*)$ are defined in Lemma. 8 and 7 respectively.*

Theorem 9. *By playing type-2, the secondary network can guarantee it ends up with an equilibrium with higher or at least equal utility.*

Proof. To prove this theorem, we only need to prove three facts: 1) under any primary network's strategy s_p, the secondary network could gain more utility by playing type-2 ($u_{s2}^*(s_p)$)than type-1 ($u_{s1}^*(s_p)$). This is because the type-2 secondary network does not need to consider its interference towards to primary network, while the type-1 secondary network needs to do so. Therefore, the strategy space of the type-2's problem ORS2 is larger

than that of type-1's problem ORS1; 2) with the increasing of primary network's stream number s_p, the secondary network's maximum utility $u^*_{s1/s2}(s_p)$ decreases. This is also due to the size of strategy space: enlarging primary network's sending-stream number will compress the secondary network's strategy space. 3) in equilibrium, the primary network always transmits larger or at least equal number of streams when coexisting with type-1 than type-2 network. This is obvious as the primary network always chooses to send its maximum number of streams when coexisting with type-1 secondary network. Assuming s^*_{p1} and s^*_{p2} are the primary network's optimal strategies when dealing with type-1 and type-2 secondary networks respectively, then we have $s^*_{p1} \geqslant s^*_{p2}$, thus $u^*_{s1}(s^*_{p1}) \leqslant u^*_{s1}(s^*_{p2})$. As we have $u^*_{s1}(s^*_{p2}) \leqslant u^*_{s2}(s^*_{p2})$, thus we can have $u^*_{s1}(s^*_{p1}) \leqslant u^*_{s2}(s^*_{p2})$. □

One straightforward insight from this theorem is that the secondary network has the incentive to violate the spectrum access rule. In the next section, we will use two case studies to verify this incentive and then explore the methodology to deal with such selfish secondary networks.

5.4 Numerical Results

5.4.1 Overview

With our equilibrium analysis algorithms in Sec. 5.3, the primary network could estimate the equilibriums and the corresponding utilities. In this section, we will run our algorithms to show several results that provide insights of the coexisting game between primary and secondary networks. We choose 4 and 2 as the antenna numbers for primary network and secondary networks respectively. We use two case studies in which the single-link primary network coexists with 2-flow and 3-flow multi-hop networks respectively. We will calculate and analyze both primary and secondary network's optimal strategies and the interference generated by secondary network's optimal response strategy. We will first show that the general multi-flow secondary networks always have incentives to play selfishly and non-compliantly, i.e., playing type-2, which is bad news for the primary networks.

Second, to deal with such selfish networks, we decompose our algorithms and analyze the intermediate status. Our analysis implies that by aggressively extending primary network's interfering range, we could enhance its own utility in the equilibrium.

5.4.2 Selfish Incentives of Secondary Networks

We will show that in general cases, the secondary networks always have the incentives to be selfish, i.e., playing type-2 rather than type-1.

To analyze the secondary network's selfish incentives, we compare its utilities by playing type-1 and type-2 respectively. We select a scenario (scenario 1 in Fig. 5.3 (a)) with a single-link primary-network flow and two single/multi-hop secondary-network flows. We run our algorithms and derive the equilibriums and the corresponding utilities. Specifically, when coexisting with type-1 secondary networks, the utilities of primary and secondary networks under equilibriums are $(4, 0)$. Meanwhile, the utilities are $(2, 1)$ when the primary network coexists with the type-2 secondary networks. To get more insights of the results, we insert breakpoints in line 2 and 4 of our Alg. 4 to observe the utilities under each of the primary network's stream-transmitting strategies. The results are shown in Fig. 5.4. From the results we can observe that 1) the primary network could always achieve higher utilities when dealing with type-1 secondary network (as shown in Fig. 5.4 (a)) and the primary network's equilibriums are transmitting 4 and 2 streams when coexisting with the two types of secondary networks respectively; 2) however, the secondary network could always obtain higher or at least equal utilities by playing type-2, i.e., being selfish and non-compliant. Similar results could be derived from another case-study (scenario 2) results shown in Fig. 5.5.

5.4.3 Countering Selfish Secondary Networks

As we have shown the secondary networks always have the incentives to behave selfishly, it is necessary for the primary network to protect its transmission against selfish secondary networks' interferences. However, the interference from secondary networks is complex as it is implicitly affected by primary network's strategies. Using our MILP problems for-

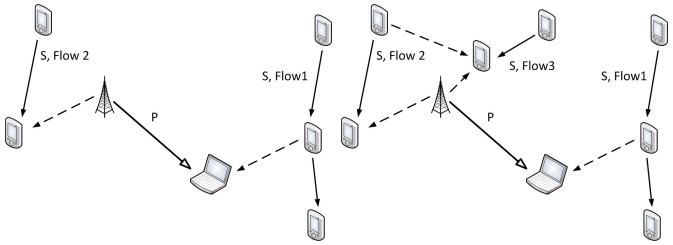

(a) (b)

Fig. 5.3. Simulation settings. (a) single-link primary network with 2-flow multi-hop secondary network. (b) single-link primary network with 3-flow multi-hop secondary network

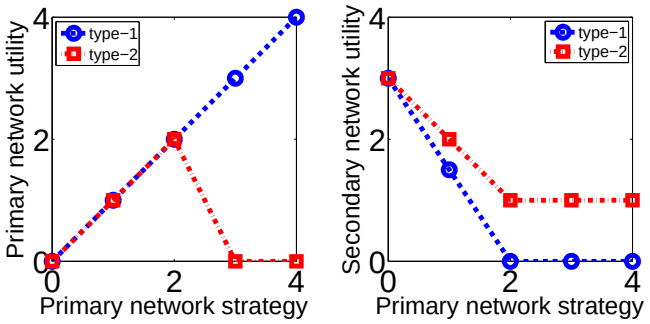

(a) (b)

Fig. 5.4. Primary-network (a) and secondary-network (b) utilities under primary network's stream-transmitting strategies.

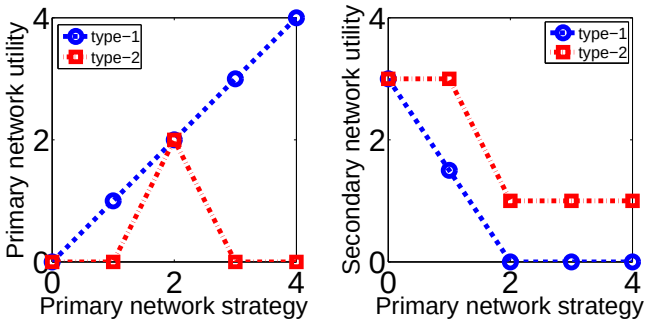

(a) (b)

Fig. 5.5. Primary-network (a) and secondary-network (b) utilities under primary network's stream-transmitting strategies.

mulation, we could precisely quantify the interferences from secondary networks through intermediate status analysis of our Alg. 4. Our intuition is that the larger degree of interferences generated by primary networks (in our system model, the interference is controlled

by the primary network's TX range and its transmitting strategies), the less interference it receives from the secondary networks in return. We validate our conjectures using our two case studies shown in Fig. 5.6.

In Fig. 5.6, we can observe that by transmitting more streams, the primary network endures less interference back from the secondary network. However, in practice the number of transmitted streams is capped by the number of antennas of the primary network thus we cannot increase the transmitting-stream number arbitrarily. Another observation is that by using long transmitting range, the primary network could also reduce the interferences generated by the secondary network through a chain of interferences out to and back from it. Though we show only two cases with two different network settings, such a phenomenon could be observed in general cases. This is because longer transmission range means larger interference degree generated on the secondary networks, thus more DoFs are consumed to perform IC at the secondary network, which otherwise could be used to transmit more streams in the secondary network. Therefore, less interferences could be fed back to the primary network in return as the interference is the result of stream transmissions. The longer transmitting range could finally enhance the utilities of the primary network in the game equilibriums, which is validated in Fig. 5.7. Note that this transmitting-range-extending approach is different from the 'tit-for-tat' approach in repeated game, as we do not force the secondary network to change into the compliant type. Instead, by using this approach, we aim at improving the primary network's utility in the equilibrium when coexisting with the non-compliant secondary network.

5.5 Summary

In this chapter, we studied the coexistence problem in cognitive radio networks with MIMO capability using game-theoretical approach. We formulate the game between the single-link primary network and the multi-hop secondary network as a Stackelberg game. To derive the equilibrium, we designed an algorithm based on the solution of a mixed-integer-linear-programming problem. Our results show that the multi-hop secondary network always has the incentive to play selfishly. The results also imply that we could enhance the

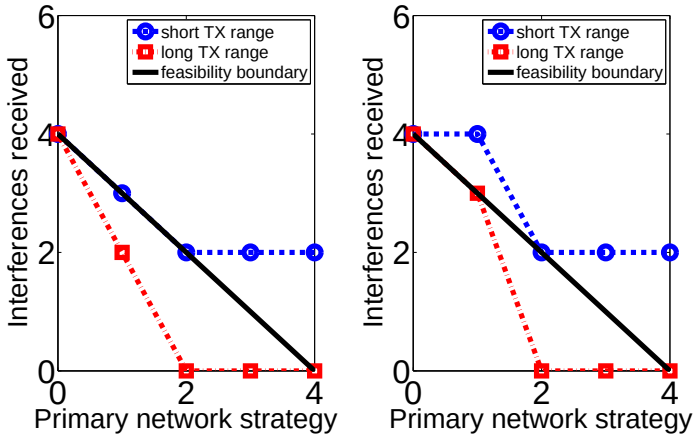

(a) (b)

Fig. 5.6. Interference towards primary network under its stream-transmitting strategies with different primary network's TX-interference ranges. (a) scenario 1. (b) scenario 2.

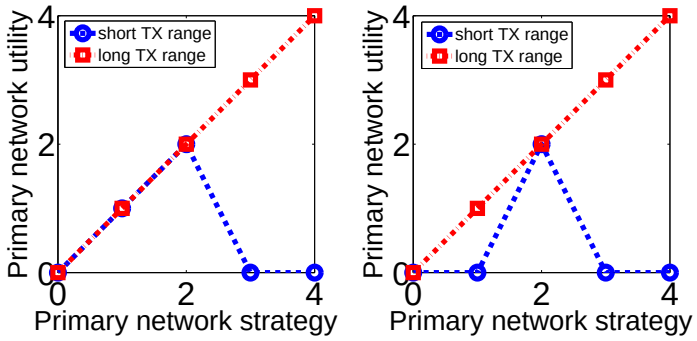

(a) (b)

Fig. 5.7. Primary network's utilities under its stream-transmitting strategies with different primary network's TX-interference ranges. (a) scenario 1. (b) scenario 2.

primary network's utility by enlarging its transmitter's interference range.

CHAPTER 6
THROUGHPUT OPTIMIZATION IN MULTI-HOP WIRELESS NETWORKS WITH RECONFIGURABLE ANTENNAS

6.1 Overview

In previous chapters, we have shown that wireless MIMO could enhance network throughput by performing IC and SM. In fact, there are other advanced physical-layer techniques that we can leverage. RA could provide the ability of swift pattern changing, thus dynamically control the transmission and interference range. Intuitively, we could control the RAs to decrease the interference degree in the network by carefully selecting the patterns. However, a tractable modeling is still missing. In this chapter, we propose the two-layer pattern-selecting and link-scheduling model. Our model successfully captures the relation between pattern selection and link-coverage/interference areas. In addition, to fully characterize the reconfigurability of antennas, we have no assumption about the shape of the pattern. Based on our model, we formulate the throughput optimization with reconfigurable antennas (TORA) problem into a mixed integer non-linear programming problem. After reformulating it into a mixed integer linear programming (MILP) problem using reformulation linearization technique (RLT), we can solve it using off-the-shelf tools such as IBMs CPLEX, which is based on the branch and bound technique. We theoretically prove the advantages brought by reconfigurable antennas using conflict-graph based approach. Through extensive evaluation results, the benefits of using reconfigurable antennas over traditional omni-directional antennas and directional antennas are validated.

6.2 Motivating Examples

As we mentioned, RA's main advantages are state diversity and fast reconfigurability, while they can also enjoy the directivity gain of directional antennas. For pattern-

reconfigurable antennas, they can achieve all-directional pattern coverage as omni-directional antennas by dynamical antenna pattern switching, meanwhile generating low-degree of interference to the unintended directions like a DA. This creates many new opportunities to optimize the performance of MWNs in link layer or network layer, which are illustrated through three simple examples in Fig. 6.1.

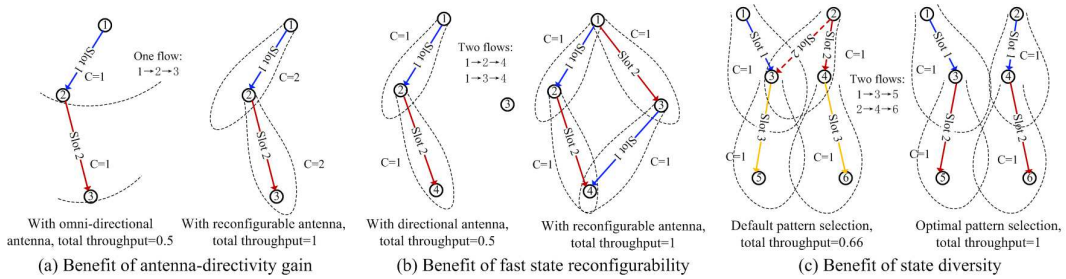

Fig. 6.1. Motivating examples: Throughput benefits brought by RAs in MWNs due to antenna-directivity gain, fast reconfigurability, and state diversity

In Fig. 6.1 (a), we show a single-flow case. Using omni-directional antenna, one path is possible which gives an end-to-end (E2E) throughput of 0.5 under the optimal schedule (assuming per-link capacity is 1). While using pattern-reconfigurable RAs (or DA), the link capacities are doubled due to *antenna-directivity gain*, which yields a twofold E2E throughput gain. In Fig. 6.1 (b), a two-flow case is shown to illustrate the benefit of fast state reconfigurability. Using legacy DAs with a fixed beam, there is one flow ($1 \rightarrow 2 \rightarrow 4$) and the DA beam at node 1 is selected to point toward node 2. The overall throughput under optimal schedule is 0.5 flow per time slot. While using RAs, node 1's transmit state can be quickly adjusted such that node 1 could fully utilize time resources to transmit one more stream, which enhances total E2E throughput (and also fairness between two flows). In Fig. 6.1 (c), a two-flow case shows the benefit of *state diversity*. In the left subfigure, node 2 uses the default state which interferes with the $1 \rightarrow 3$ link. Thus nodes 1 and 2 have to transmit at separate time slots. In the right subfigure, optimal state selection is used by adopting another state at node 2 (e.g., a different pattern) such that now $1 \rightarrow 3$ and $2 \rightarrow 4$ can transmit simultaneously in slot 1, which yields a higher throughput. Note that, the above scenarios are only an exemplary subset; in general, there are many ways that RAs

can enhance the E2E performance, including throughput, delay, and energy-efficiency. In this chapter we focus on throughput optimization.

6.3 Modeling and Formulation

6.3.1 Antenna Model

In this work, we consider three types of antennas: OAs, DAs, and RAs. OAs (a.k.a. isotropic antennas) transmit and receive signals equally in all directions. DAs can radiate signals in a certain direction. We assume the directional antenna is able to choose any of its signal direction from all candidates, but cannot swiftly change the direction [28, 31, 56–59]. Compared with DAs, RAs can swiftly reconfigure antenna states in terms of frequency, polarization, and radiation pattern. In our work we focus on the reconfigurability of pattern, where each node's antenna has multiple candidate radiation patterns, which in general can be in any shape. We assume the patterns can be overlapped with each other. RAs can perform very fast pattern switching choosing from all candidate patterns within negligible time [23]. In this work, the pattern selection is considered only at the transmitter side.

We adopt the protocol model [60] due to its simplicity and mathematical tractability, which has been widely used previously [18, 28, 61, 62]. We assume at each time slot the transmitter selects a pattern k associating with a geographical area $\mathcal{T}_{i,k}$, within which the receivers are reachable by this transmitter. (The area of this pattern could be derived using path-loss model or experimental method, which is out of the scope of this work.) We also use $\mathcal{I}_{i,k}$ to denote the interference area, within which the transmitted signal's power is too large to be treated as background noise for all unintended devices. It is easy to see that normally we have $\mathcal{T}_{i,k} \subseteq \mathcal{I}_{i,k}$. However, to make our model more general, such a relation is not considered necessary. We consider multiple flows with predefined routes in our MWNs.

6.3.2 Link-Layer Model of RAs in Multi-hop Networks

1) Overview: Next we present our basic idea of link-layer modeling of RAs in MWNs. As we mentioned, such modeling is challenging due to dynamic antenna pattern selection

across time, which affects both network topology (whether a link is established in the graph at time t) and interference (whether two established links interfere with each other at time t). In addition, one link can be covered by multiple overlapping antenna patterns due to pattern diversity.

To capture the above characteristics, our model conceptually consists of two modules. Module one is antenna pattern selection, in which the radiation pattern is chosen by each node. The choices of patterns determine the link-coverage and interference relations. The second module is link scheduling, which determines the set of links that are active during each time slot, while considering interference constraints. Logically these two modules are hierarchical: link scheduling is performed after antenna pattern selecting, because no link can be established unless one of the covering patterns is chosen first. Based on the link-layer model, we can maximize the throughput by optimally selecting antenna patterns and the interference-free link sets in each slot.

2) Modeling Details: We model the MWN as a directed graph $G(\mathcal{V}, \mathcal{E})$, where each node is equipped with a single RA. We assume that T time slots are available to the network under a single frequency (alternatively one can model it using multiple frequency bands). We do not consider power control in this work. Let Ω represent the set of multi-hop flows in the network, and r_f denote the rate of flow $f \in \Omega$. In case that routing scheme is given, we denote $\mathcal{L}$ the set of links in the flows. Let $z_l(t)$ denote whether link l is actively transmitting in slot t. All variables and parameters are shown in Table. 6.1.

We use $x_i(t)$ and $y_i(t)$ to denote whether node i transmits or receives in time slot t. Assuming half-duplex operation on each transceiver, we have the following link-rate constraint:

$$x_i(t) + y_i(t) \leqslant 1 \qquad (\forall i \in \mathcal{N}) \tag{6.1}$$

Given the ability of fast antenna reconfiguration, at each time slot t, node i selects a transmit antenna pattern k, which can be different across time slots. In addition, since we assume a general antenna model, the patterns can be of any shape and multiple patterns can be arbitrarily overlapped. However, each node can only select one pattern from its set

Table 6.1. Major Notations

$x_i(t), y_i(t)$	whether node i transmits/receives at time slot t
$p_{i,k}(t)$	whether node i selects pattern k at slot t
$\mathcal{L}, \mathcal{N}, \Omega$	the selected link set, node set and flow set
$\alpha_{i,j}(t)$	whether link (i,j) is in node i's transmitting area at slot t
$\beta_{i,j}(t)$	whether link (i,j) is in node i's interference area at slot t
$\theta_{i,j}(t)$	the link (i,j)'s capacity at slot t
$A_{i,j,k}$	transmission area parameter, denotes whether link (i,j) is in node i's transmitting area under pattern k
$B_{i,j,k}$	interference area parameter, denotes whether link (i,j) is in node i's interference area under pattern k
$\Theta_{i,j,k}$	link capacity parameter, denotes link (i,j)'s capacity under node i's pattern k
$z_{i,j}(t)$	whether link (i,j) is active at slot t
$c_{i,j}$	overall capacity of link (i,j)
$r_{i,j,f}$	rate of link (i,j) on flow f
r_f	rate of flow f
$a_{i,j}(t), b_{i,j}(t), m_{i,j}(t), \phi_{i,j}(t), \psi_{i,j}(t), w_{i,j}(t)$	intermediate variables for linearization reformulation

of candidate patterns $\mathcal{K}_i$ in each time slot, and we introduce a binary variable $p_{i,k}(t) = 1$ to denote such a selection:

$$\sum_{k \in \mathcal{K}_i} p_{i,k}(t) = x_i(t) \quad (\forall i \in \mathcal{N}) \tag{6.2}$$

To capture the hierarchical relation between pattern selection and link scheduling, we use the variable $\alpha_{i,j}(t)$ to denote whether link (i,j) is covered by any pattern selected by node i in slot t (i.e., whether link (i,j) is in $G_r(\mathcal{V}_{r,t}, \mathcal{E}_{r,t})$, which denotes the dynamic topology due to pattern reconfigurability in time slot t). An example is shown in Fig. 6.2, where the link $(1,2)$ is available at that time slot as it is covered by the pattern selected, thus we have $\alpha_{1,2}(t) = 1$. Note that it does not mean link $(1,2)$ is active, but only makes it an available candidate ready for scheduling. To denote whether link (i,j) is covered in G_r under the transmitting node's pattern k, we use $A_{i,j,k}$, a binary link-pattern parameter. By selecting a pattern $p_{i,k}(t)$ in slot t, $\alpha_{i,j}(t)$ is determined by:

$$\alpha_{i,j}(t) = \sum_{k \in \mathcal{K}_i} p_{i,k}(t) \cdot A_{i,j,k}, \quad (\forall (i,j) \in \mathcal{L}) \tag{6.3}$$

We use $\theta_{i,j}(t)$ to denote the link capacity in time slot t. $\Theta_{i,j,k}$ refers to the link-capacity parameter, which denotes link (i,j)'s capacity under its transmitter's antenna pattern k. In reality, the capacity is a function of transmitting power, antenna gain, channel gain, etc. This parameter can be derived based on either experimental measurements (e.g., data rate multiplies packet deliver probability), or channel capacity model. In Sec. 6.5, we adopt an existing channel-capacity model $\Theta_{i,j} = W * log_2(1 + P_t \cdot G_a \cdot G_{ij}/P_N)$ [63] to calculate link capacity. This is Shannon capacity which only considers SNR instead of SINR, since we adopt a protocol model. However, we can use reality check technique [63] to make sure the scheduling solution is feasible when considering the aggregated interference from all the transmitters, which is orthogonal to our work. Similar to constraint (6.3), by selecting a pattern $p_{i,k}(t)$, link (i,j)'s capacity is computed as:

$$\theta_{i,j}(t) = \sum_{k \in \mathcal{K}_i} p_{i,k}(t) \cdot \Theta_{i,j,k}, \quad (\forall (i,j) \in \mathcal{L}) \tag{6.4}$$

The selection of patterns affects the interference relation in the network. We use $\beta_{i,j}(t)$ to denote whether the transmission of node i can interfere with another node j when j is receiving data from another source. An example is shown in Fig. 6.2, in which link $(1,2)$ and $(1,3)$ are interfering links, thus $\beta_{1,2}(t) = \beta_{1,3}(t) = 1$. $B_{i,j,k}$ is the link-interference parameter, which denotes whether node j is in the interference area under the transmitting node i's antenna pattern k. Similarly, once the pattern is selected, the interference relation is determined as:

$$\beta_{i,j}(t) = \sum_{k \in \mathcal{K}_i} p_{i,k}(t) \cdot B_{i,j,k}, \quad (\forall (i,j) \in \mathcal{L}) \tag{6.5}$$

In our model, we assume that each transceiver can only transmit to/receive from one link concurrently. Thus we use primary interference to denote the transmission conflicts of all the links sharing a transmitter/receiver. The binary variables $x_i(t)$ and $y_i(t)$ stipulate that only one link/stream is active at each node i in each slot:

$$x_i(t) = \sum_{(i,j) \in \mathcal{L}_{i,out}} z_{i,j}(t), \quad (\forall i \in \mathcal{N}) \tag{6.6}$$

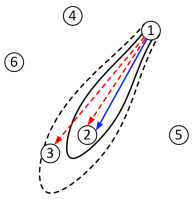

Fig. 6.2. An illustration of link-coverage and interference area. $\alpha_{1,2}(t) = 1$. $\beta_{1,2}(t) = \beta_{1,3}(t) = 1$.

$$y_i(t) = \sum_{(j,i)\in\mathcal{L}_{i,in}} z_{j,i}(t), \quad (\forall i \in \mathcal{N}) \tag{6.7}$$

Only if the link (i, j) is covered in time slot t, can it then be activated. In other words, if link (i, j) is active in slot t, i.e. $z_{i,j}(t) = 1$, then we must have $\alpha_{i,j}(t) = 1$:

$$\sum_{(i,j)\in\mathcal{L}} z_{i,j}(t) \cdot (1 - \alpha_{i,j}(t)) = 0 \tag{6.8}$$

$c_{i,j}$ denotes the link capacity averaged over all slots when this link is active:

$$c_{i,j} = 1/T \cdot \sum_{t}^{T} z_{i,j}(t) \cdot \theta_{i,j}(t), \quad (\forall (i, j) \in \mathcal{L}) \tag{6.9}$$

We define secondary interference as the transmission conflicts among different interfering-links without common nodes. The secondary interference at receiver side must be taken into account to avoid conflict. If node i is receiving, i.e $y_i(t) = 1$, then any potential interfering source must not transmit in the same slot unless it is transmitting to node i:

$$y_i(t) \cdot \sum_{(j,i)\in\mathcal{L}_{i,in}} \beta_{j,i}(t) \cdot (1 - z_{j,i}(t)) \cdot x_j(t) = 0 \tag{6.10}$$

Let $r_{i,j}$ denote the link rate. For intermediate nodes, the overall input rate equals the output rate. For source and receiving nodes, the output/input rates equal the flow rate:

$$\sum_{(j,i)\in\mathcal{L}_{i,in}} r_{j,i,f} = \sum_{(i,g,f)\in\mathcal{L}_{i,out}} r_{i,g,f}, \quad (\forall i \in \mathcal{N}, \forall f \in \Omega) \tag{6.11}$$

$$\sum_{(j,i)\in\mathcal{L}_{i,in}} r_{j,i,f} = r_f, \quad (\forall i \in \mathcal{N}, \forall f \in \Omega) \tag{6.12}$$

$$\sum_{(i,j)\in\mathcal{L}_{i,out}} r_{i,j,f} = r_f, \quad (\forall i \in \mathcal{N}, \forall f \in \Omega) \tag{6.13}$$

The achievable link rate should always be upper-bounded by its capacity, thus we have the following link-rate constraint:

$$\sum_{f} r_{i,j,f} \leqslant c_{i,j} \quad (\forall (i,j) \in \mathcal{L}) \tag{6.14}$$

From a high level, a feasible solution satisfying the above constraints essentially finds non-interfering concurrent transmitting links along with their antenna patterns from the network at every time slot t.

6.3.3 Optimization Formulation

Based on the link-layer model, we formulate the throughput optimization with reconfigurable antennas (TORA) problem, where we aim at maximizing the overall throughput of one or multiple multi-hop flows, while satisfying all the constraints above. The TORA problem is shown in Fig. 6.3. $h(\cdot)$ denotes a general linear weighted function, e.g., $u = \eta_1 r(f_1) + \eta_2 r(f_2)$. For simplicity, in our evaluation, we assume $\eta_i = 1$ for all flows. TORA is a mixed non-linear integer programming problem, which is generally NP-hard.

In the above, $x_i(t)$, $y_i(t)$, $\alpha_{i,j}(t)$, $\beta_{i,j}(t)$, $z_{i,j}(t)$, $p_{i,k}(t)$ are all binary variables, $c_{i,j}, \theta_{i,j}(t), r_{i,j,f}, r_f$ are continuous. Currently, TORA only considers transmitter-side pattern reconfigurability. But it can be easily extended to support polarization/frequency reconfigurability by introducing another antenna state variable at the receiver side, which will be our future work.

Reformulation: In our formulation, several constraints are non-linear. Therefore, we use RLT to linearize these constraints. We first set $z_{i,j}(t) \cdot \alpha_{i,j}(t) = a_{i,j}(t)$. Then constraint

$$\max\ u = \sum_{f \in \Omega} h(r(f))$$

s.t. Half duplex constraints:(6.1);
Pattern selection constraint:(6.2);
Link coverage constraint(6.3);
Link capacity constraint:(6.4);
Link interference constraint:(6.5);
Transmitter conflict constraint:(6.6);
Receiver conflict constraint:(6.7);
Link coverage and link active constraint:(6.8);
Link capacity constraint:(6.9);
Receiver interference constraint:(6.10);
Route balance constraints:(6.11 – 6.13);
Link rate constraint:(6.14);

Fig. 6.3. Throughput optimization problem in multi-hop networks with reconfigurable antennas (TORA)

(6.8) is reformulated into:

$$\sum z_{i,j}(t) - \sum a_{i,j}(t) = 0 \tag{6.15}$$

In addition, several new constraints are needed after we introduce the new variable:

$$a_{i,j}(t) \geqslant 0; \quad z_{i,j}(t) - a_{i,j}(t) \geqslant 0; \quad \alpha_{i,j}(t) - a_{i,j}(t) \geqslant 0;$$
$$1 - \alpha_{i,j}(t) - z_{i,j}(t) + a_{i,j}(t) \geqslant 0 \tag{6.16}$$

In (6.9), we set $m_{i,j}(t) = z_{i,j}(t) \cdot \theta_{i,j}(t)$, and constraint (6.9) becomes:

$$c_{i,j} = 1/T \cdot \sum_{t}^{T} m_{i,j}(t), \tag{6.17}$$

and several new constraints are added after introducing new variable $m_{i,j}(t)$:

$$m_{i,j}(t) \geqslant 0; \quad z_{i,j}(t) - m_{i,j}(t) \geqslant 0; \quad \theta_{i,j}(t) - m_{i,j}(t) \geqslant 0;$$
$$1 - \theta_{i,j}(t) - z_{i,j}(t) + m_{i,j}(t) \geqslant 0 \tag{6.18}$$

In constraint (6.10), we first set $y_i(t) \cdot x_j(t) = w_{i,j}(t)$, then we set $\beta_{j,i}(t) \cdot w_{i,j}(t) = \phi_{i,j}(t)$, $z_{i,j}(t) \cdot \beta_{i,j}(t) = b_{i,j}(t)$, and $b_{j,i}(t) \cdot w_{i,j}(t) = \psi_{i,j}(t)$. Then we have:

$$\sum \phi_{i,j}(t) - \sum \psi_{i,j}(t) = 0; \tag{6.19}$$

Again, by introducing the new variables, we have the constraints:

$$b_{i,j}(t) \geqslant 0; \quad z_{i,j}(t) - b_{i,j}(t) \geqslant 0; \quad \beta_{i,j}(t) - b_{i,j}(t) \geqslant 0;$$
$$1 - \beta_{i,j}(t) - z_{i,j}(t) + b_{i,j}(t) \geqslant 0 \tag{6.20}$$

$$w_{i,j}(t) \geqslant 0; \quad x_j(t) - w_{i,j}(t) \geqslant 0; \quad y_i(t) - w_{i,j}(t) \geqslant 0;$$
$$1 - x_j(t) - y_i(t) + w_{i,j}(t) \geqslant 0 \tag{6.21}$$

$$\phi_{i,j}(t) \geqslant 0; \quad \beta_{j,i}(t) - \phi_{i,j}(t) \geqslant 0; \quad w_{i,j}(t) - \phi_{i,j}(t) \geqslant 0;$$
$$1 - \beta_{j,i}(t) - w_{i,j}(t) + \phi_{i,j}(t) \geqslant 0 \tag{6.22}$$

$$\psi_{i,j}(t) \geqslant 0; \quad b_{j,i}(t) - \psi_{i,j}(t) \geqslant 0; \quad w_{i,j}(t) - \psi_{i,j}(t) \geqslant 0;$$
$$1 - b_{j,i}(t) - w_{i,j}(t) + \psi_{i,j}(t) \geqslant 0 \tag{6.23}$$

So far, all the constraints have been linearized through reformulation, thus TORA can be solved using the branch and bound technique. Note that some equations (e.g., Eq.6.16) could be further simplified after the formal reformulating, which however do not change the optimization results. We use IBM's off-the-shelf tool CPLEX to solve our problem.

6.3.4 Variations of TORA using Traditional Antennas

We use OAs and DAs as comparisons in our work. For DAs, we assume they can select any pattern, which is then fixed across all slots. We show that the same throughput-optimization problem using omni-directional antennas (TOOA) and directional antennas (TODA) are special cases of our problem (TORA).

For omni-directional antennas, since there is only one antenna pattern, we can simplify the constraints (6.3)-(6.5) as:

$$\alpha_{i,j}(t) = A^o_{i,j}, \theta_{i,j}(t) = \Theta^o_{i,j}, \beta_{i,j}(t) = B^o_{i,j} \ (\forall (i,j) \in \mathcal{L}) \tag{6.24}$$

By removing (6.2), we obtain the TOOA problem. We can reduce it to TORA by introducing the pattern variable p_i and constraint (6.2) and set $A^r_{i,j,k} = A^o_{i,j}, B^r_{i,j,k} = B^o_{i,j}, \Theta^r_{i,j,k} = \Theta^o_{i,j}, \forall k$. We can see that the reduced form of TOOA is just a special case of TORA in which all the transmission area, interference area, and link capacity parameters are the same under all patterns.

Formulation of the TODA problem is similar by simply replacing $A^o_{i,j}, B^o_{i,j}, \Theta^o_{i,j}$ with $A^d_{i,j}, B^d_{i,j}, \Theta^d_{i,j}$ in (6.24), where the antenna directions (patterns) are arbitrary and predetermined. As the link-coverage and interference areas are static, the models with omni-directional and directional antennas are simpler and the two corresponding problems are easier to solve.

6.4 Theoretical Throughput Gain Analysis of RAs

In this section, we study the gain brought by reconfigurable antennas in MWNs. We can prove the superiority of RAs in terms of overall network throughput compared with OAs and DAs in certain conditions.

Theorem 10. *Given a network $G(\mathcal{V}, \mathcal{E})$ equipped with omni-directional antennas or reconfigurable antennas respectively, if $\forall i, \mathcal{T}_{i,OA} \subseteq \bigcup_k \mathcal{T}_{i,k,RA}$, and $\bigcup_k \mathcal{I}_{i,k,RA} \subseteq \mathcal{I}_{i,OA}$, for the overall maximum throughput in TORA and TOOA problems, we always have $u_{RA} \geqslant u_{OA}$.*

In Theorem 10, the rationale is that RAs can maintain/improve network connectivity degree while reducing the interference degree. This can be formally proved using conflict-graph based methodology [60]. For detailed proof, please refer to our technical report [64]. Theorem 10 can be extended to the general form:

Theorem 11. *Given a network $G(\mathcal{V}, \mathcal{E})$ equipped with two general types of reconfigurable antennas RA_1 and RA_2, if $\forall i, k_2, \exists \mathcal{K}, s.t. \mathcal{T}_{i,k_2,RA_2} \subseteq \bigcup_{k_1 \in \mathcal{K}} \mathcal{T}_{i,k_1,RA_1}$ and $\bigcup_{k_1 \in \mathcal{K}} \mathcal{I}_{i,k_1,RA_1} \subseteq \mathcal{I}_{i,k_2,RA_2}$, then we have $u_{RA_1} \geqslant u_{RA_2}$.*

For comparison with DAs, we can prove RA's superiority using similar approach.

6.5 Evaluation

In this section, we will evaluate the network throughput of MWNs with RAs through simulations. We solve our TORA problem using CPLEX in Virtual C++ environment and compare the results with TOOA and TODA problems. We first use some simple case studies to show the advantage of RAs through inspecting the link scheduling in details. Then we randomly generate multiple flows to validate the superiority of RAs in the average cases.

6.5.1 Simulation Setting

We place 60 nodes randomly distributed in a 100×100 square area. Time is divided into $T = 8$ slots. We assume each node has K candidate patterns to choose from. Each pattern covers a fan-shape area with $2\pi/K$ angle (note that the pattern could be of any shape in our general model, but here we use fan-shape to simplify the simulation). By using RAs, each node can swiftly change its pattern between any two adjacent time slots, resulting in different transmission and interference areas. By using DAs, the patterns are fixed a priori as DAs cannot perform swift pattern switching. Note that when $K = 1$, it is equivalent to the case of using OAs. In subsection B and first part of subsection C, we explore the throughput gain brought by RAs due to pattern diversity and fast reconfigurability. To eliminate the uncertain influence brought by antenna-directivity gain, we assume antenna gain is fixed when using RAs and DAs, thus the transmission and interference ranges are

not extended. (This could be implemented in practice by performing power control but is out of the scope of this work.) In addition, when increasing K, we satisfy the conditions in Theorem 11. In the second part of subsection C, we test the influence of antenna-directivity gain by considering it variable.

Table 6.2. Link scheduling details for case study 1

Flows	Path Link	RA Slots	Rate	OA Slots	Rate
Flow 1	$18 \rightarrow 6$	6,7	0.25	6	0.125
	$6 \rightarrow 10$	3,4	0.25	4	0.125
Flow 2	$5 \rightarrow 6$	0,1	0.25	1	0.125
	$6 \rightarrow 36$	2,5	0.25	7	0.125
Flow 3	$5 \rightarrow 13$	2,3,4,6	0.5	0,3,5	0.375
	$13 \rightarrow 27$	0,1,5,7	0.5	2,4,7	0.375

Table 6.3. Link scheduling details for case study 2

Flows	Path Link	RA Slots	Rate	RA-OL Slots	Rate
Flow 1	$44 \rightarrow 25$	0,4	0.25	3,4,5,6	0.5
	$25 \rightarrow 13$	1,7	0.25	0,1,2,7	0.5
	$13 \rightarrow 5$	3,5	0.25	3,4,5,6	0.5

6.5.2 Case Study

First, we use two examples to show the benefits brought by using RAs. Given fixed antenna gain, transmission and interference ranges are set as $(30, 50)$. To better illustrate the benefits of pattern reconfigurability and diversity, we temporarily simplify the link-capacity model by normalizing link capacity as 1 for all links covered by the transmission range of node i, $\forall i \in N$. Case 1 is shown in Fig. 6.4(a) where we can transmit three flows using RAs. The details of scheduling are shown in Table 6.2. Among these flows, the normalized throughput is 0.25 for each of flows 1 and 2, and 0.5 for flow 3, thus the overall network throughput is 1. To achieve this, swift pattern switching is performed. Node 5 chooses pattern 3 to transmit to node 6 on slots $1, 2$ and chooses pattern 8 to transmit to node 13 in slots $2, 3, 4$, and 6. Node 6 chooses pattern 3 to transmit to node 36 in slots $2, 5$ and chooses pattern 5 to transmit to node 10 in slots $3, 4$. Now assuming we use DAs instead

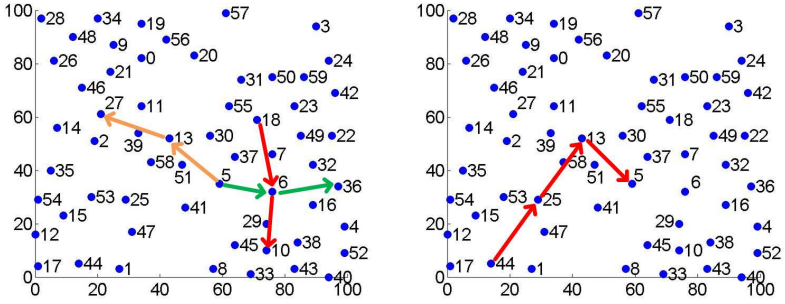

(a) (b)

Fig. 6.4. Examples of fast reconfigurability (a) and pattern diversity (b). (a) three flows coexist by utilizing pattern-switching capability of RAs. Flow 1: 18 → 6 → 10. Flow 2: 5 → 6 → 36. Flow 3: 5 → 13 → 27. (b) Flow: 44 → 25 → 13 → 5 by using 50% pattern overlapping (OL).

of RAs, it is not difficult to see that the maximum throughput can never be larger than 0.5 by using any pre-fixed antenna pattern (the best case is only transmitting one flow, e.g., flow 3, which achieves the normalized overall throughput as 0.5). The reason is the lack of ability to perform fast pattern selection when using traditional DAs. In this case, nodes 5 and 6 cannot fully utilize the transmitting opportunities in different directions, which leads to a lower overall network throughput.

On the other hand, by using OAs, the throughput of flows $1, 2$, and 3 is $0.125, 0.125$, and 0.375, respectively, which is also lower than the throughput using RAs. This is due to the enlarged interference degree brought by OAs. In this case, each node needs to avoid generating interference to the nodes locating in a broader region, thus limiting its opportunity to transmit.

Table 6.4. Reconfigurability Benefits: RA vs. OA

	1 pattern (OA)	2 patterns	4 patterns	8 patterns
1 flow	100 %	116.3 %	122.6 %	122.8 %
2 flows	100 %	129.2 %	146.5 %	155.2 %

In case 2, we continue exploring the benefits brought by RAs. In Fig. 6.4 (b), we show that the network throughput can be enhanced by exploiting pattern diversity and the details

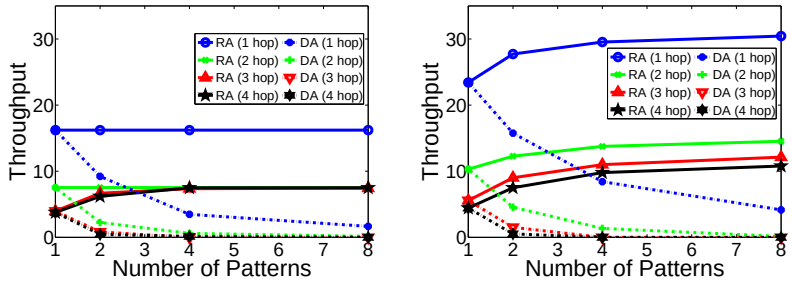

(a) (b)

Fig. 6.5. The average network throughputs (in bps/Hz) comparison by using RAs, OAs, and DAs. Pattern number 1 denotes the OAs case. (a) single flow scenarios; (b) two concurrent-flow scenarios.

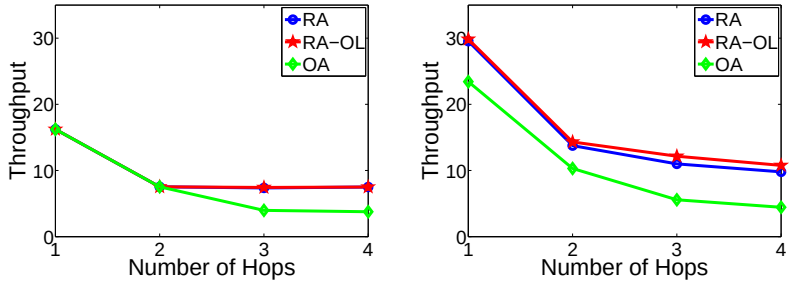

(a) (b)

Fig. 6.6. The average network throughputs (in bps/Hz) comparison by using RAs, RA-OL, and OAs under different hop numbers for each flow. Total pattern beam width γ is set as $\pi/2$ for RAs and RA-OL(50% overlapping). (a) single flow scenarios; (b) two concurrent-flow scenarios.

Table 6.5. Pattern Diversity Benefits: RA, RA-OL vs. OA

	1 hop	2 hops	3 hops	4 hops
1 flow RA	100 %	100 %	185.1 %	199.2 %
1 flow RA-OL	100 %	100 %	187 %	199.2 %
2 flow RA	126.1 %	133.4 %	197.3 %	220.7 %
2 flow RA-OL	127.4 %	138.8 %	218.1 %	242.7 %

of scheduling are shown in Table 6.3. In case 1, each link is exclusively covered by only one pattern, that is, no pattern overlaps with others. Intuitively, larger pattern diversity provides more pattern-selection choices for each node, maintaining the network connectivity degree while further decreasing the interference degree. Therefore, the network throughput can be further improved. In Fig. 6.4(b), when considering no pattern overlapping (OL),

link $13 \rightarrow 5$ is covered by only one pattern that inevitably generates interference to node 25. Therefore, nodes 13 and 44 cannot transmit concurrently and the total network throughput is 0.25. When considering pattern overlapping (which brings pattern diversity), link $13 \rightarrow 5$ can be covered by another pattern that does not generate interference to node 25. By selecting this pattern at some slot t, link $13 \rightarrow 5$ is covered (i.e., $\alpha_{13,5}(t) = 1$), meanwhile the link $13 \rightarrow 25$ is not interfering (i.e., $\beta_{13,25}(t) = 0$). As the interference degree is reduced, more links can transmit concurrently in one slot, leading to a higher network throughput of 0.5. This example also shows the distinctiveness of our work compared with previous research on steerable beam antennas such as [65], which determines the antenna direction simply based on antenna-directivity gain, instead of joint optimization of pattern selection and link scheduling.

6.5.3 Average Throughput Result

We test the average throughput gain of RAs compared with traditional DAs and OAs. In each simulation we repeatedly carry out 50 independent tests. The parameters are chosen as: transmission power $P_t = 20dBm$, noise level $P_N = -93dBm$, [9] transmitting frequency $f = 2.4GHz$ and W is normalized as 1. We adopt the free-space path-loss model to calculate channel gain G_{ij}. We first test the fixed antenna-gain case by setting the antenna gain as 1. The transmission and interference ranges are set as $(30, 50)$. We take all parameters into our link-capacity model to calculate the link capacity. The average throughputs are shown in Fig. 6.5. We can observe that with the increase of pattern number, the throughput decreases by using DAs while it always increases by using RAs. The reason is that DAs degrade the network connectivity while RAs maintain the connectivity degree and decrease the interference degree. Note that when the pattern number is 1 (i.e., $K = 1$), it is equivalent to the case of OAs. The throughput benefits of RAs vs. OAs in percentages are shown in Table 6.4. The larger number of candidate patterns we have, higher the throughput benefit is due to reconfigurability.

In addition to showing the gain brought by pattern reconfigurability, we perform another simulation to test the throughput gain brought by pattern diversity through pattern

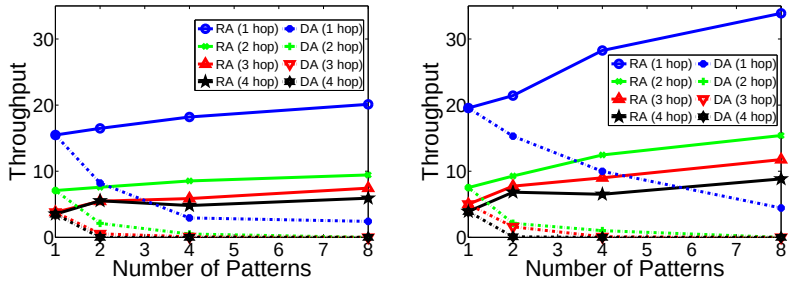

Fig. 6.7. The average network throughputs (in bps/Hz) comparison with variable antenna-directivity gain by using RAs, OAs, and DAs. Note that when pattern number is 1, it is equivalent to the OAs case. (a) single flow scenarios; (b) two concurrent-flow scenarios.

Table 6.6. Reconfigurability Benefits: RA vs. OA (with variable antenna-directivity gain)

	1 pattern (OA)	2 patterns	4 patterns	8 patterns
1 flow	100 %	117.4 %	125.2 %	143.7 %
2 flows	100 %	125.8 %	156.2 %	194.1 %

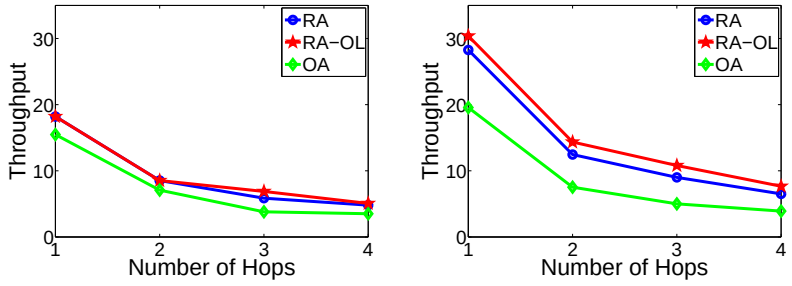

Fig. 6.8. The average network throughputs (in bps/Hz) comparison with variable antenna-directivity gain by using RAs, RA-OL, and OAs under different hop numbers for each flow. Total pattern beam width γ is set as $\pi/2$ for RAs and RA-OL(50% overlapping). (a) single flow scenarios; (b) two concurrent-flow scenarios.

Table 6.7. Pattern Diversity Benefits: RA, RA-OL vs. OA (with variable antenna-directivity gain)

	1 hop	2 hops	3 hops	4 hops
1 flow RA	117.5 %	120.5%	154.3 %	137.0 %
1 flow RA-OL	117.5 %	120.5 %	181.2 %	144.4 %
2 flow RA	144.5 %	165.5 %	179.8 %	166.5 %
2 flow RA-OL	155.3 %	190.1 %	215.7 %	196.0 %

overlapping. The results are shown in Fig. 6.6. From this figure, we can find that: 1) by increasing the pattern diversity, the network throughput can always be enhanced. The reason is that increasing pattern diversity can also decrease interference degree while maintaining the connectivity degree. 2) With the increase of hop count, the throughput decreases. The reason is straightforward as more hops brings more competitions within the network (due to interference and half-duplex) thus cutting down the network throughput in each flow. The results also validate our theoretical analysis in Sec.6.4.

The simulation results above illustrate the throughput gains brought by pattern reconfigurability and diversity. When considering variable antenna-directivity gain, it becomes more complicated and the overall throughput gain/loss will be uncertain. The reason is that by focusing the transmitting power towards a fixed direction, the transmission range as well as interference range in this direction are enlarged. While enlarged antenna gain increases link capacity and transmission range, it can also increase the interference degree which can degrade overall network throughput. The transmission and interference ranges of OAs are set as $(40, 60)$. We derive the RAs and DAs antenna-directivity gain as $2/(1 - cos(\gamma/2))$ based on the power-density-analysis approach [66] where γ is the pattern's beam width. From the results shown in Fig. 6.7 and 6.8, we can find: 1) the overall throughput by using RAs is higher than the one by using DA. 2) With the increase of pattern number, the network throughput increases in general but in some cases (e.g., with 4-hop RAs from 2 patterns to 4 patterns in Fig. 6.7. (b)) the throughput decreases due to the enlarged interference degree brought by antenna-directivity gain. To solve this issue, some solutions such as precise power control can be employed, which however is beyond the scope of this dissertation and will be studied in our future work.

6.6 Summary

In this chapter, we studied the throughput gain brought by reconfigurable antennas (RAs) in multi-hop wireless networks (MWNs). We proposed a novel tractable link-layer model which successfully captures the dynamic antenna pattern-link relations. Based on our model, the throughput optimization problem with RAs (TORA) was proposed. We

formulated our problem as an MINLP problem and then reformulated it into an MILP problem using RLT technique before solving it with CPLEX. We theoretically proved the superiority of RAs to traditional omni-directional and directional antennas using a conflict-graph based methodology. The benefits of RAs are validated by several case studies and extensive simulations. Our optimization results provide a performance bound in terms of overall throughput for any future link-layer-distributed-protocol design with RAs in MWNs.

CHAPTER 7
CONCLUSIONS AND FUTURE RESEARCH

7.1 Conclusions

In this chapter, we summarize our contributions in this dissertation and draw conclusions. Then we will outline several future directions of interference mitigation in wireless networks.

In the coexistence of wireless networks, most previous works are limited to the traditional omni-directional antennas. Recent advances in wireless MIMO and reconfigurable antennas have been proven to remarkably enhance the coexistence performance of wireless networks. However, these works focus on the physical-layer design. In my work, we study the coexistence problem at the network level. Specifically, we use global optimization approaches to derive the performance upper bounds of multi-hop networks' coexistence problem. For the practical-distributed approach, we use game-theoretical method to study the coexistence problem of wireless networks.

In Chapter 2, we study the coexistence problem of a multi-hop BAN against the external CTI, especially those from non-protocol-compliant sources that are much harder to mitigate than the CTI from 802.x devices. We formulate a joint routing and power control problem aiming at overcoming the impact of such strong CTI in a BAN, while using minimal overall energy consumption. The optimal results are derived by using CPLEX after reformulated into linear form. We then propose a practical JRPC protocol which exploits passive measurement and prediction to model the uncertain impact of CTI on link qualities, and then propose a heuristic algorithm to efficiently solve our JRPC problem. Remarkably, evaluation results show that our JRPC protocol can effectively enlarge the "reliability zone" of the BAN, even when the CTI source is closest to the body. Our protocol also achieves high efficiency, low-energy consumption and overhead. Future work will focus on distributed

algorithms.

In Chapter 3, we performed a study of the cooperative cross-technology interference mitigation (CIM) paradigm for heterogeneous multi-hop networks in unplanned settings. The main technical challenges are due to the lack of a predefined network priority in unplanned deployments, and to various forms of network heterogeneity. We first show that general technology-independent interference cancellation (TIIC) is feasible for heterogeneous multi-hop networks with different protocol standards, and then introduce our two CIM models with different interference cancellation (IC) techniques. We characterize the performance bounds of CIM via deriving the Pareto-optimal throughput curve. Through extensive simulation results we show that the CIM paradigms with full IC and receiver-side IC can both offer significant performance gains in throughput to the coexisting networks compared with the traditional interference-avoidance (IAV) paradigm. The models and results will guide practical CIM protocol design, and pave the way to ultimately change the coexistence paradigm for unplanned heterogeneous networks in unlicensed bands and TV white spaces.

In Chapter 4, we study the coexistence problem of MIMO wireless networks. Different from previous works, we focus on this problem from a new point of view at a higher level: the incentive of complying with/violating the underlying MAC protocols. We establish a new multi-level game framework which incorporates both the high-level cooperative/non-cooperative strategies, and the low-level DoF allocation strategies. The game is played in two rounds, in which the first round is modeled as a static game and the second round is modeled as a Stackelberg game. Both the utilities and strategies in equilibrium are analyzed and derived in this chapter. By studying the equilibriums in different scenarios, we have insights of the cooperation incentives in the coexistence of single-link MIMO wireless networks, which could be used as guidance in network design in spectrum-scarce scenarios.

In Chapter 5, we extend our game-theoretical approach to the multi-hop cases, specifically in the domain of cognitive radio networks. We analyze both the primary and secondary networks' optimal strategies in the coexistence game. We study two different types of sec-

ondary networks, categorized by their selfish behaviors. The first type is selfish-compliant in following the spectrum access rules and does not generate any interference to the primary network. The secondary type is selfish-non-compliant secondary network, which maximizes its own throughput without caring its interference to the primary network. We derive the equilibriums of both primary networks and each of the two types of secondary networks respectively. Our results imply that the secondary networks always have the incentive to play selfishly, as doing so could enhance its average throughput. To defend against the selfish secondary networks, we could enlarge the interference areas of the primary network's transmitter, which could enhance its throughput in the equilibrium through an implicit interference chain between the primary network and the secondary network.

In Chapter 6, we study the throughput gain brought by reconfigurable antennas (RAs) in multi-hop wireless networks (MWNs). We propose a novel tractable link-layer model which successfully captures the dynamic antenna pattern-link relations. Based on our model, the throughput optimization problem with RAs (TORA) was proposed. We formulate our problem as a MINLP problem and then reformulate it into a MILP problem using RLT technique before solving it with CPLEX. We theoretically prove the superiority of RAs to traditional omni-directional and directional antennas using a conflict-graph based methodology. The benefits of RAs are validated by several case studies and extensive simulations. Our optimization results provide a performance bound in terms of overall throughput for any future link-layer-distributed-protocol design with RAs in MWNs.

7.2 Future Research Directions

In the area of body area networks coexisting with cross-technology interferences, the major future direction is to develop a distributed algorithm, instead of our centralized optimization/heuristic algorithm. A distributed scheme could reduce the computational overhead at the central controller, though this is not an overkill in a small-size body area network. Another direction is to improve our link-PDR estimation and prediction algorithm to make it robust against fast-changing and unpredictable interferences. In addition, defending against malicious interfering signals is also worth of studying. Theoretically, the

attacker could perform smart jamming only at the data-transmitting phase, but keep silent at the link-measuring phase. In this case, the interference degree will be underestimated by the BANs.

In the area of cooperative interference mitigation of heterogeneous wireless MIMO networks, One future direction is a more precise modeling. Our current model is based on a global node-cancellation order. However, this ordering is sufficient but not necessary. The sufficient and also necessary modeling is still an open problem. Our goal is to design another model to further enhance the overall-throughput-performance bounds. Another direction is the distributed algorithm design. While our work derives the upper bound of the coexisting networks' throughputs, a distributed algorithm run on each network/node is more practical in reality. Ideally, such algorithms should not rely on the global topology/interference information, thus incurring less communication overhead within the networks.

In the area of a game-theoretical approach to study the coexistence of MIMO wireless networks, the major future direction is the analysis of multiple multi-hop networks' coexistence. However, this is a challenge as the strategy space is large due to the intricacy of link scheduling. We need an efficient algorithm to determine the leader network's optimal strategy. In addition, as our results show that the secondary networks always have the incentive to play selfishly, we need to design a scheme to enforce cooperation by the secondary network, which is necessary for primary network's reliable transmission.

In the area of throughput optimization in wireless networks with reconfigurable antennas, one future direction is to study the coexistence problem of multiple wireless networks with reconfigurable antennas, just like our work in Chapter 3. Ideally, the throughput region could be improved by cooperatively using reconfigurable antennas to reduce the interference degree. Another direction is modeling of frequency and polarization reconfigurability. Currently we only model the pattern reconfigurability. By considering the other two types of reconfigurability, we could further improve the overall throughput performance.

REFERENCES

[1] K. Lorincz, D. Malan, T. Fulford-Jones, A. Nawoj, A. Clavel, V. Shnayder, G. Mainland, M. Welsh, and S. Moulton, "Sensor networks for emergency response: challenges and opportunities," *IEEE Pervasive Computing*, vol. 3, no. 4, pp. 16–23, Oct.-Dec. 2004.

[2] J. Bernhard, J. Reed, and J. M. Park, "Final report of the national science foundation workshop on. enhancing access to the radio spectrum (ears)," *http://www.nsf.gov/funding/pgm_summ.jsp?pims_id=503480*, 2010.

[3] C. Liang, N. Priyantha, J. Liu, and A. Terzis, "Surviving wi-fi interference in low power zigbee networks," in *ACM SenSys*. ACM, 2010, pp. 309–322.

[4] R. Shah and L. Nachman, "Interference detection and mitigation in ieee 802.15. 4 networks," in *IEEE IPSN*, 2008, pp. 553–554.

[5] M. Patel and J. Wang, "Applications, challenges, and prospective in emerging body area networking technologies," *Wireless Communications, IEEE*, vol. 17, no. 1, pp. 80 –88, february 2010.

[6] A. Gaffney, "Fcc releases regulations governing medical body area network devices." [Online]. Available: http://www.raps.org/focus-online/news/news-article-view/article/2225/

[7] Shimmer, "Wireless strain gauge." [Online]. Available: http://www.shimmer-research.com/p/products/sensor-units-and-modules/wireless-strain-gauge

[8] K. Chowdhury and I. Akyildiz, "Interferer classification, channel selection and transmission adaptation for wireless sensor networks," in *Communications, 2009. ICC '09*, june 2009, pp. 1 –5.

[9] Y. Hou, M. Li, and S. Yu, "Surviving the rf smog: Making body area networks robust to cross-technology interference," in *Sensor, Mesh and Ad Hoc Communications and Networks (SECON), 2013 10th Annual IEEE Communications Society Conference on*, June 2013, pp. 353–361.

[10] D. Tse and P. Viswanath, *Fundamentals of wireless communication.* New York, NY, USA: Cambridge University Press, 2005.

[11] S. Gollakota, S. D. Perli, and D. Katabi, "Interference alignment and cancellation," *SIGCOMM Comput. Commun. Rev.*, vol. 39, no. 4, pp. 159–170, Aug. 2009. [Online]. Available: http://doi.acm.org/10.1145/1594977.1592588

[12] V. Cadambe and S. Jafar, "Interference alignment and degrees of freedom of the k -user interference channel," *Information Theory, IEEE Transactions on*, vol. 54, no. 8, pp. 3425–3441, Aug 2008.

[13] S. Gollakota, F. Adib, D. Katabi, and S. Seshan, "Clearing the rf smog: making 802.11n robust to cross-technology interference," in *Proceedings of the ACM SIGCOMM 2011 conference*, ser. SIGCOMM '11. New York, NY, USA: ACM, 2011, pp. 170–181. [Online]. Available: http://doi.acm.org/10.1145/2018436.2018456

[14] K. Sundaresan, R. Sivakumar, M.-A. Ingram, and T.-Y. Chang, "Medium access control in ad hoc networks with mimo links: optimization considerations and algorithms," *Mobile Computing, IEEE Transactions on*, vol. 3, no. 4, pp. 350–365, 2004.

[15] R. Bhatia and L. Li, "Throughput optimization of wireless mesh networks with mimo links," in *IEEE INFOCOM 2007*, 2007, pp. 2326–2330.

[16] L. Cortes-Pena, J. Barry, and D. Blough, "Jointly optimizing stream allocation, beamforming and combining weights for the mimo interference channel," *Wireless Communications, IEEE Transactions on*, vol. 14, no. 4, pp. 2245–2256, April 2015.

[17] B. Hamdaoui and K. G. Shin, "Characterization and analysis of multi-hop wireless mimo network throughput," in *ACM MobiHoc '07*. New York, NY, USA: ACM, 2007, pp. 120–129. [Online]. Available: http://doi.acm.org/10.1145/1288107.1288124

[18] X. Yuan, C. Jiang, Y. Shi, Y. Hou, W. Lou, S. Kompella, and S. Midkiff, "Toward transparent coexistence for multihop secondary cognitive radio networks," *Selected Areas in Communications, IEEE Journal on*, vol. 33, no. 5, pp. 958–971, May 2015.

[19] H. Zeng, Y. Shi, Y. Hou, W. Lou, S. Kompella, and S. Midkiff, "On interference alignment for multi-hop mimo networks," in *INFOCOM, 2013 Proceedings IEEE*, April 2013, pp. 1330–1338.

[20] D. Blough, G. Resta, P. Santi, R. Srinivasan, and L. Cortes-Pena, "Optimal one-shot scheduling for mimo networks," in *IEEE SECON 2011*, 2011, pp. 404–412.

[21] Y. Hou, M. Li, X. Yuan, Y. Hou, and W. Lou, "Cooperative cross-technology interference mitigation for heterogeneous multi-hop networks," in *INFOCOM, 2014 Proceedings IEEE*, April 2014, pp. 880–888.

[22] K. C.-J. Lin, S. Gollakota, and D. Katabi, "Random access heterogeneous mimo networks," in *Proceedings of the ACM SIGCOMM 2011 Conference*, ser. SIGCOMM '11. New York, NY, USA: ACM, 2011, pp. 146–157. [Online]. Available: http://doi.acm.org/10.1145/2018436.2018454

[23] J. Costantine, Y. Tawk, S. E. Barbin, and C. G. Christodoulou, "Reconfigurable antennas: Design and applications," *Proceedings of the IEEE*, vol. 103, no. 3, pp. 424–437, 2015.

[24] M. Yllmaz, M. Abdallah, H. El-Sallabi, J. Chamberland, K. Qaraqe, and H. Arslan, "Joint subcarrier and antenna state selection for cognitive heterogeneous networks with reconfigurable antennas," *Communications, IEEE Transactions on*, vol. 63, no. 11, Nov 2015.

[25] B. Cetiner, H. Jafarkhani, J.-Y. Qian, H. J. Yoo, A. Grau, and F. De Flaviis, "Multi-functional reconfigurable mems integrated antennas for adaptive mimo systems," *Communications Magazine, IEEE*, vol. 42, no. 12, Dec 2004.

[26] J. Boerman and J. Bernhard, "Performance study of pattern reconfigurable antennas in mimo communication systems," *Antennas and Propagation, IEEE Transactions on*, vol. 56, no. 1, Jan 2008.

[27] F. Babich and M. Comisso, "Throughput and delay analysis of 802.11-based wireless networks using smart and directional antennas," *Communications, IEEE Transactions on*, vol. 57, no. 5, May 2009.

[28] P. Li, C. Zhang, and Y. Fang, "The capacity of wireless ad hoc networks using directional antennas," *Mobile Computing, IEEE Transactions on*, vol. 10, no. 10, Oct 2011.

[29] U. Kumar, H. Gupta, and S. Das, "A topology control approach to using directional antennas in wireless mesh networks," in *IEEE International Conference on Communications, 2006*, vol. 9, June 2006.

[30] X. Yuan, Z. Li, D. Rodrigo, H. Mopidevi, O. Kaynar, L. Jofre, and B. Cetiner, "A parasitic layer-based reconfigurable antenna design by multi-objective optimization," *Antennas and Propagation, IEEE Transactions on*, vol. 60, no. 6, pp. 2690–2701, June 2012.

[31] R. Ramanathan, "On the performance of ad hoc networks with beamforming antennas," in *Proceedings of ACM MobiHoc'01*. New York, NY, USA: ACM, 2001.

[32] V. Navda, A. P. Subramanian, K. Dhanasekaran, A. Timm-Giel, and S. Das, "Mobisteer: Using steerable beam directional antenna for vehicular network access," in *Proceedings of the 5th International Conference on Mobile Systems, Applications and Services*, ser. MobiSys '07. New York, NY, USA: ACM, 2007, pp. 192–205.

[33] W. Xu, "On adjusting power to defend wireless networks from jamming," in *MOBIQUITOUS '07*. Washington, DC, USA: IEEE Computer Society, 2007, pp. 1–6. [Online]. Available: http://dx.doi.org/10.1109/MOBIQ.2007.4451072

[34] O. Durmaz Incel, A. Ghosh, B. Krishnamachari, and K. Chintalapudi, "Fast data collection in tree-based wireless sensor networks," *Mobile Computing, IEEE Transactions on*, vol. 11, no. 1, pp. 86 –99, jan. 2012.

[35] Q. Wang, M. Hempstead, and W. Yang, "A realistic power consumption model for wireless sensor network devices," in *IEEE SECON '06*, vol. 1, sept. 2006, pp. 286 –295.

[36] J. Zhu, "On the power efficiency and optimal transmission range of wireless sensor nodes," in *IEEE EIT'09*, june 2009, pp. 277 –281.

[37] H. D. Sherali and W. P. Adams., "A reformulation-linearization technique for solving discrete and continuous nonconvex problems," *Springer*, 2010.

[38] H. Zeng, Y. Shi, T. Hou, W. Lou, H. Sherali, R. Zhu, and S. Midkiff, "A scheduling algorithm for mimo dof allocation in multi-hop networks," *Mobile Computing, IEEE Transactions on*, vol. PP, no. 99, pp. 1–1, 2015.

[39] H. Zeng, Y. Shi, Y. Hou, and W. Lou, "An efficient dof scheduling algorithm for multi-hop mimo networks," in *INFOCOM, 2013 Proceedings IEEE*, April 2013, pp. 1564–1554.

[40] S. Lin, G. Zhou, K. Whitehouse, Y. Wu, J. A. Stankovic, and T. He, "Towards stable network performance in wireless sensor networks," in *RTSS '09*, 2009, pp. 227–237.

[41] J. Huang, S. Liu, G. Xing, H. Zhang, J. Wang, and L. Huang, "Accuracy-aware interference modeling and measurement in wireless sensor networks," in *ICDCS '11*, 2011, pp. 172–181.

[42] S. Liu, G. Xing, H. Zhang, J. Wang, J. Huang, M. Sha, and L. Huang, "Passive interference measurement in wireless sensor networks," in *IEEE ICNP*, oct. 2010, pp. 52 –61.

[43] S. Xiao, A. Dhamdhere, V. Sivaraman, and A. Burdett, "Transmission power control in body area sensor networks for healthcare monitoring," *IEEE JSAC*, vol. 27, no. 1, pp. 37 –48, january 2009.

[44] H. Madsen, *Time Series Analysis: Forecasting and Control*. CRC Press, 2008, vol. 77.

[45] X. Li, N. Mitton, and D. Simplot-Ryl, "Mobility prediction based neighborhood discovery in mobile ad hoc networks," in *IFIP NETWORKING'11*, 2011, pp. 241–253.

[46] X. Liang, X. Li, Q. Shen, R. Lu, X. Lin, X. Shen, and W. Zhang, "Exploiting Prediction to Enable Secure and Reliable Routing in Wireless Body Area Networks," in *INFOCOM*, Orlando, FL, 2012.

[47] Y. Liu, Q. Zhang, and L. Ni, "Opportunity-based topology control in wireless sensor networks," *IEEE TPDS*, vol. 21, no. 3, pp. 405 –416, march 2010.

[48] X. Zhang and K. G. Shin, "Gap sense: Lightweight coordination of heterogeneous wireless devices," in *INFOCOM, 2013 Proceedings IEEE*, 2013.

[49] S. Toumpis and A. Goldsmith, "Capacity regions for wireless ad hoc networks," *Wireless Communications, IEEE Transactions on*, vol. 2, no. 4, pp. 736–748, 2003.

[50] Y. Shi, J. Liu, C. Jiang, C. Gao, and Y. Hou, "An optimal link layer model for multi-hop mimo networks," in *INFOCOM, 2011 Proceedings IEEE*, 2011, pp. 1916–1924.

[51] Q. Spencer, A. Swindlehurst, and M. Haardt, "Zero-forcing methods for downlink spatial multiplexing in multiuser mimo channels," *Signal Processing, IEEE Transactions on*, vol. 52, no. 2, pp. 461–471, 2004.

[52] A. Goldsmith, *Wireless communications*. Cambridge university press, 2005.

[53] S. Sharma, Y. Shi, Y. Hou, H. Sherali, and S. Kompella, "Cooperative communications in multi-hop wireless networks: Joint flow routing and relay node assignment," in *INFOCOM, 2010 Proceedings IEEE*, 2010, pp. 1–9.

[54] Y. Hou, M. Li, and D. Yang, "A game theoretical approach to coexistence of heterogeneous mimo wireless networks with interference cancellation," http://wiser.arizona.edu/publications/techreport_icnc_2016.pdf, October 2015.

[55] X. Yuan, C. Jiang, Y. Shi, Y. T. Hou, W. Lou, and S. Kompella, "Beyond interference avoidance: On transparent coexistence for multi-hop secondary cr networks," in *2013 IEEE International Conference on Sensing, Communications and Networking (SECON)*, June 2013, pp. 398–405.

[56] S. Yi, Y. Pei, and S. Kalyanaraman, "On the capacity improvement of ad hoc wireless networks using directional antennas," in *Proceedings of the 4th ACM International Symposium on Mobile Ad Hoc Networking & Computing*, ser. MobiHoc '03. New York, NY, USA: ACM, 2003.

[57] C. Peraki and S. D. Servetto, "On the maximum stable throughput problem in random networks with directional antennas," in *Proceedings of the 4th ACM International Symposium on Mobile Ad Hoc Networking & Computing*, ser. MobiHoc '03. New York, NY, USA: ACM, 2003.

[58] O. Bazan and M. Jaseemuddin, "On the design of opportunistic mac protocols for multihop wireless ; networks with beamforming antennas," *Mobile Computing, IEEE Transactions on*, vol. 10, no. 3, March 2011.

[59] W. Wong and S.-H. Chan, "Topology optimization for wireless mesh with directional antennas," in *Communications (ICC), 2014 IEEE International Conference on*, June 2014, pp. 2791–2796.

[60] K. Jain, J. Padhye, V. N. Padmanabhan, and L. Qiu, "Impact of interference on multi-hop wireless network performance," in *Proceedings of the 9th Annual International Conference on Mobile Computing and Networking*, ser. MobiCom '03. New York, NY, USA: ACM, 2003.

[61] P. Gupta and P. R. Kumar, "The capacity of wireless networks," *Information Theory, IEEE Transactions on*, vol. 46, no. 2, pp. 388–404, 2000.

[62] X. Huang, J. Wang, and Y. Fang, "Achieving maximum flow in interference-aware wireless sensor networks with smart antennas," *Ad Hoc Netw.*, vol. 5, no. 6, Aug. 2007.

[63] Y. Shi, Y. T. Hou, J. Liu, and S. Kompella, "Bridging the gap between protocol and physical models for wireless networks," *IEEE Transactions on Mobile Computing*, vol. 12, no. 7, July 2013.

[64] Y. Hou and M. Li, "Throughput optimization in mwns with reconfigurable antennas," *Technical Report*, 2016. [Online]. Available: http://wiser.arizona.edu/papers/RAtechrep.pdf

[65] R. Choudhury, X. Yang, R. Ramanathan, and N. Vaidya, "On designing mac protocols for wireless networks using directional antennas," *Mobile Computing, IEEE Transactions on*, vol. 5, no. 5, May 2006.

[66] J. E. Hill, "Gain of directional antennas," *Watkins-Johnson Company, Tech-notes*, 1976.

CURRICULUM VITAE

Yantian Hou

Published Journal Articles

- Yantian Hou, Ming Li, Shucheng Yu, "Making Wireless Body Area Networks Robust under Cross-Technology Interference," IEEE Transactions on Wireless Communications (TWC), in major revision.
- Yantian Hou, Ming Li and Xu Yuan, Y. Thomas Hou, Wenjing Lou "Cooperative Interference Mitigation for Heterogeneous Multi-hop Networks Coexistence," IEEE Transactions on Wireless Communications (TWC), accepted.

Published Conference Papers

- Yantian Hou, Ming Li and Dejun Yang, A Game Theoretical Approach to Coexistence of Heterogeneous MIMO Wireless Networks with Interference Cancellation, IEEE International Conference on Computing, Networking and Communication (IEEE ICNC'16), Feb. 15-18 2016, Kauai, HI.)
- Yantian Hou, Ming Li, Ruchir Chauhan, Ryan. M. Gerdes, and Kai Zeng, "Message Integrity Protection over Wireless Channel by Countering Signal Cancellation: Theory and Practice", the 10th ACM Symposium on Information, Computer and Communications Security (ACM ASIACCS'15),Singapore, Apr. 2015.
- Boyang Wang, Yantian Hou, Ming Li, Haitao Wang, Hui Li and Fenghua Li, "Tree-based Multi-Dimensional Range Search on Encrypted Data with Enhanced Privacy," in Proceedings of the 10th International Conference on Security and Privacy in Communication Networks (SecureComm'14), Beijing, China, September 24-26, 2014.

- Boyang Wang, Yantian Hou, Ming Li, Haitao Wang and Hui Li, "Maple: Scalable Multi-Dimensional Range Search over Encrypted Cloud Data with Tree-based Index," in Proceedings of the 9th ACM Symposium on Information, Computer and Communication Security (ACM ASIACCS 2014), pp.111-122, Kyoto, Japan, June 3-6, 2014.

- Yantian Hou, Ming Li, Xu Yuan, Y. Thomas Hou, and Wenjing Lou, "Cooperative Cross-Technology Interference Mitigation for Heterogeneous Multi-hop Networks", The 33nd IEEE International Conference on Computer Communication (IEEE INFOCOM'14), Toronto, ON, Canada, Apr. 27 - May 2, 2014.

- Yantian Hou and Ming Li, "Enforcing Spectrum Access Rules in Cognitive Radio Networks through Cooperative Jamming".International Conference on Wireless Algorithms, Systems, and Applications (WASA 2013), Zhangjiajie, Hunan, China, August 7-10, 2013..

- Yantian Hou, Ming Li and Shucheng Yu, "Surviving the RF Smog: Making Body Area Networks Robust to Cross-Technology Interference", 10th Annual IEEE Communications Society Conference on Sensor, Mesh and Ad Hoc Communications and Networks (IEEE SECON'13), New Orleans, Jun. 24-27, 2013.

- Yantian Hou, Ming Li, and Joshua. D. Guttman, "Chorus: Scalable In-band Trust Establishment for Multiple Constrained Devices over the Insecure Wireless Channel", The 6th ACM Conference on Security and Privacy in Wireless and Mobile Networks (ACM WiSec'13), Budapest, Hungary, April 17-19, 2013.